8-2013

Formation, Deformation, and Incision of Colorado River Terraces Upstream of Moab, Utah

Andrew P. Jochems
Utah State University

FORMATION, DEFORMATION, AND INCISION OF COLORADO RIVER TERRACES UPSTREAM OF MOAB, UTAH

by

Andrew P. Jochems

A thesis submitted in partial fulfillment
of the requirements for the degree

of

MASTER OF SCIENCE

in

Geology

Approved:

_____	_____
Dr. Joel L. Pederson Major Professor	Dr. Patrick Belmont Committee Member
_____	_____
Dr. Tammy M. Rittenour Committee Member	Dr. Mark R. McLellan Vice President for Research and Dean of the School of Graduate Studies

UTAH STATE UNIVERSITY
Logan, Utah

2013

ABSTRACT

Formation, Deformation, and Incision of Colorado River Terraces

Upstream of Moab, Utah

by

Andrew P. Jochems, Master of Science

Utah State University, 2013

Major Professor: Dr. Joel L. Pederson
Department: Geology

Fluvial terraces contain information about incision, deformation, and climate change. In this study, a chronostratigraphic record of Colorado River terraces is constructed from optically stimulated luminescence (OSL) dating of Pleistocene alluvium and real-time kinematic (RTK) GPS surveys of terrace form. This record is analyzed to relate terrace formation to late Pleistocene climate fluctuations, and terrain analyses and longitudinal profile patterns reveal recent salt-related activity in the northern Paradox Basin as well as patterns in Colorado Plateau incision.

A well-preserved, correlative suite of mainstem (M) fluvial deposits exists along the Colorado River upstream of Moab, Utah. Absolute dates indicate sedimentation >70 ka (M7, M6/M5), 70-50 ka (M4), 50-40 ka (M3), and 35-25 ka (M2). The M4 and M2 formed during the crescendo to glacial maxima, but the M7, M6/M5, and M3 were deposited during variable climate of marine isotope stages (MIS) 5 and 3. Deposits include thin (<7 m) strath terraces and thick (10-20 m) fill terraces.

Our results suggest that terrace sedimentation is linked to enhanced sediment flux during glaciations in Rocky Mountain headwaters (M4 and M2), but major deposits also formed during dryland tributary sediment loading with markedly different timing (M6/M5 and M3). Conversely, incision may be driven by higher deglacial flows. Clast provenance data demonstrate greater percentages of locally-sourced sediment in M6/M5 and M3 deposits. Valley-bottom geometry and neotectonics control terrace form, with strath terraces found in bedrock-restricted reaches and fill terraces in wider valleys.

Previously speculated salt deformation in this area is confirmed by localized collapse preserved in M4 stratigraphy in the Cache Valley graben and ~15 m of broader subsidence upstream. Concavity and knickzone distributions in tributary profiles are discordant and represent subtle expressions of salt-tectonic activity. Finally, a surprisingly rapid incision rate of ~900 m/Ma over the past ~70 ka suggests that the Colorado River may be responding to flexural rebound in the central plateau, but is faster than that predicted by the debated bull's-eye pattern of regional incision. This locally high rate may also reflect a transient wave of incision, as suggested by increased Pleistocene rates interpreted by studies in Glen and Grand canyons.

(193 pages)

PUBLIC ABSTRACT

FORMATION, DEFORMATION, AND INCISION OF COLORADO RIVER TERRACES UPSTREAM OF MOAB, UTAH

The history of rivers is laid down as sediment in all landscapes, typically as a function of climate, geologic structures, and/or changes in sea level. When a river abandons its floodplain, this sediment collectively constitutes a landform called a fluvial terrace. Terraces are used to unlock prior characteristics of a river flowing through a given area at both local and regional scales. Dating terrace sediment allows comparison to known changes in climate and geologic deformation, two significant controls on the hydraulics of rivers and the deposition of their sediment loads.

The importance of terraces lies in their utility as markers of climate change and geologic deformation. By constructing a record of terrace formation by large rivers such as the Colorado, we develop the capacity to predict how a river system will respond to changing climate or geologic events such as the rupturing of faults or the uplift of the Earth's surface. These capabilities permit informed decisions wherever humans live along or otherwise depend on rivers, including water management and floodplain zoning.

We describe the history of the Colorado River upstream of Moab, Utah over the last 100,000 years. By dating terrace sediment and taking topographic surveys of terrace shape and form, we identify patterns in climate change and geologic deformation related to subsurface salt deposits. Our findings imply that the Colorado River is sensitive to both of these controls, especially in terms of where it deposits its sediment load, how much sediment is deposited, and the timing of floodplain abandonment.

Andrew P. Jochems

ACKNOWLEDGMENTS

I wish to thank my committee members, Dr. Tammy Rittenour and Dr. Patrick Belmont, for their valuable advice and guidance throughout the execution of this research. I greatly appreciate the help and company of many field hands: Natalie Bursztyn, Santiago Flores, Faye Geiger, Troy Siddoway, and Cianna Wyshnytzky. Michelle Nelson in the Utah State Luminescence Laboratory was integral to the processing and analysis of luminescence results. I am grateful to the USU Department of Geology for the Peter R. McKillop Memorial Scholarship, and for financial support in the form of research and teaching assistantships.

The support of my family and my significant other, Amanda Gallegos, was instrumental during my time at Utah State. My grandfather, Willis Nigh, graciously lent his geologic expertise and inexhaustible encouragement. Finally, I must express extreme gratitude to my advisor, Dr. Joel Pederson, for his patience and scientific insight, which will continue to inspire my development as both a geoscientist and human being long after I depart Logan.

Andy Jochems

CONTENTS

Page

LIST OF TABLES

LIST OF TABLES (CONT.)

LIST OF TABLES (CONT.)

LIST OF FIGURES

LIST OF FIGURES (CONT.)

CHAPTER 1

INTRODUCTION

Colorado River terraces provide a valuable record of cyclical fluvial aggradation and incision over the late Pleistocene, and can serve as markers of salt tectonism in the Colorado Plateau. However, the links between climate drivers and the processes behind terrace formation remain unresolved. Optically stimulated luminescence (OSL) dating of terrace sediment and real-time kinematic (RTK) GPS topographic surveys of terrace form are used to construct a chronostratigraphy that spans two major glacial-interglacial cycles. Geographic information system (GIS) analyses allow for quantitative assessment of landscape dynamics in the study area in response to salt tectonism. Together, these analyses paint a picture of late Quaternary geomorphic evolution of the Colorado River in the iconic Colorado Plateau drylands upstream of Moab, Utah, USA.

This thesis consists of two related studies set in the highly erosional landscape of the central Colorado Plateau. The first is a study of the formation of Colorado River terraces upstream of Moab, and the second is a study of salt tectonism and incision along the river and its local tributaries.

More specifically, Chapter 2 details the construction of a chronostratigraphy of Colorado River terraces in the study area. Previous models of terrace formation are reviewed and provide a foundation from which we build our model for the genesis of mainstem deposits in this dryland setting. This study employs OSL dating and RTK GPS surveys of terrace deposits. The results lead to a new conceptual model for the formation of fluvial terraces along the Colorado River above Moab. This chapter is intended to be a

draft manuscript coauthored by Dr. Joel Pederson and myself, targeted for the *Geological Society of America Bulletin* or *Quaternary Science Reviews*.

Chapter 3 is a study of evidence from the mainstem terrace record for recently active salt tectonism, late Pleistocene incision rates of the Colorado River, and the characterization of topography in the study area using GIS metrics. OSL dating and RTK survey results permit the calculation of incision rates and deformation of terraces by hypothesized salt tectonism. Calculated spatial metrics include the normalized steepness index (k_{sn}) and concavity of tributary channel profiles, which are used to assess the varying controls on stream-profile shape in the study area. This chapter is intended to be a concise draft manuscript coauthored by Dr. Joel Pederson and myself, for submission to the journal *Geology*.

Chapter 4 is a summary of these two studies and their implications for the interpretation of fluvial records and landscape dynamics in the central Colorado Plateau.

CHAPTER 2

CONTROLS ON THE FORMATION OF COLORADO RIVER TERRACES UPSTREAM OF MOAB, UTAH

ABSTRACT

Fluvial terraces contain information about incision, deformation, and climate change, but our poor understanding of the linkages between climate drivers and the processes behind terrace formation renders them an imprecise tool. We attempt to unlock this information through analysis of the chronostratigraphic record and longitudinal profile patterns of Colorado River terraces upstream of Moab, Utah, USA. Terrace sediments were dated using optically stimulated luminescence (OSL) and the spatial patterns of deposits were determined through real-time kinematic (RTK) GPS surveys.

There are six correlative late Pleistocene mainstem (M) terraces designated as M7-M2 along the Colorado River upstream of Moab. OSL ages indicate sedimentation at >70 ka (M7, M6/M5), ~70-50 ka (M4), ~50-40 ka (M3), and ~35-25 ka (M2). M1 is a minor Holocene deposit. Sedimentation of the M4 and M2 occurs during the build-up to and height of glaciations, but the M7, M6/M5, and M3 are instead deposited during the highly variable climate of marine isotope stages (MIS) 5 and 3. Incision occurs during interglacials or periods of low ice volume. Deposits vary from thin (<7 m) strath terraces in bedrock-restricted reaches upstream to unexpectedly thick (10-20 m) fill terraces in broad Professor Valley.

These results suggest that terrace sedimentation in the central Colorado Plateau is linked to enhanced sediment supply and perhaps reduced peak flows during full glacial

conditions in the Rocky Mountain headwaters (M4 and M2). However, major terrace deposits are also formed during pulses of dryland tributary sediment loading with markedly different timing (M7, M6/M5, and M3). Conversely, incision may be driven by higher peak flows such as during the current interglacial. Local canyon/valley-bottom geometry and neotectonics control terrace form in this setting. Long-profile survey data also show that terraces are deformed by subsidence resulting from tectonism of Paradox Basin evaporites. This deformation and variable valley geometry obfuscate any climate-related information specifically within terrace form.

INTRODUCTION

Fluvial terraces are important landscape markers that contain information about incision, deformation, and climate change. Yet understanding their formation has long been a fundamental problem in geomorphology. Many studies have sought to identify the climatic or tectonic conditions under which terraces form (e.g., Pazzaglia and Gardner, 1993; Fuller et al., 2009; Pazzaglia, in press). Researchers have also attempted to discern the conditions under which fill (depositional) and strath (erosional) terraces are produced. In general, depositional terraces have been thought to reflect aggradation events controlled by climate or baselevel change, whereas erosional terraces have been considered tectonically-controlled features (Bull, 1990). However, recent studies have uncovered more complicated patterns in strath terrace formation (Hancock and Anderson, 2002; Pan et al., 2003), and climate or intrinsic dynamics have been found to be the primary driver of terrace genesis even in tectonically active regions (e.g., Finnegan and Dietrich, 2011; DeVecchio et al., 2012). Although baselevel fall ultimately drives

incision (e.g., Merritts et al., 1994), terraces may be formed during superimposed climate oscillations that alter the balance between sediment load and transport capacity. Thus, our poor understanding of the linkages between climate drivers and the processes behind terrace formation renders them an imprecise tool.

The drainages of the Rocky Mountains and Colorado Plateau have inspired significant work on these issues. Hancock and Anderson (2002) modeled strath terrace formation in the Wind River Mountains of Wyoming, finding that straths there form during the transition from full glacial conditions to interglacial periods. High sediment flux and river transport capacity associated with glaciations leads to increased aggradation of terrace deposits, and subsequent incision and abandonment of these surfaces occurs during deglaciation. However, it is uncertain how hydrologic and sedimentologic signals in the upper Colorado River basin promote terrace formation far downstream during Rocky Mountain glaciations. The chronostratigraphy, morphology, and spatial characteristics of mainstem Colorado River terraces in eastern Grand Canyon have been investigated in recent studies and compared to late Pleistocene climate oscillations in the Rocky Mountains. For example, Anders et al. (2005) found significant differences in the chronostratigraphy of local tributary drainages and the mainstem Colorado River. Their results highlight unresolved issues including the influence of changes in distant hydrology versus local sediment flux in controlling incision or sedimentation, and whether transient sediment signals confound the time-correlation of terraces across a large watershed. The interplay of climate in the Rocky Mountain headwaters of the Colorado River and downstream effects on terrace formation throughout its longitudinal profile provides the opportunity to study the relative influence

of climate change, tectonic activity, and canyon/valley-bottom geometry of large river systems. However, few data exist on the ages and morphologic characteristics of terraces in the Colorado Plateau upstream of Grand and Glen canyons.

Colorado River terraces upstream of Moab, Utah provide a rich record for study because their deposits are well exposed, can be readily dated using optically stimulated luminescence (OSL), and include suites of both fill and strath terrace deposits. Terraces in the study area are also possibly deformed by salt tectonism in this part of the Paradox Basin (Colman, 1983; Trudgill, 2011). Finally, age and survey data obtained for terraces allow for the calculation of incision rates in the context of regional patterns associated with heavily debated tectonic drivers (e.g., Darling et al., 2012; Karlstrom et al., 2012; Pederson et al., 2013). Tectonic issues are examined in Chapter 3.

The purpose of this study is to construct a chronostratigraphic record of Colorado River terraces and to survey and record their longitudinal profile patterns upstream of Moab. Geochronology is vital to testing the hypothesis that terraces are produced under distinct climatic scenarios, and OSL is used to date mainstem Colorado River terrace deposits in the study area. Age control on terrace formation in this area will help to establish relationships to past climate and allow correlations throughout the study area, despite any changes in the spatial and morphologic characteristics of terraces. We propose that Colorado River terraces upstream of Moab were formed in response to both glacial-interglacial hydrology changes in Rocky Mountain headwaters as well as increased local sediment loading from the plateau drylands with more poorly understood connections to climate shifts. Furthermore, terrace form here is not simply related to climate dynamics, but also to variable local valley geometry and neotectonic activity.

BACKGROUND

Regional setting

The Colorado Plateau spans portions of Arizona, Colorado, New Mexico, and Utah, and is bordered on the east and southeast by the central and southern Rocky Mountains and Rio Grande Rift. The Basin and Range defines its western extent. The Colorado River drains the entire plateau and heads in the high Rockies near La Poudre Pass, Colorado (Fig. 2.1). The river extends some 2,330 km from its headwaters until it dies out north of the Gulf of California, with a total drainage area of ~640,000 km^2. Rocky Mountain tributaries funnel snowmelt into the larger system, providing nearly the entire discharge of the Colorado until its confluence with the Green River in southeastern Utah. The annual hydrograph of the Colorado is dominated by Rocky Mountain snowpack and runoff.

Colorado River gravels preserved beneath late Miocene basalt flows near Grand Junction, CO suggest that the river was flowing west out of the Rocky Mountains onto the Colorado Plateau as early as 11 Ma (Aslan et al., 2010). The river was integrated into approximately its modern drainage configuration ~6 Ma, resulting in baselevel fall and enhanced erosion of the landscape (Lucchitta, 1979; Pederson et al., 2002). The majority of the sediment load in the Colorado drainage is supplied by plateau drylands and canyons, accounting in part for the famously rapid erosion and high sediment load transported by the Colorado River.

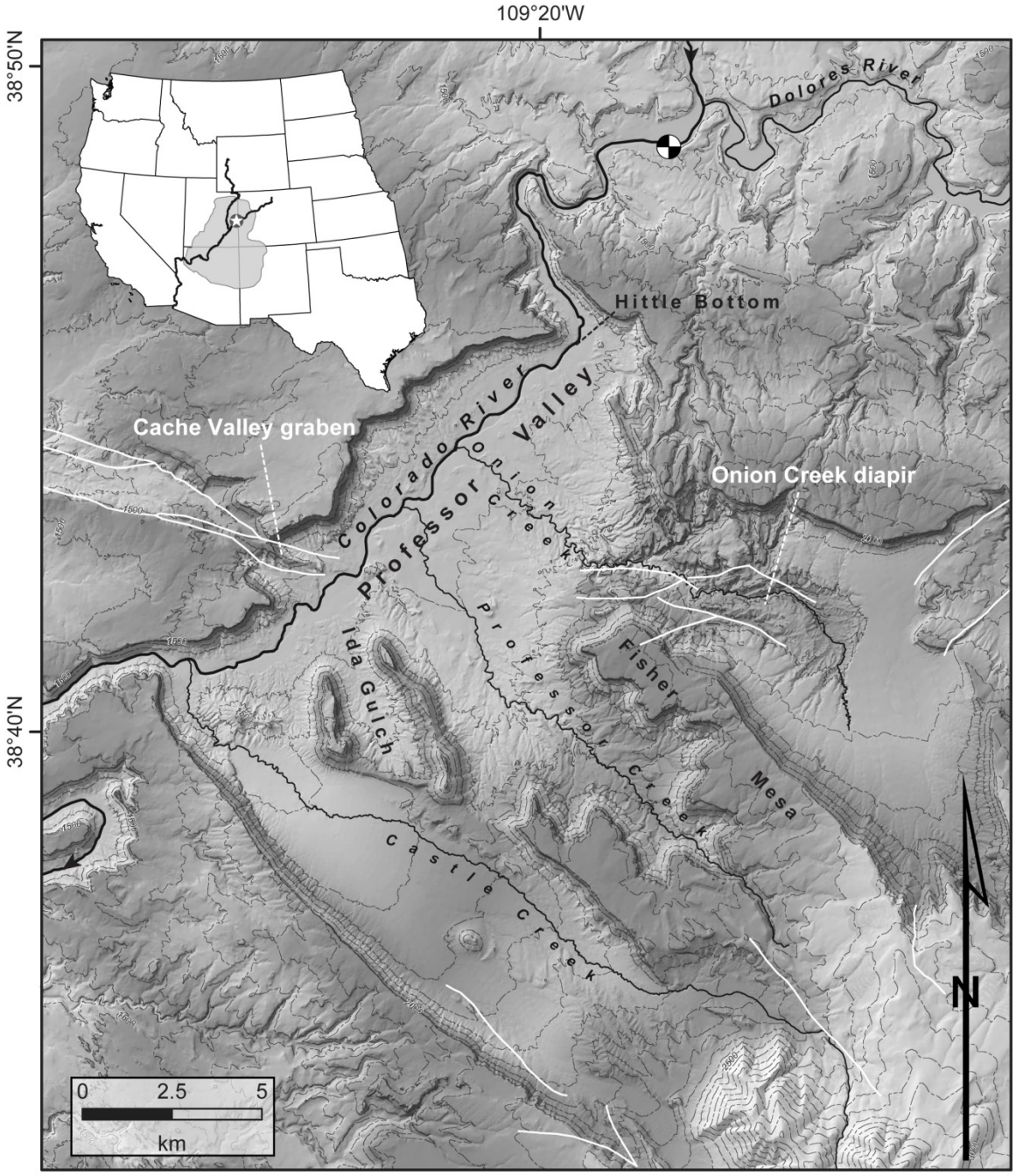

Figure 2.1. Map of Colorado River study area north of Moab, southeastern Utah, southwestern USA. Shaded area on inset map shows Colorado Plateau and study location. White lines are major Quaternary faults and folds (Doelling, 2001). Dewey Bridge stream gage station (USGS 09180500) is shown in northern study area. Light gray lines are 100 m contours. Black arrows show flow direction.

Local setting

The terraces examined in this study include flights of both strath and fill deposits preserved along a ~30 km stretch of the Colorado River between its confluence with the Dolores River and Castle Creek downstream. USGS gage 09180500 (Colorado River near Cisco, UT; Fig 2.1) is located in the study area just downstream of the Dolores (11,998 km^2 drainage area). The area of the upper Colorado River basin above the gage is ~62,700 km^2. The Colorado River here has a median discharge of 203 cubic meters per second (cms), a mean annual maximum discharge of 1013 cms, and several floods exceeding 1700 cms since AD 1913. The modern channel of the Colorado River is 90-105 m wide where restricted by canyon walls, and up to 165 m in Cache Valley graben. Mean annual precipitation is 17.8-22.9 cm and mean annual temperature is 11.7-12.8° C in the study area (USDA, 2011). This area of the Colorado Plateau has been near the northern limit of the late summer monsoon over the late Quaternary (Shafer, 1989).

Relief in the study area ranges from 1847 m on the Dome Plateau northwest of the river to 1223 m at the river's confluence with Castle Creek (Fig. 2.1). Mt. Waas, the northernmost peak of the nearby La Sal Mountains, stands at 3758 m. Soils in the study area consist of entisols and inceptisols no more than ~20-30 cm thick and often thinner or absent. Local hillslopes and cliffs are weathering-limited and are examples of bedrock sub-threshold hillslopes (Montgomery, 2001) with low soil production; rates of baselevel fall are lower than those required for threshold slopes. Based on similar deposits in eastern Grand Canyon (Anders et al., 2005), colluvial deposits stored beneath cliffs, ledges, and slopes are transported to drainages primarily through mass movements.

Three perennial tributaries enter the Colorado River in the study area (Fig. 2.1). From upstream to downstream, they are Onion Creek (51.5 km^2 drainage area), Professor Creek (87 km^2), and Castle Creek (139 km^2). Sediment transport in tributary catchments takes place primarily through debris flows and flashfloods, as suggested by medium to large boulders (≥0.5 m) present in gravel bars in the lower 1-2 km of each tributary. Tributary confluences with the Colorado are characterized by bouldery debris fans forming rapids.

The study area consists of five distinct reaches of the Colorado River, defined by varying geology and valley-bottom geometry (Fig. 2.2). These reaches are designated, from upstream to downstream, as the Dewey Bridge, Dewey Canyon, Professor Valley, Cache Valley graben, and Ida Gulch/Castle Valley reaches.

In the Dewey Bridge reach, the river passes through the Jurassic Morrison, Entrada, and Navajo formations. The river flows through Dewey Canyon, where it is bound on either side by sandstone cliffs of the Jurassic Glen Canyon Group, as well as mudstones and sandstones of the Triassic Chinle and Moenkopi formations. It crosses the northwest trending Sagers Wash syncline north of Dewey Bridge, and the inactive, down-to-the-south Blue Chief Mesa normal fault in Dewey Canyon (Doelling, 1996).

Downstream, Dewey Canyon broadens into the Professor Valley reach at Hittle Bottom. Here, the landscape is dominated by piedmont slopes southeast of the Colorado River, and cliffs and ledges of late Paleozoic and Mesozoic strata rising over 500 m to the Dome Plateau to the northwest. Onion, Professor, and Castle creeks have eroded into conglomerate and sandstone of the Permian Cutler Formation, which are commonly mantled by tributary piedmont gravel (Colman and Hawkins, 1985). Professor Valley

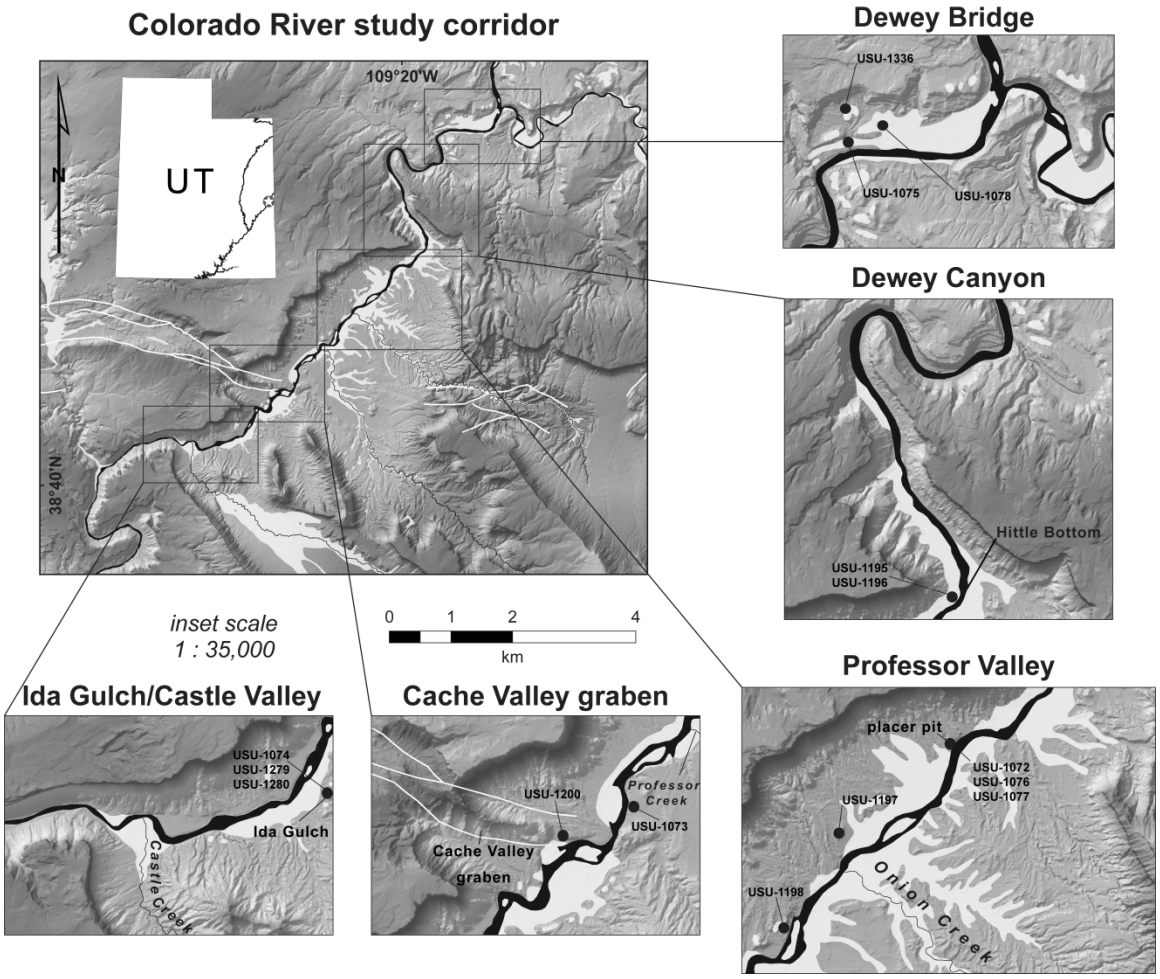

Figure 2.2. Five study reaches, with previously mapped deposits of Quaternary gravel and alluvium (Doelling, 2001). Study area marked by star on inset map. White areas are late Pleistocene and Holocene alluvium, including mainstem terrace gravels and local piedmont. White lines are major Quaternary faults and folds. Black dots show OSL sampling locations with sample numbers.

borders Cache Valley graben at its southwestern extent. Deformation in this feature occurred as subsurface evaporites of the Pennsylvanian Paradox Formation flowed away from its core or were dissolved and gradually removed by the Colorado River throughout the Cache Valley graben reach (Doelling et al., 1988; Doelling and Ross, 1998).

In the Ida Gulch/Castle Valley reach, monuments capped by sandstones of the Wingate and Kayenta formations rise between the river and the intrusive rocks of the La Sal Mountains to the southeast. Castle Creek drains the northwest flank of the La Sals and meets the Colorado River before bedrock canyon walls of Mesozoic strata rise above the river along its course toward Moab (Fig. 2.1).

Quaternary deposits in the study area include sediment deposited by the Colorado River, its tributary drainages, eolian processes, and hillslope systems. Mainstem Colorado River terrace gravels are generally moderately sorted, sub-rounded to rounded, poorly stratified gravel with varying percentages of exotic clasts from Rocky Mountain source areas. They are rarely more than 7 m thick near Dewey Bridge, but commonly approach or exceed 10 m in Professor Valley. Piedmont gravels are thin (<3 m), poorly to moderately sorted, sub-angular to sub-rounded, and lack far-traveled clasts.

The nearby La Sal Mountains feature glacial deposits of lateral moraines and U-shaped valleys that are primarily associated with the marine isotope stage (MIS) 2 Pinedale glaciation (Richmond, 1962; Doelling, 2001). Some glacial deposits may be of MIS 6 Bull Lake age (~140-130 ka). Harden and others (1985) described the carbonate morphology of soils developed on these deposits as well as inset terraces at lower elevations. They identified syn-glacial fluvial gravels in Spanish Valley associated with both the Pinedale and Bull Lake glaciations based on carbonate accumulation rates.

Paleoclimate of the Rocky Mountains

Correlation of Rocky Mountain glaciers to global climate events over the late Pleistocene is a necessary component of establishing the fluvial behavior of rivers that head in the Rockies. Pertinent global, regional, and local paleoclimate records are shown in Fig. 2.3 and discussed below.

The Milankovitch theory of orbitally-controlled insolation has been proposed as the primary driver of ice sheet growth and decay (Hays et al., 1976; Cheng et al., 2009). However, ice sheet dynamics are complex, and late Pleistocene glacial-interglacial cycles do not necessarily correlate to solar insolation minima or maxima due to time lags or intricate feedback mechanisms (Fig. 2.3A).

Global ice volume is indicated by ^{18}O-enriched marine waters (Fig. 2.3B), and high-latitude ice sheets in the northern hemisphere are thought to have lowered temperatures in proglacial regions by 4-10° C relative to the present (Thompson et al., 1993). The height of these ice sheets may have forced the jet stream south, focusing precipitation in the central Rockies and increasing the extent of alpine glaciers. However, new data suggest that this southern shift may have been minimal or nonexistent, and that tropical teleconnections could have played a more significant role in the delivery of moisture to the western United States during the Last Glacial Maximum (LGM) after ~21 ka (Lyle et al., 2012). Although broadly synchronous with the global LGM of ~26.5-19 ka (Clark et al., 2009), the LGM is observed at varying times in the Rocky Mountain headwaters of the Colorado River (Fig. 2.3D).

A uranium-series dated record of vein calcite growth in Devils Hole, NV provides a $\delta^{18}O$ record for the interior western US (Fig 2.3C; Winograd et al., 2006). Vein calcite

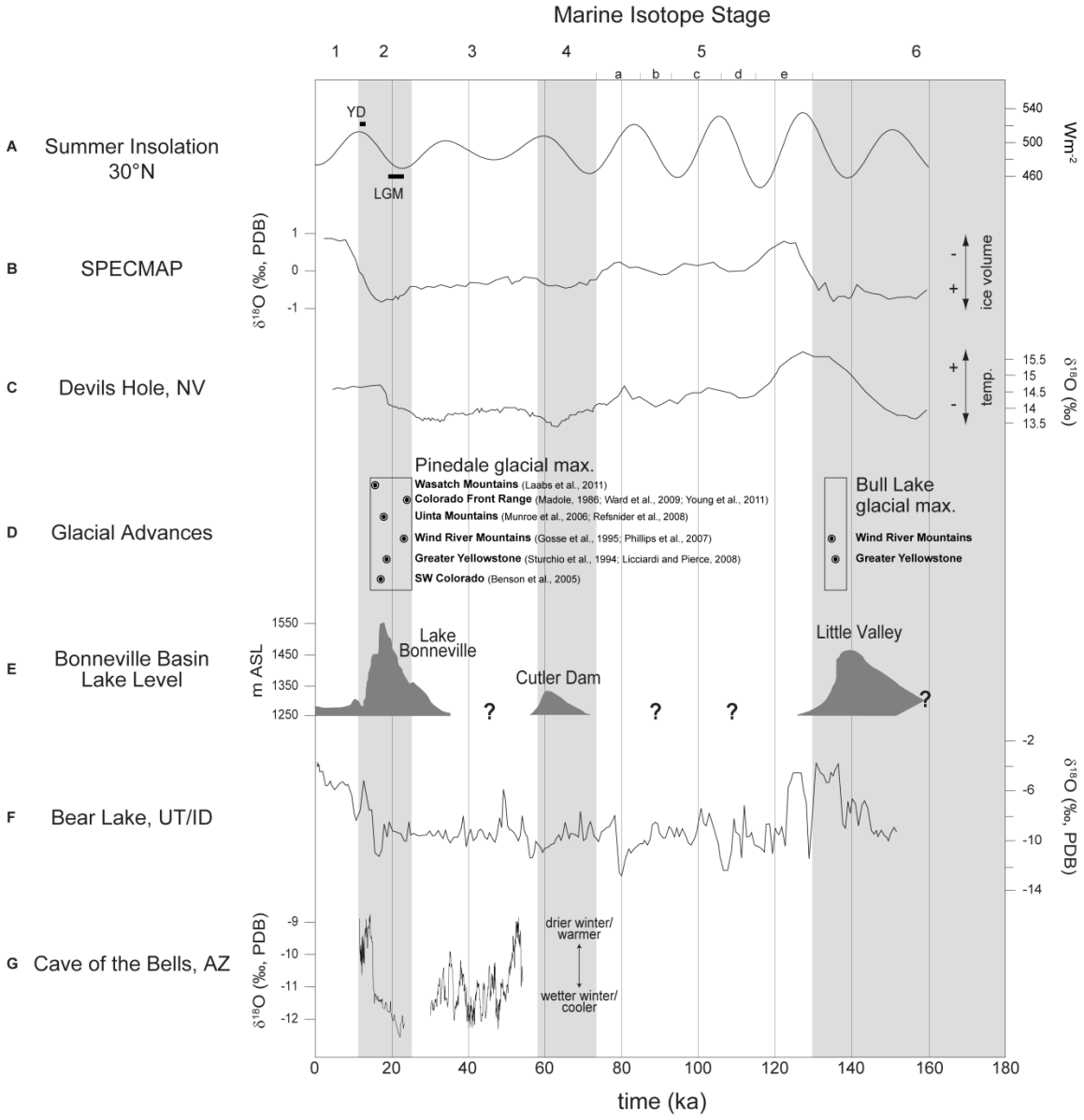

Figure 2.3. Global and regional paleoclimate records. (A) Summer solstice solar insolation curve at 30°N, with MIS 2 climate events marked by bars (modified from Berger and Loutre, 1991). LGM – Last Glacial Maximum; YD – Younger Dryas. (B) SPECMAP marine oxygen isotope curve indicating global ice volume extent (modified from Martinson et al., 1987). PDB – PeeDee Belemnite. (C) Oxygen isotope curve constructed from vein calcite $\delta^{18}O$, Devils Hole, NV (modified from Winograd et al., 1992, 2006). (D) Rocky Mountain glacial records dated using cosmogenic nuclides and radiocarbon. Circles represent earliest maximum advance dates from each area. (E) Lake Bonneville hydrograph showing three major late Pleistocene lake cycles (modified from Benson et al., 2011). (F) Bear Lake, UT/ID, oxygen isotope record constructed from ostracode $\delta^{18}O$ (modified from Bright et al., 2006). (G) Cave of the Bells, AZ, speleothem $\delta^{18}O$ record (modified from Wagner et al., 2010).

records paleotemperature, and the Devils Hole record is considered a proxy for eastern Pacific sea surface temperatures and $\delta^{18}O$ records of global ice volume (Winograd et al., 1992, 2006). This record correlates well with sea surface temperature changes in the eastern Pacific over the last ~160 ka, and indicates a common atmospheric teleconnection between late Pleistocene Northern Hemisphere paleoclimate records. This linkage could have resulted in enhanced Pleistocene moisture availability in the western US, including the Rockies.

Rocky Mountain glacial advances and retreats (Fig. 2.3D) have been determined for the late Pleistocene through extensive mapping of glacial landforms (Pierce, 1979) and confirmed using a variety of methods, including cosmogenic radionuclide (CRN) and radiocarbon dating. Licciardi and Pierce (2008) dated Yellowstone moraines to 136 ± 13 ^{10}Be ka and 18.8 ± 0.9 to 13.5 ± 1.1 ^{10}Be ka for the Bull Lake and Pinedale glaciations, respectively. The LGM has been dated to 16.8 ± 0.7 ka in the southwestern Uinta Mountains, UT (Munroe et al., 2006), and 13.8 ± 0.6 to 11.4 ± 0.5 ka in the Wind River Mountains of Wyoming (Gosse et al., 1995), based on sampling of moraine-crest boulders. Phillips et al. (1997) dated Wind River moraine and fluvial-terrace outwash boulders to ~130 ka, although Sharp et al. (2003) used uranium-series dating of pedogenic carbonate in Wind River terraces to demonstrate possible ice advance ~150 ka. In the Arkansas River basin of Colorado, Young et al. (2011) found asynchronous Pinedale maxima ~22-16 ka based on ages of moraine boulders/pebbles and terrace boulders. An array of recent regional cosmogenic studies support these ages (e.g., Chadwick et al., 1997; Benson et al., 2005; Munroe et al., 2006; Refsnider et al., 2008; Ward et al., 2009), as well as radiocarbon ages obtained from sediment cores of glacial

Lake Devlin, CO that suggest LGM advances in the Colorado Front Range occurred ~23.5-21 ka (Madole, 1986).

Regional evidence for the LGM in the central Rockies and the Great Basin includes the hydrograph of pluvial Lake Bonneville (Fig. 2.3E). The size of Lake Bonneville has been correlated to glacial extent in the Wasatch and western Uinta ranges (Benson et al., 2011). Glacial extent may therefore have been related to the "lake-effect" of precipitation, with earlier glacial maxima (~25-18 ka) observed in the orographically-shielded Uintas than in the Wasatch (~16 ka; Lips et al., 2005). Additionally, the timing of the Bull Lake and Pinedale glaciations is supported by pollen and ostracode $\delta^{18}O$ analyzed from core samples of Bear Lake, UT/ID (Fig. 2.3F). The $\delta^{18}O$ of lake waters decreases when the Bear River drains into the lake, which is currently topographically closed; this is particularly true during periods of glacial melting (Bright et al., 2006). The Bear Lake record demonstrates a general correlation between hydrologic changes observed in the depletion or enrichment of $\delta^{18}O$ in ostracodes, regional vegetation, and global ice volume and summer insolation (Jiménez-Moreno et al., 2007). It is generally in agreement with the Devils Hole record (e.g., during MIS 5; Fig. 2.3C, F), though the Bear Lake record implies a different timing for the MIS 6 Bull Lake glaciation and subsequent interglacial conditions after ~140 ka (Bright et al., 2006; Winograd et al., 2006).

The highly variable climate of MIS 3 is revealed in the Cave of the Bells, AZ, speleothem $\delta^{18}O$ record (Fig. 2.3G; Wagner et al., 2010). Forced south by atmospheric changes linked to North Atlantic ocean circulation, precipitation from westerly storms enters the cave during winter as dripwater, carrying a $\delta^{18}O$ signature largely independent of temperature. Drier instadial conditions are marked by higher $\delta^{18}O$ values in this record,

whereas wetter stadial conditions are marked by the reverse trend. The Cave of the Bells curve demonstrates climatic variability in the southwestern United States on a millennial timescale between 54 and 30 ka.

Locally, alternating eolian deposition and pedogenesis in upland portions of Canyonlands National Park indicate sediment production during climatic transitions over the late Pleistocene and Holocene, as vegetation was destabilized by drought or sediment was eroded during periods of high runoff (Reheis et al., 2005). These patterns are observed after ~20 ka in Canyonlands. In addition, packrat midden data imply drier conditions in southeastern Utah as glacial conditions strengthened ~25 ka (Betancourt, 1990; Sharpe, 1991).

Conceptual models of terrace formation

Fluvial terraces are the abandoned floodplains of streams and rivers, and consist of unconsolidated deposits with basal unconformities known as straths and bench-like tops known as treads (Ritter et al., 2002). Strath terraces result from lateral planation of rivers across valley floors, whereas fill terraces are formed by valley aggradation and subsequent entrenchment into alluvial fills. Terraces reflect the adjustment of rivers to climatic perturbations or the lowering of baselevel, the ultimate level of fluvial erosion. However, terrace genesis may also be attributed to intrinsic controls such as meander growth and cutoff (Finnegan and Dietrich, 2011) or complex response (Schumm and Parker, 1973). Thin strath and thick fill terrace deposits generally reflect different regimes in rivers with respect to changing balances in transport capacity and sediment supply (Lane, 1955; Hancock and Anderson, 2002). Terraces may be paired or unpaired,

depending on the continuity of fluvial deposition along a valley (Davis, 1902; Bull, 1991). Fluvial modeling and mapped relationships of terrace deposits suggest that fill terraces are commonly formed in canyons where valley walls are composed of resistant bedrock, while strath terraces are frequently associated with weaker bedrock (e.g., shale) that permits lateral planation and the beveling of wide valley bottoms (Hancock and Anderson, 2002; Wegmann and Pazzaglia, 2002).

Gilbert (1877) first proposed that sediment supply moderates bedrock-incision rates and the formation of terraces through channel armoring effects. This hypothesis remains valid today, though there are many complexities in the manner in which rivers aggrade, incise, and form terraces. Stream power is particularly important to understanding bedrock stream erosion and stream power equations incorporate terms related to sediment supply and transport (Whipple and Tucker, 1999). However, river channels undergoing adjustment to long-term, steady uplift demonstrate a nonlinear relationship between erosion and sediment load, rather than proportionality to stream power (Sklar and Dietrich, 2001). Sediment supply can in turn be controlled by climate, with changes in threshold properties of hillslopes contributing excess sediment to stream systems as suggested by increased paleo-erosion rates during wetter periods due to more frequent deep-seated landslides (e.g., Fuller et al., 2009). Elevated sediment supply in turn armors the channel bed and inhibits vertical incision. The balance between sediment supply and transport capacity is thus key to the formation of terraces.

The aggradational and erosional patterns of rivers change in response to tectonic perturbations. It is widely accepted that rivers increase their incision rates to match increased uplift (Merritts et al., 1994; Riihimaki et al., 2007). For example, high

Holocene incision rates calculated in the Clearwater River of the Olympic Mountains, WA, may result from the river attempting to achieve a graded (equilibrium) concavity as its bedrock channel was uplifted (Wegmann and Pazzaglia, 2002). Molnar and others (1994) likewise documented enhanced fluvial incision driven by active uplift in the Tien Shan, China, during glacial periods that would be expected to favor aggradation. Incision is hindered by climatically-induced sedimentation that armors the channel. Hillslope destabilization and ensuing liberation of sediments transported to and by the fluvial system may also be controlled by climate, possibly tipping the balance between incision and sediment storage. However, there may be intrinsic modifications of sediment storage and supply, particularly in smaller ephemeral systems (Schumm and Hadley, 1957; Patton and Boison, 1986).

It is imperative to judge the applicability of different models of terrace formation as they apply to Colorado River terraces. Although straths are traditionally thought to be beveled at the low point of a bedrock channel, sediment-loading effects suggest that straths may be formed by lateral planation after bed sedimentation and adjustment to a new baselevel (Hancock and Anderson, 2002; Burbank and Anderson, 2011). Alternatively, basin-ward aggradation and incision in river systems draining actively uplifting mountains may be superimposed on steady uplift, initiating upstream migration of knickpoints that incise previously formed straths (Finnegan and Balco, 2013).

The numerical modeling of Hancock and Anderson (2002) of Wind River terraces suggests that strath terraces can result from deposition and lateral planation during the high sediment flux and low transport capacity associated with glacial conditions, which promote effective weathering of material in glaciated headwater catchments. Terraces are

formed when the river abandons planated surfaces as transport capacity (effective discharge) overcomes the lowered sediment loads of the transition to interglacial conditions (Fig. 2.4). This model also implies that, in general, strath terraces are expected to form in broad floodplains while fill terraces form in more restricted reaches where canyon walls consist of lithologies that are less easily eroded. Wegmann and Pazzaglia (2002) suggested an alternative model in which lateral cutting is followed by sedimentation and finally incision, all occurring during deglaciations (cf. Bull, 1991; Pazzaglia and Brandon, 2001).

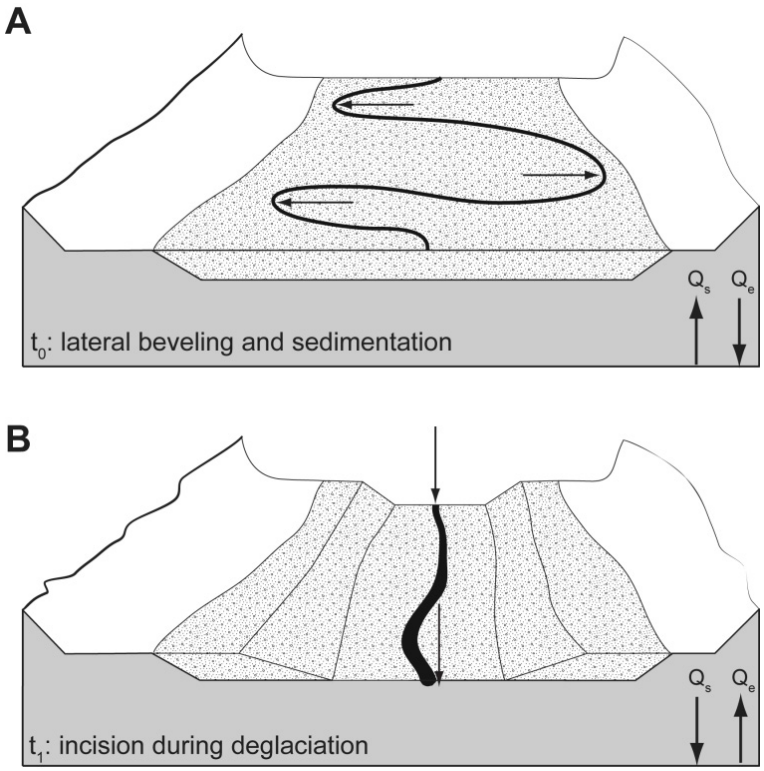

Figure 2.4. Fill-and-bevel model of fluvial terrace formation (modified from Hancock and Anderson, 2002). (A) Conditions of high sediment load (Q_s) and low effective discharge (Q_e), e.g., during glacial maxima. (B) Conditions of low sediment load and high effective discharge, e.g., during deglaciations.

The terraces modeled by Hancock and Anderson (2002) are located much closer to glaciated headwaters (10s of km) than the Colorado River terraces (~400 km) in southeastern Utah, but climate controls may still operate on terrace formation in the study area. Bull (1991) notes that geomorphic responses downstream of glaciated regions depend on the balance between sediment yield and critical stream power, which in turn depend on factors such as the sensitivity of bedrock to different weathering regimes associated with climate change. These factors vary considerably in the extensive Colorado River drainage.

METHODS

Our research design is focused on establishing a chronostratigraphy of terrace deposits using luminescence dating and topographic surveys of terraces in cross-section. We correlate these data in the context of a longitudinal profile through the study area, and consider lithologic clast-count data for the bedload provenance of the Colorado River and its local tributaries through time.

Geochronology

In addition to relative stratigraphic relationships between terraces, this study relies on numeric dating of deposits using optically stimulated luminescence (OSL) on quartz grains and infrared stimulated luminescence (IRSL) on feldspar grains. Luminescence is a burial dating technique that determines the amount of time elapsed since grains were last exposed to light during transport (Huntley et al., 1985), and can be used to determine the burial age of terrace sediments up to ~300 ka in age with errors of approximately 5-

10% (Murray and Olley, 2002). Luminescence was used to date depositional episodes associated with lateral planation of strath terraces or aggradation of fill terraces, with intervening episodes of incision inferred as time gaps between dated deposits.

Sediment samples were collected from four of the five main reaches along the Colorado River, the exception being Dewey Canyon where mainstem alluvial deposits are uncommon. Samples were taken in opaque metal tubes or large plastic film canisters, preventing exposure to light during transport to the laboratory. Sampled sediment consisted of fine to medium-grained sand with primary sedimentary structures and no indication of bioturbation or soil development. All samples were taken at least 1 m below the geomorphic surface to avoid a significant cosmic dose rate and the influence of pedogenesis and bioturbation. Uncertainty in luminescence ages from fluvial deposits may arise from partial bleaching effects, as rivers with large suspended loads may inhibit resetting of the luminescence signal in individual quartz grains. However, these effects are expected to be minor in proportion to the large equivalent dose (D_e, described below) of the older Pleistocene samples examined here (Murray and Olley, 2002; Rittenour, 2008).

Luminescence is induced upon exposure to light or heat, which zeroes or resets the signal (Huntley et al., 1985). The magnitude of the signal is proportional to the time elapsed since grains were deposited and shielded from further exposure to light or heat. The signal is measured in the laboratory when the sample is exposed to blue wavelength stimulation (~340 nm). The optical response is termed the natural dose (N). Samples are then dosed with radiation, with repeated doses producing luminescence responses that bracket N. The hypothetical radiation dose producing the same response as N is the

equivalent dose, D_e, and represents the amount of radiation the sample was exposed to during burial. The procedure described above is known as the single-aliquot regenerative-dose (SAR) protocol, which measures luminescence signals from multiple aliquots of the same sample to generate multiple D_e estimates (Murray and Wintle, 2000). Analyses were performed on grain-size fractions between 75 and 250 μm, and quartz grains were separated from heavier minerals using sodium polytungstate (Na-polytungstate) of density 2.7 g/cm^3. Separated quartz was then etched and purified using hydrofluoric acid. An ideal age obtained for a sample is derived from measurements of ≥20 acceptable aliquots based on criteria related to optical properties. Each aliquot is 1 mm in diameter and contains ~20 grains of sand. All samples were processed and analyzed at the Utah State University Luminescence Laboratory, where the luminescence signal of each sample was measured on Risø TL/OSL-DA-20 readers equipped with photomultipliers and irradiators.

IRSL was used to test the accuracy of quartz OSL for select samples. The SAR protocol was applied to IRSL samples in the same way as quartz samples, with regenerative radiation doses compared to the natural luminescence response in order to determine D_e (Wallinga et al., 2000). Samples processed for IRSL were selected based on their response to feldspar IR checks performed at the end of quartz OSL runs, with exceptionally high peak to background ratios of luminescence responses indicating samples with high feldspar content. Feldspars were separated from other minerals using Na-polytungstate of density 2.58 g/cm^3. Risø reader diodes were set to emit only infrared wavelength stimulation (800-900 nm) for IRSL analyses.

To calculate ages from measured D_e, environmental dose rates were determined from sediment surrounding the sample. The luminescence signal accrues due to this dosing by natural radiation from the decay of U, Th, Rb, and K, as well as from cosmic radiation. Dose rate samples were collected within a 30 cm radius of the luminescence sample. These samples were split in the laboratory to approximately 100 g subsamples. Subsamples were sent to ALS Geochemistry, Elko, NV, where elemental analysis was performed through inductively coupled plasma mass spectrometry (ICP-MS) and atomic emission spectroscopy (ICP-AES). Dose rate conversions for U, Th, Rb, K, and H_2O attenuation follow Guérin et al. (2011). Total 2σ errors on luminescence ages include random and systematic errors from equivalent dose scatter (overdispersion), uncertainties in the calculation of environment dose rates, and instrumental error.

Once elemental concentrations of dose rate subsamples were determined, ages were calculated using the central age model (CAM) of Galbraith et al. (1999). The age of an OSL sample is the equivalent dose divided by the dose rate. With only 2 samples having generated $\geq$20 satisfactory aliquots, all ages are reported as preliminary in our results.

Survey data

High-resolution topographic data were obtained for the elevations and locations of terrace deposits in the study area using a real-time kinematic (RTK) TopCon HiPer GA GPS. A stationary base receiver was set at a static point (without established ground control), and measurements of terrace straths, risers, treads, piedmont surfaces, and bedrock were collected using a mobile rover receiver. All spatial data were post-

processed using the Online Positioning User Service (OPUS), which compares and corrects observations according to the National Geodetic Survey Continuously Operating Reference Station (NGS-CORS) network. Post-processing improved spatial errors to ≤3 cm vertically and ≤1.5 cm laterally.

Spatial analyses

Spatial analyses were performed in ArcGIS (ESRI, 2011). These included measurements of channel and valley-bottom width, and calculated gradient and stream power through the five study reaches. Spatial results were plotted along a longitudinal profile constructed from USGS and Bureau of Reclamation survey data (USGS, 1948).

Channel and valley-bottom width were measured at 100 m intervals throughout the study reaches. Widths were taken from the modern channel based on USGS 7.5' topographic quads, and elevations 5 and 50 m above the modern channel based on contours constructed from a 10 m digital elevation model (DEM). These heights represent the level above Holocene valley-bottom surfaces and underlying alluvial deposits observed across the Colorado Plateau (e.g., Hereford et al., 1996; Pederson et al., 2006), and an older Pleistocene valley-bottom surface, respectively. All width calculations were averaged by study reach. Gradient was also calculated at 100 m intervals and averaged across each of the study reaches. Finally, these measurements were used to determine unit stream power of the Colorado River, which is calculated as follows:

$$\Omega_u = \frac{\gamma Q S}{w}, \quad (1)$$

where Ω_u is unit stream power (W/m), γ is the specific weight of water (kN/m^3), Q is discharge (m^3/s), S is gradient, and w is channel or valley-bottom width (m). Bankfull discharge of the 2.5-year flood ($Q_{2.5}$) was calculated from annual stream gage data at USGS gage station 09180500. This value is widely considered an approximation of the effective channel-forming flow (e.g., Leopold and Maddock, 1953). A specific weight of water of 9.8 kN/m^3 was used.

Bedload provenance

The lithology of terrace gravels is indicative of upstream geology, and may be used to delineate bedload provenance and sediment contributions from the trunk river versus tributary streams. The lithology and median diameter of modern gravels and late Pleistocene terrace gravels in the study area were documented through lithologic clast counts in an attempt to resolve distal versus local sources. Modern patterns of lithology/provenance were documented through counts of 100 clasts at the Colorado River above and below its confluence with the Dolores, the Colorado River in Cache Valley graben, the Dolores River ~2 km upstream of its confluence with the Colorado, and the channels of Onion, Professor, and Castle creeks within 1.5 km of their confluences with the Colorado. Terrace gravel provenance patterns through time were recorded from all mainstem terraces throughout the field area. Where possible, clasts were collected at 0.5 m intervals over lateral transects of 30 and 20 m; otherwise, clasts were collected by random selection from characteristic transects of each deposit (Wolman, 1954).

RESULTS

Chronostratigraphy

Preliminary luminescence age control for the study terraces is shown in Table 2.1, with additional information for OSL and dose rate analysis results found in Appendix A. Fifteen OSL samples were analyzed from thirteen terrace deposits between Dewey Bridge and Castle Creek. Age results range from 84 ± 31 ka to 27 ± 6 ka (MIS 5-2). Notably, average dose rates are high (2.6-3.4 Gy/ka), with an outlier of 7.9 Gy/ka for a sample from the uppermost M3 deposit near Onion Creek. High equivalent doses result in luminescence curves that are approaching saturation and effectively limit OSL dating to <150 ka (e.g., DeVecchio et al., 2012). One sample was processed for IRSL and two samples required subtraction of the early background luminescence signal.

The spatial form of terrace deposits changes greatly throughout the study area, both in terms of thickness and relative heights of basal straths above the modern river. These changes and the chronostratigraphy of the study reaches are described below.

Dewey Bridge reach

Four mainstem Colorado River terraces (M7, M4, M3, and M2) were surveyed at Dewey Bridge (Fig. 2.5). The M4, M3, and M2 terraces are best preserved in this reach, whereas the M7 is a single isolated remnant (Fig. 2.5A). All surveyed terraces are found on river right (when travelling downstream), on the north side of the river (Fig. 2.5B). Only higher terraces and minor M2 deposits are found on river left. Dewey Bridge terraces are strath terraces (<8-10 m in total thickness) with ≤7.2 m of sediment thickness (Table 2.2). Higher terraces were mapped at Dewey Bridge by Doelling (1996), but were

TABLE 2.1 SUMMARY OF PRELIMINARY OSL AGE CONTROL FOR COLORADO RIVER TERRACE DEPOSITS

Deposit[a]	Sample[b]	USU Sample #	Depth (m)	# Aliquots	Dose Rate, Gy/ka	Equivalent Dose (D_e), Gy (overdispersion, %)	OSL Age, ka[c]
M2	AJ-DB-T2A	USU-1075	1.7	13 (29)	3.42 ± 0.18	98.63 ± 15.54 (22.5)	29 ± 5
M2	AJ-HB-M2	USU-1195	2.8	16 (19)	3.56 ± 0.20	121.82 ± 15.83 (23.4)	34 ± 6
M2	AJ-CVG-T2Au	USU-1073	2.5	23 (30)	2.81 ± 0.15	75.04 ± 13.73 (39.7)	27 ± 6
M3	AJ-DB-T3	USU-1078	1.8	12 (31)	3.54 ± 0.19	124.85 ± 13.08 (0.0)	35 ± 5[d]
M3	AJ-HB-M3	USU-1196	1.5	5 (5)	5.07 ± 0.29[e]	197.55 ± 20.33 (5.5)	39 ± 5[e]
M3	AJ-PV-T3usAu	USU-1072	3.0	17 (30)	3.12 ± 0.14[f]	137.10 ± 24.00 (33.5)	~44[f]
M3	AJ-PV-T3uAu	USU-1076	3.0	20 (28)	3.21 ± 0.17	170.34 ± 26.76 (32.5)	53 ± 10
M3	AJ-PV-T3lAu	USU-1077	8.0	4 (5)	2.62 ± 0.64	114.70 ± 18.66 (8.8)	37 ± 6
M3	AJ-IG-T3g	USU-1074	1.5	19 (25)	3.25 ± 0.17	133.92 ± 20.87 (31.0)	41 ± 8
M4	AJ-DB-M4	USU-1336	1.5	18 (31)	3.12 ± 0.16	164.44 ± 32.98 (40.0)	53 ± 12
M4	AJ-CVG-M3o	USU-1200	9.4	12 (28)	3.15 ± 0.17	218.59 ± 48.76 (34.1)	69 ± 17
M4	AJ-IG-M3	USU-1280	8.0	18 (35)	3.40 ± 0.19	197.86 ± 21.90 (20.3)	58 ± 9
M5	AJ-PV-M4B	USU-1198	2.0	16 (26)	2.88 ± 0.15	142.16 ± 28.38 (35.6)	52 ± 12[d]
M6	AJ-IG-M5	USU-1279	1.5	19 (33)	2.64 ± 0.14	196.80 ± 43.43 (45.4)	75 ± 18
M7	AJ-PV-M4	USU-1197	2.3	10 (15)	2.71 ± 0.14	222.46 ± 78.02 (49.7)	84 ± 31

[a] Organized by stratigraphic position; "M" is mainstem Colorado River deposit.

[b] DB = Dewey Bridge, HB = Hittle Bottom, PV = Professor Valley, CVG = Cache Valley graben, IG = Ida Gulch.

[c] Reported ages with 2σ error.

[d] Sample corrected for falling $D_e(t)$ using early background subtraction.

[e] Age calculated from infrared luminescence performed on feldspar grains.

[f] Mean dose rate of other samples used due to erroneously high chemistry results (see text); age is only an estimate.

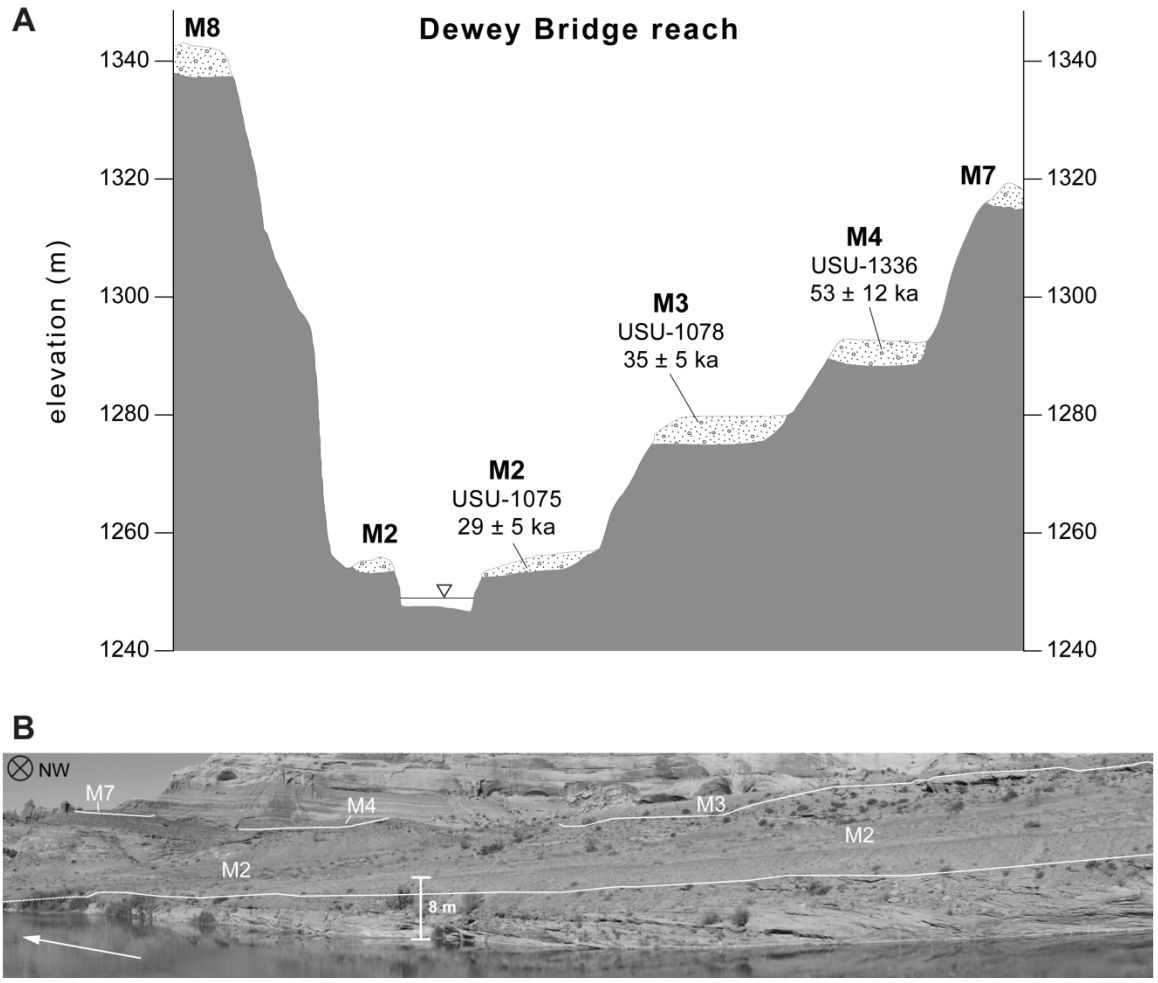

Figure 2.5. Dewey Bridge reach cross-section and annotated photograph. (A) Schematic cross-section of Dewey Bridge terrace stratigraphy and local OSL age constraints. Dewey Bridge strath terraces are thin (≤7.2 m) and have low-relief strath surfaces. (B) Photograph looking downstream. The Dewey Bridge reach is moderately restricted by canyon walls of Jurassic strata, such as the Entrada Sandstone pictured in the background. White arrow indicates direction of flow.

TABLE 2.2 STRATH ELEVATIONS AND TERRACE THICKNESSES

	Dewey Bridge reach			Professor Valley reach			Cache Valley graben reach			Ida Gulch/Castle Valley reach		
Deposit	Min ht. (m)[a]	Max ht. (m)[b]	Max thickness (m)[c]	Min ht. (m)	Max ht. (m)	Max thickness (m)	Min ht. (m)	Max ht. (m)	Max thickness (m)	Min ht. (m)	Max ht. (m)	Max thickness (m)
M2	5.2	6.5	5.9	NA[d]	NA[d]	NA[d]	NA[d]	NA[d]	NA[d]	NA[d]	NA[d]	NA[d]
M3	26.2	28.6	7.2	3.0	NA[e]	19.8	11.0	23.0	21.8	6.0	7.8	20.4
M4	41.0	43.3	5.3	38.7	40.1	6.1	24.3	27.7	17.0	27.3	36.2	10.1
M5				44.4	48.5	6.2				37.7	42.3	9.0
M6				44.7	48.3	9.0	52.5	55.1	9.0	59.4	63.8	13.1
M7	66.7	68.6	5.2	59.0	69.5	13.1						

Note: All spatial and form measurements taken from RTK GPS surveys. Horizontal precision ± 1.5 cm, vertical precision ± 3 cm.

[a] Minimum height of strath above the modern channel.

[b] Maximum height of strath above the modern channel.

[c] Maximum alluvial thickness, measured as difference between minimum strath and maximum tread elevations.

[d] Strath below grade.

[e] Only one strath elevation surveyed.

not included in this study due to our focus on the best preserved, datable late Pleistocene stratigraphy. The Holocene M1 deposit is largely absent in this reach.

Dewey Bridge terraces are underlain by 3-7 m of tabular to broadly lenticular, clast-supported, imbricated, moderately sorted, sub-rounded to well-rounded, pebble-cobble gravel with thin to medium-scale (3-10 cm) cross-beds. Matrix material is poorly sorted, sub-angular to sub-rounded, fine to very coarse sand. Interbedded with these gravel beds are occasional 7-15 cm thick, ripple laminated, normally graded, moderately-well sorted lenses of fine to medium sand. Additionally, the M2 terrace has a ~2 m cap of normally graded, moderately-well sorted, medium-grained fluvial sand variably preserved atop gravels. This sandy cap has been deflated from higher terraces, decreasing their total height and thickness. Soils are variably preserved on terrace benches in this reach. Where they exist, they are primarily thin (<30 cm) entisols with abundant eolian material.

The unsurveyed M8 deposit at Dewey Bridge has been mapped at ~82 m above grade (Fig. 2.5A; Doelling, 1996). The strath of the M7 deposit in this reach lies 67-69 m above river level (Table 2.2). These highest deposits are not constrained by OSL dating due to the paucity of sand lenses within these isolated gravels. Ages were obtained for the more extensive M4, M3, and M2 deposits (Table 2.1), and were determined from sampled sand lenses at least 2 m below the top of each landform. The M4 strath is 41-43 m above grade and its deposits have been dated to 53 ± 12 ka (USU-1336). The M3 strath is 26-29 m above grade and its associated deposit has been dated to 35 ± 5 ka (USU-1078). An OSL age of 29 ± 5 ka (USU-1075) was obtained for sediment of the M2 terrace, which lies 5-6.5 m above grade.

Professor Valley reach

The long Professor Valley reach (~8 km; Fig. 2.2) includes a diverse suite of terrace deposits that are typically thicker than their counterparts upstream at Dewey Bridge (Table 2.2). Six mainstem late Pleistocene Colorado River terraces (M7-M2) and two tributary piedmont deposits (P3, P2) were recorded in this reach (Fig. 2.6A), which includes the M3 and M2 at Hittle Bottom. High terrace remnants in Professor Valley are straths with thicker (typically ≤9 m) deposits, whereas the lower M3 and M2 are notably thicker (≤20 m), sandier fill packages. The M7-M5 are preserved as high isolated deposits (Fig. 2.6B), whereas the M4-M2 deposits are more common. The ubiquitous P3 and P2 deposits in this reach commonly grade downslope to the M3 and M2 terraces, respectively. The M7 and M4-M2 terraces are found on either side of the river, but the M6 and M5 deposits are found only on river right above the confluence of Professor Creek. Silty sand packages of the Holocene M1 terrace are also found in this reach, but were not a focus of our efforts.

The Professor Valley M7-M4 deposits are underlain by 3-9 m of tabular to broadly lenticular, thin to thick-bedded (3-100 cm), clast-supported, imbricated, moderately sorted, well rounded, pebble-cobble gravel. Matrix material consists of poorly sorted, sub-angular to sub-rounded, fine to very coarse sand. Interbedded lenses are more common in these deposits than at Dewey Bridge, and are typically ≤20 cm of moderately sorted, sub-angular to rounded, fine to coarse sand.

The M3 deposit dominates the Professor Valley reach. At Hittle Bottom (Fig. 2.1, 2.2), it is a tabular to lenticular, clast to matrix-supported, imbricated, poorly to moderately sorted, well rounded, pebble-cobble gravel with thin (1-3 cm) cross-beds. Its

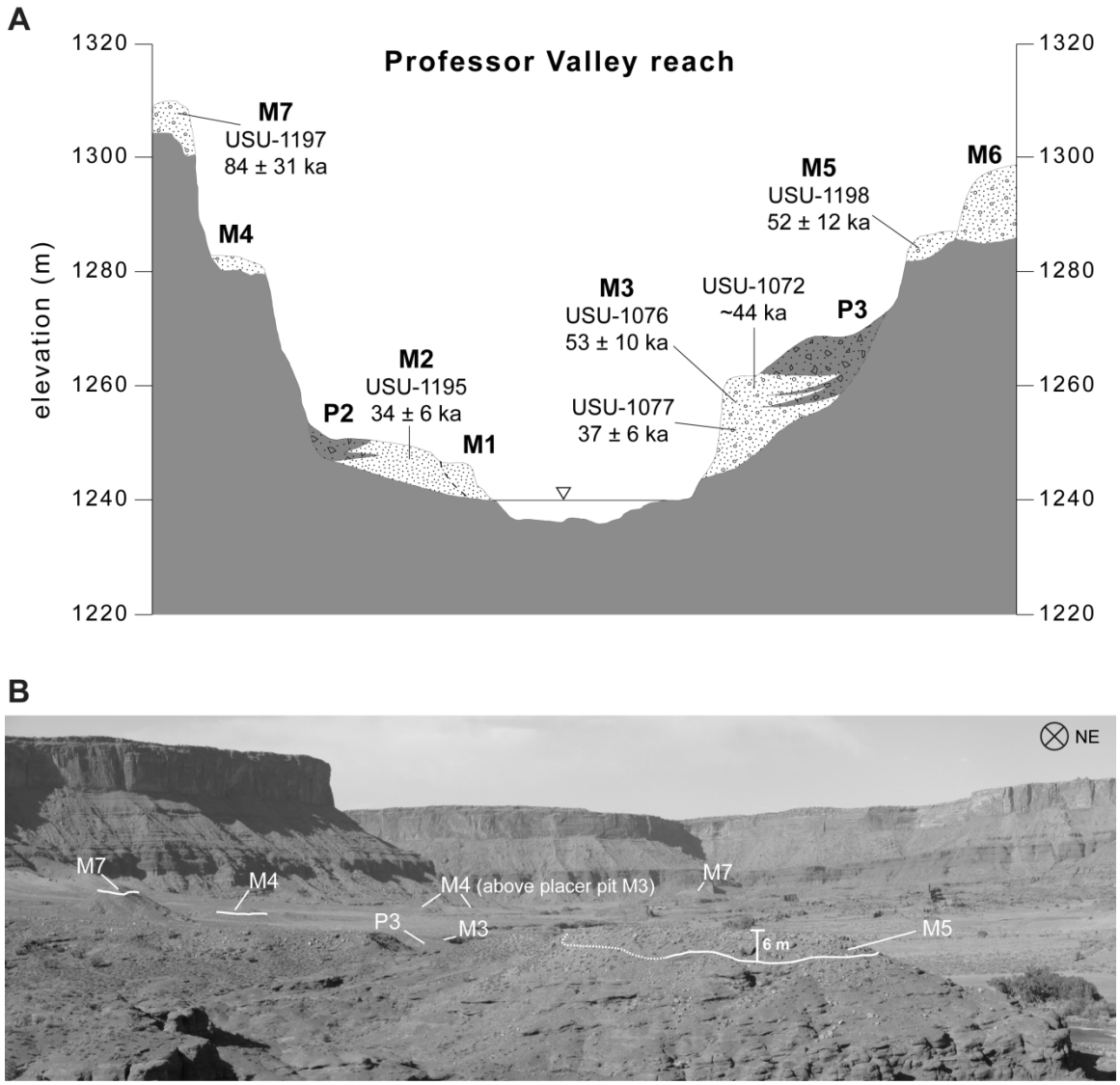

Figure 2.6. Professor Valley reach cross-section and annotated photograph. (A) Schematic cross-section of Professor Valley reach terrace stratigraphy and local OSL age constraints. Terrace deposits here thicken considerably from those at Dewey Bridge, and commonly interfinger with piedmont gravels. (B) Photograph looking upstream from M6 terrace ~2 km below confluence of Onion Creek, illustrating examples of terraces preserved in this wide reach and their position in the landscape.

matrix consists of moderately sorted, silt to fine sand. This deposit has ~0.75 m thick capping lenses of silt to fine sand similar in texture and composition to the matrix, and with low angle cross-bedding and massive or weakly ripple-laminated sand. The M3 gravel commonly interfingers with or underlies local prograding piedmont gravel in this reach.

Two km downstream of Hittle Bottom on river right, an abandoned placer mining pit provides the best exposure of the M3 in the study area (Fig. 2.2). Here, the deposit is more than 13 m of medium to thick (10-100 cm) interbedded gravel with finer-grained overbank sediments (Fig. 2.7). This thick deposit includes four packages displaying overall reverse grading, as well as a lower gravel mostly obscured by colluvial cover. Where exposed, the lower unit is a tabular, clast to matrix-supported, imbricated, poorly sorted, sub-rounded to well rounded, pebble-cobble gravel. The lowest well-exposed package is a 0-4.4 m deposit consisting of thin to medium-bedded (3-10 cm), massive to cross-bedded, moderately-well sorted, silt to fine sand (unit I, Fig. 2.7). This deposit includes a lower 1.5 cm lens of variably oxidized or reduced, carbonate-cemented, silt to very fine sand. Unit II is a 0-4.8 m, moderately to very well sorted, silt to medium sand with medium to thick (10-100 cm) cross-bed sets or massive sands and a 0.4 m mud interbed. Unit III is a 1.9-4.5 m clast to matrix-supported, imbricated, moderately sorted, sub-rounded to well rounded, pebble-cobble gravel with thick (≤100 cm) tabular cross-bed sets. Its matrix material consists of poorly sorted, silt to medium sand. Unit III includes a 0.5 m bioturbated, well sorted lens of very fine to fine sand. Unit IV is a 1.6 m moderately-well sorted, sub-angular to sub-rounded, pebble-cobble gravel with thick (≤100 cm) beds and numerous clasts of local origin indicating intermixing of local

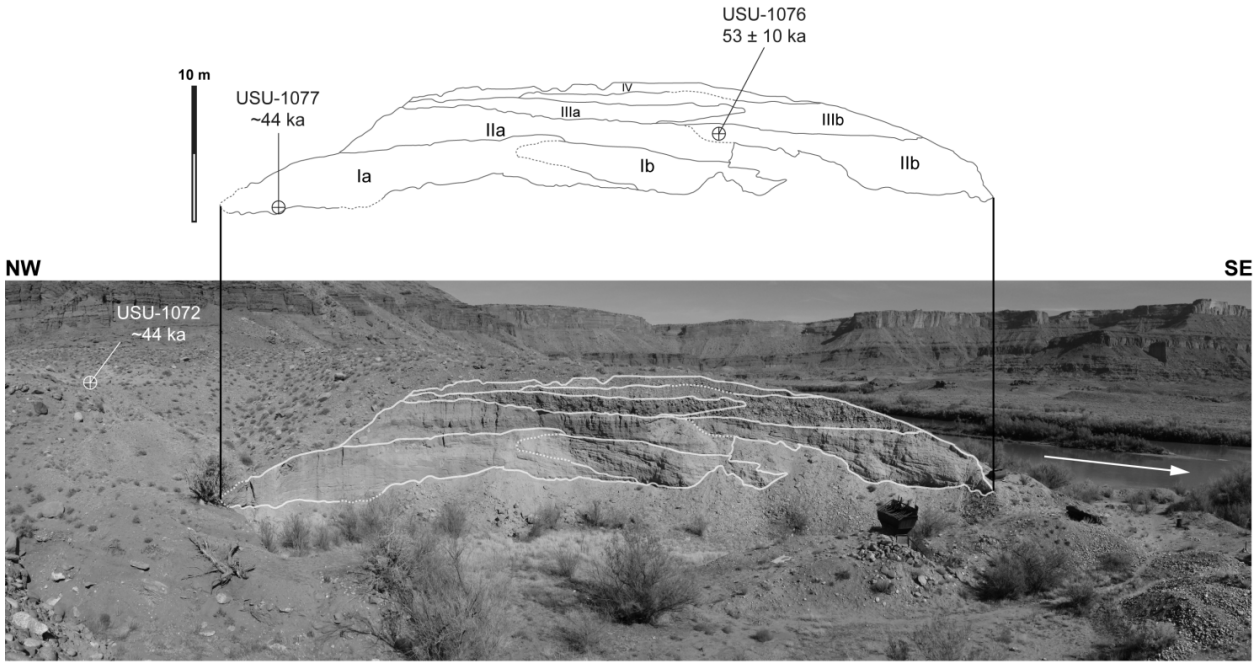

Unit descriptions:

IV: (1.6 m) Thick-bedded, moderately-well sorted, sub-angular to sub-rounded, pebble-to-cobble gravel interfingering with local piedmont

IIIb: (0-4.5 m) Thick-bedded, moderately sorted, sub-angular to well rounded, imbricated pebble-to-cobble gravel; matrix of silt to medium sand; includes 0.5 m lens of well sorted, very fine to fine sand with bioturbation

IIIa: (1.9 m) Thick-bedded, moderately sorted, sub-angular to sub-rounded, mostly cobble gravel; matrix of silt to fine sand

IIb: (0-4.8 m) Medium-bedded, very well sorted, silt to fine sand, locally cross-bedded with overbank topples

IIa: (0-4 m) Medium to thick-bedded, moderately-well sorted, fine to medium, massive sand with well cemented 0.4 m massive mud interbed

Ib: (2.9 m) Medium-bedded, moderately-well sorted, silt to fine sand with planar cross-bedding

Ia: (0-4.4 m) Thin-bedded, moderately-well sorted, silt to very fine sand with climbing ripples and local redox features

Figure 2.7. Photograph with annotated stratigraphy of >10 m thick placer pit M3 deposit. Basal bedload gravel is covered by colluvium and is exposed in northeast-facing outcrop (not shown). Units I and II are interpreted as mainstem channel-margin sandbar deposits with minor interfingering of piedmont deposits observed in Unit II. Unit III is interpreted as gravel bar/bedload deposits. Unit IV is interpreted as a piedmont debris flow deposit. White arrow indicates direction of flow.

piedmont gravels. Its matrix was not described in the field but is likely similar in texture and composition to the matrix of unit III, but with abundant local material and perhaps greater proportions of clay. The placer pit M3 is partially capped by ~2 m of mainstem fluvial sand mixed with eolian deposits of silt to very fine sand. In overview, this deposit is interpreted as mainstem channel margin sandbar/floodplain sediment (units I and II), coarsening upward during aggradation to gravel bar/bedload gravels (unit III), and piedmont debris-flow gravels (unit IV) capped by mixed mainstem overbank and alluvial-eolian deposits. Thus, the M3 here records most of a depositional cycle, as opposed to the latter stages of aggradation observed in other study area deposits.

The M3 deposit ~3 km downstream near the confluence of Onion Creek (Fig. 2.1, 2.2) is 19.8 m thick and displays similar stratigraphy to the placer pit deposit. Local P3 gravels prograde from at least 1 km upslope to over the top of the M3 along the Colorado River.

The well-preserved M2 deposit at Hittle Bottom (Fig. 2.1, 2.2) is underlain by 5.1 m of thick to very thick-bedded (0.3->1 m), clast to matrix-supported, imbricated, poorly to moderately sorted, sub-angular to well rounded, pebble-cobble gravel. Its matrix is poorly sorted, silt to medium sand. The Hittle Bottom M2 interfingers with a 1 m lens of ripple-laminated, moderately sorted, silt to fine sand. Downstream at the Onion Creek confluence, the M2 deposit prominently interfingers with piedmont deposits exposed in cut banks of Onion Creek. The exposed portion of the mainstem deposit consists of ~2 m of broadly lenticular, medium to thick (10-100 cm) bedded, mostly massive, well sorted, silty clay to fine sand. Climbing ripples, cross-stratified ripples, and reverse grading may be observed in places. This package is interpreted as a flood/overbank deposit, and

interfingers with broadly lenticular, poorly sorted, sub-angular to sub-rounded piedmont gravel with medium to thick bedding.

Piedmont deposits in the Professor Valley reach are commonly <2 m, broadly lenticular, clast-supported, ripple laminated to massive, reverse graded, poorly sorted, sub-angular to sub-rounded, granule-boulder gravels with medium to thick (10-100 cm) bedding. Matrix material is typically poorly sorted, clay to medium sand. The chaotic orientation of piedmont clasts implies transport via debris flows.

The Professor Valley M7 strath is found 59-69.5 m above river level (Table 2.2). Figure 2.6A shows the Professor Valley terrace suite in schematic cross-section, including the strath geometry of the higher M7 deposit. This deposit has been dated to 84 ± 31 ka (Table 2.1). The M6 and M5 upstream of the Professor Creek confluence lie 44-48.5 m above grade. Their similar landscape position (Fig. 2.6A) implies that they may constitute the same deposit. A stratigraphically improbable luminescence age of 52 ± 12 ka (USU-1198) was obtained near the top of the M5 terrace (Table 2.1); this result could be erroneous due to the incorporation of younger sediment during sampling. The Professor Valley M4 is undated with a strath 39-40 m above grade. M3 straths in this reach range from 3 m above river level to below grade, as the M3 begins to converge with the modern profile. A luminescence sample taken 1.5 m below the tread of the M3 at Hittle Bottom returns an age of 39 ± 5 ka (USU-1196) based on only five accepted aliquots. The placer pit M3 includes a stratigraphically impossible OSL age of 37 ± 6 ka (USU-1077) from basal unit I (Fig. 2.7). This sample has only 4 accepted aliquots (Table 2.1) and its age may increase with further analysis. However, greenish coloration around this sample indicates that reduction has occurred in the surrounding sediment due to the

presence of groundwater over at least a portion of its burial history. Thus, its actual age may be closer to ~44 ka if a saturated water content of 20% is assumed. Another OSL age of 53 ± 10 ka (USU-1076) was determined from a sample taken from 3 m below the top of the exposure (a sand lens in unit II). A silt-rich lens near piedmont deposits capping the M3 returns an age of 18 ± 4 ka, with an anomalously high dose rate of 7.93 ± 0.41 Gy/ka. This sample has an equivalent dose of 137.10 ± 24.00 Gy (Table 2.1), similar to nearby samples, but its high dose rate results in a greatly underestimated age. If the mean dose rate of all other samples in this study (3.1 Gy/ka) is assumed for this sample, the deposit yields an age of ~44 ka (USU-1072). This is similar, within error, to the date from unit II. Finally, the M2 deposit at Hittle Bottom yields a luminescence age of 34 ± 6 ka (USU-1195). The strath of this deposit is 5.5 m above the river at Hittle Bottom, but lowers downstream and is below grade throughout the rest of the Professor Valley reach.

Cache Valley graben reach

The Cache Valley graben reach is short (<2.5 km) and is characterized by salt-tectonic structures intersecting the Colorado River (Doelling et al., 1988; Trudgill, 2011). Four deposits are preserved in this reach (M6, M4, M3, M2), all of which were surveyed (Fig. 2.8A). These deposits remain thick through the graben (Table 2.2). The M6 exists here as an isolated remnant on river left. The M4 and M3 are prevalent within the graben itself on river right (Fig. 2.2, 2.8B). The M3 is preserved to a greater extent on both sides of the river, and the M2 is also common throughout the reach. The M1 deposit is found

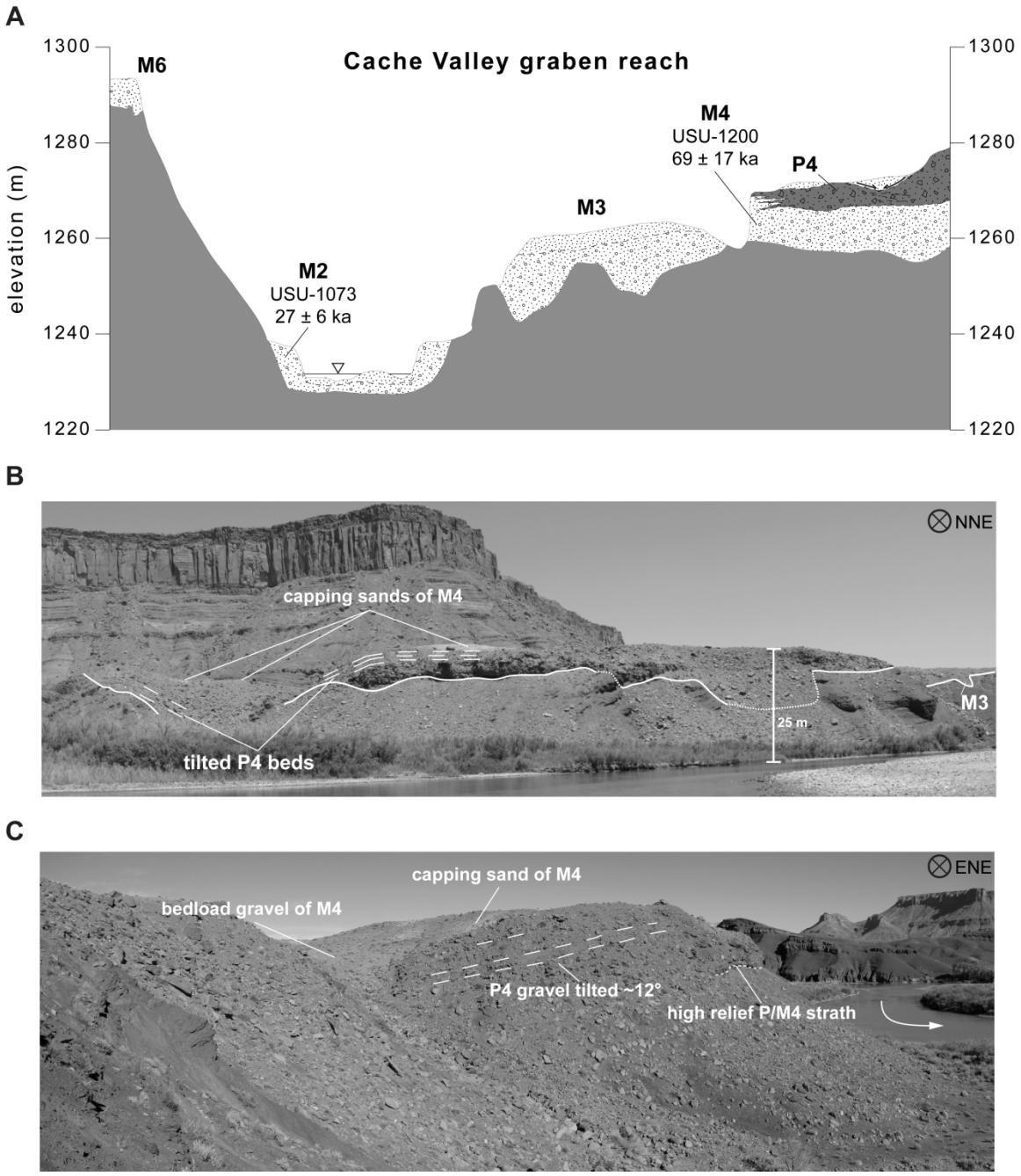

Figure 2.8. Cache Valley graben reach cross-section and annotated photographs. (A) Schematic cross-section of Cache Valley graben terrace stratigraphy and local OSL age constraints. M4 and M3 deposits have highly irregular strath surfaces, and the M2 dips below grade. Warping of the M4 and associated P4 deposits is shown. (B) Photograph looking upstream from river level, illustrating irregular strath surfaces of the M4 and M3 terraces and collapsed P4 gravels. (C) Photograph looking upstream from level of M4 bedload gravels, showing warping of piedmont gravels in relation to M4 deposits. White arrow indicates direction of flow.

throughout this reach, with or without capping silty sand. Piedmont deposits are also common within the graben.

The tread of the M6 on the upstream flank of the graben was thought to be tilted several degrees upstream (Colman, 1983), but its strath is relatively uniform and does not vary more than ~2.5 m in relief. This terrace is underlain by 6.5-9 m of tabular to broadly lenticular, medium to thick-bedded (30-100 cm), clast-supported, imbricated, moderately sorted, sub-rounded to well rounded, pebble-cobble gravel. Its matrix is poorly sorted, sub-angular to sub-rounded, fine to very coarse sand.

The M4 deposit in the upstream portion of the graben is a 12-17 m thick, tabular, thick-bedded (30-100 cm), moderately sorted, sub-rounded to well rounded, pebble-cobble gravel. This gravel is capped by well sorted, silt to fine sand that is variably preserved atop basal gravel and best exposed in the cut banks of ephemeral washes draining the center of the graben. Ribbons of tributary piedmont material within this deposit are locally sourced, poorly sorted, sub-rounded to sub-angular, very fine to coarse sand with few granules. Importantly, very coarse piedmont gravels are locally deformed in the M4 deposit on river right, with imbricated bedding dips of ~11-13° (Fig. 2.8C). The area of localized collapse indicated by tilted gravels and irregular straths is no more than ~3,000 m^2. We did not observe other locally collapsed areas in the field.

The M3 in the graben reach is 12.5-22 m thick and similar in geometry and texture to the M4. Its capping sands are better preserved than those of the M4 and consist of 8-9 m thick, broadly lenticular, well sorted, silt to very fine sand with climbing ripples. In places, mainstem fluvial sand caps interfinger with ≤1.5 m, poorly sorted, sub-angular to sub-rounded, very fine to coarse piedmont sand. P3 deposits are less common than

those grading to the M4, even though the M3 is more preserved over a greater area in this reach.

Bedload gravels of the M2 terrace in the Cache Valley graben reach drop below grade, but are capped by up to 2.3 m of laterally discontinuous, thinly laminated to massive, moderately sorted, silt to medium sand.

The M6 strath is 52.5-55 m above grade (Table 2.2), and has no age constraint in this reach. The M4 strath is 24-28 m above grade, and sand from the upper M4 deposit returns an OSL age of 69 ± 17 ka (USU-1200; Table 2.1). The strath of the M3 varies from 11-23 m above river level; its age is not constrained in this reach. The base of the M2 remains below grade in this reach, but a luminescence age of 27 ± 6 ka (USU-1073) was determined from a sample taken from its capping sand in the upstream segment of the graben.

Ida Gulch/Castle Valley reach

Four terrace deposits (M6-M3) were surveyed in the Ida Gulch/Castle Valley reach (Fig. 2.9A). The M6-M4 deposits thin from the Cache Valley graben reach above, but the M3 deposit thickens slightly and is lower in the landscape (Table 2.2). The M6 and M5 are found only on river left as small, isolated remnants. Deposits of the M4 and M3 are widely preserved in this reach, the M3 on both sides of the river (Fig. 2.9B). The M2 and Holocene M1 deposits are uncommon in this reach.

The M6-M4 deposits in Ida Gulch (Fig. 2.1, 2.2) display similar stratigraphy to one another. The M4 deposit is more extensive than the isolated erosional remnants of the M6 and M5. The M6 is a 5-13 m thick, tabular to lenticular, clast-supported, imbricated,

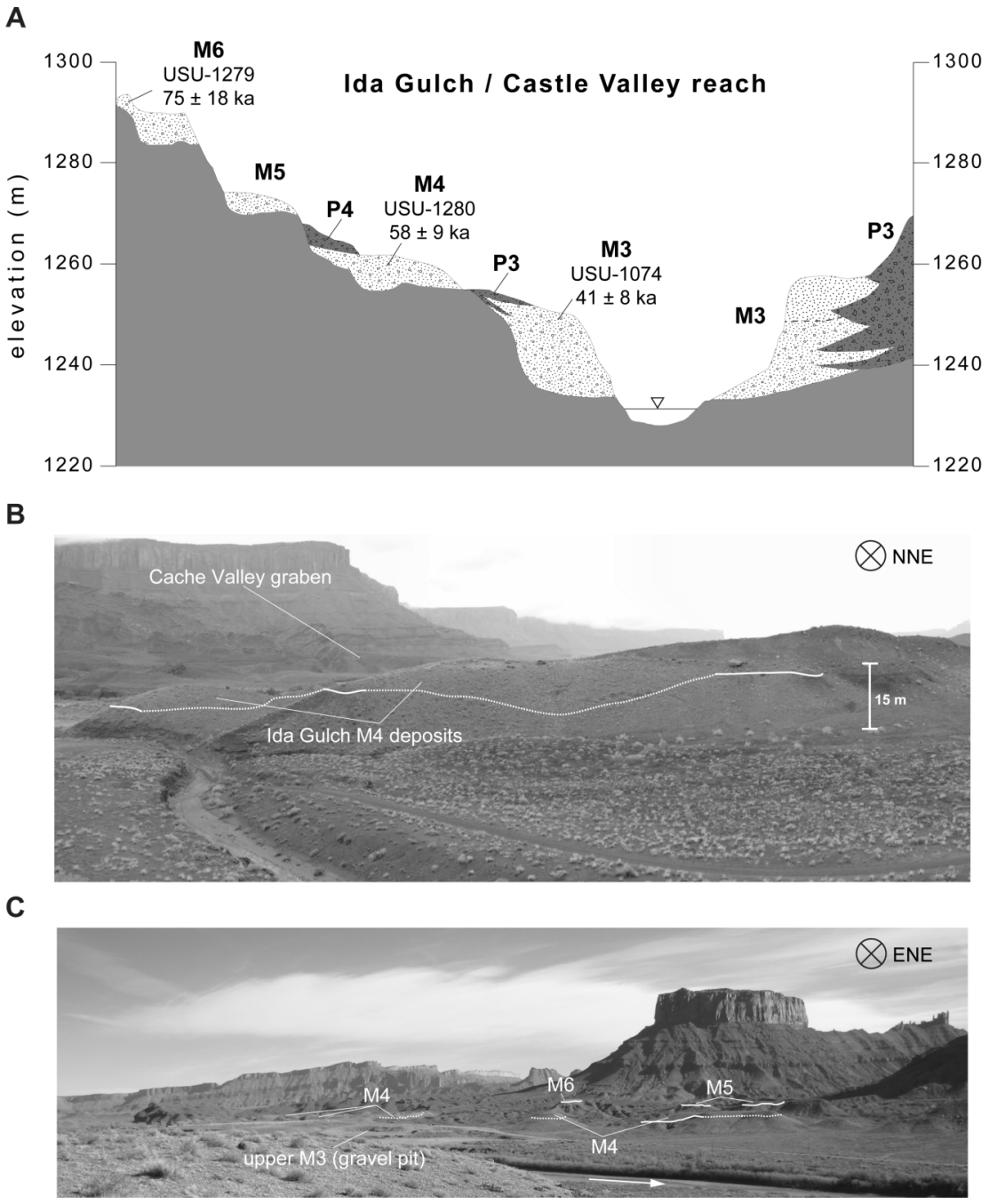

Figure 2.9. Ida Gulch/Castle Valley reach cross-section and annotated photographs (A) Schematic cross-section of Ida Gulch/Castle Valley terrace stratigraphy and local OSL age constraints. The M3 deposit remains thick, and the strath surfaces of the M6 and M4 are irregular. Piedmont gravels remain common in the landscape. (B) Photograph looking upstream from P4 deposit, showing irregular strath of M4. (C) Photograph looking upstream showing Ida Gulch terrace suite. The M4 and M3 deposits are more extensive than isolated M6 and M5 remnants. White arrow indicates direction of flow.

moderately sorted, sub-rounded to rounded, pebble-cobble channel fill gravel. The matrix of the M6 is poorly sorted, sub-angular to sub-rounded, silt to coarse sand. The M6 gravel includes <30 cm lenses of medium (10-30 cm) bedded, ripple laminated sand similar in texture to the matrix. The M6 deposit is capped in places by modest gypsic soil development (<15 cm). The M4 has a >5 m thick cap of silt to fine sand with ripple cross-beds. P4 gravel has prograded over the capping M4 sand in many places.

The M3 deposit at Ida Gulch is exposed in a Utah Highway Department gravel pit adjacent to the Colorado River. It is a 20.4 m thick, tabular, thin to thick-bedded (3-100 cm), clast to matrix-supported, normally graded, moderately sorted, sub-angular to rounded, pebble-cobble gravel. Its matrix is composed of moderately sorted, sub-rounded to rounded, medium to coarse sand. Capping sands of the Ida Gulch M3 deposit are laterally discontinuous and may interfinger with graded piedmont deposits of similar texture and composition to those in the Professor Valley reach. Four km downstream, the M3 deposit is found near the confluence of Castle Creek (Fig. 2.1, 2.2) on river left at the western flank of the Castle Creek debris fan. The M3 changes in texture and composition from its correlative deposit at Ida Gulch. Here, it is consists of thick-bedded (30-100 cm), ripple laminated to massive, very well sorted, silt to fine sand that commonly interfingers with piedmont gravels of Castle Creek. This sediment represents overbank/flood deposits overlying mostly obscured basal gravels of the mainstem Colorado, as evident from relations observed in remnants of the M3 on river right.

The terrace suite of the Ida Gulch/Castle Valley reach is shown in schematic cross-section in Fig. 2.9A. The strath of the M6 is found 59-64 m above grade (Table 2.2). The capping sand of this deposit has been dated to 75 ± 18 ka (USU-1279; Table

2.1). The M5 strath lies 38-42 m above river level; the M5 deposit has an unconstrained age. The M4 strath lies 27-36 m above river level, and yields an OSL age of 58 ± 9 ka (USU-1280). The M3 strath is found 6-8 m above grade. A sand lens in the upper 1.5 m of the M3 deposit at Ida Gulch has an OSL age of 41 ± 8 ka (USU-1074).

Regional correlations

The extent to which fluvial activity of the Colorado River correlates to regional paleoclimate records can be assessed based on preliminary OSL age results. Periods of terrace sedimentation are highly variable in relation to late Pleistocene glacial advances (Fig. 2.10). Some terraces formed during major glacial advances (M4 and M2 during MIS 4/early MIS 3 and latest MIS 3, respectively), while others formed during periods of irregular climate fluctuations (M3 during mid-MIS 3).

Terrace sedimentation in the Colorado Plateau has been synchronous at times but not at others (Fig. 2.10). Both the Colorado River upstream of Moab and the Green River at Crystal Geyser, UT were depositing sediment during MIS 3, ~50-40 ka (Pederson et al., in review). However, these time-correlative M3 deposits are found at different positions in the landscape, with the Green River M3 ~12-15 m above modern grade and the study area M3 up to 30 m above modern grade. Additionally, a minor pause inferred from the mainstem chronostratigraphy at Lee's Ferry, AZ (M3y) may have occurred synchronously with study area sedimentation during MIS 3 (Pederson et al., 2013), perhaps representing a decrease in sediment supply downstream. There may also be a correlation between study area M3 deposits and side tributary sedimentation in eastern Grand Canyon during MIS 3, as the M3 upstream of Moab has been dated to a similar

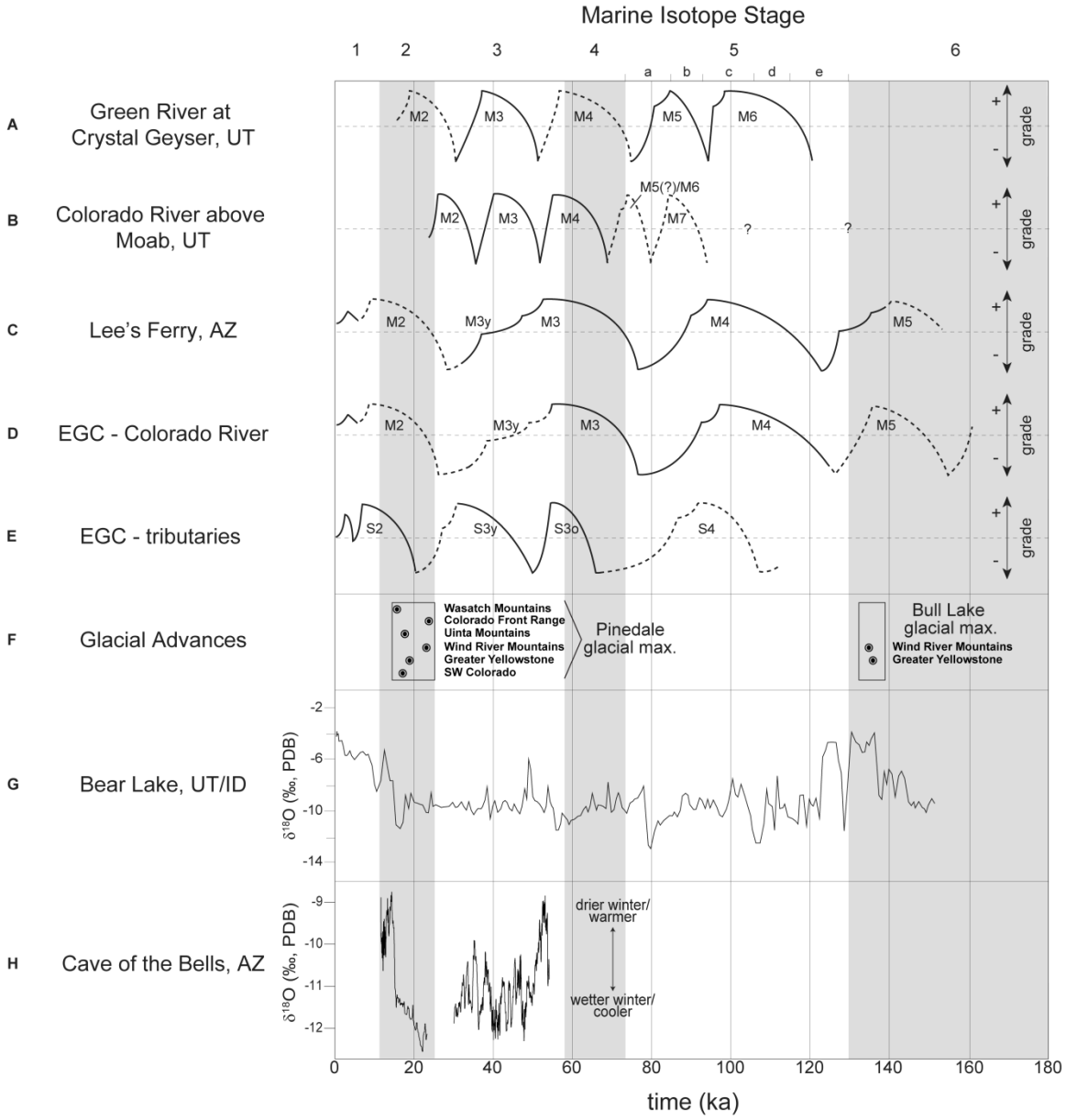

Figure 2.10. Regional chronostratigraphy and paleoclimate records. (A-E) Regional chronostratigraphy, including Green River at Crystal Geyser, UT, study area alluvial stratigraphy, Lee's Ferry, AZ, and eastern Grand Canyon (EGC) Colorado River terraces. Sedimentation is broadly synchronous during MIS 4 and 2 (Crystal Geyser, Lee's Ferry, and eastern Grand Canyon sedimentation curves from Pederson et al., in review; Pederson et al., 2013; and Anders et al., 2005, respectively). (F-H) Regional paleoclimate records. Study area M4 and M2 deposits record sedimentation during the build-up to glaciations during MIS 4 and latest MIS 3, respectively. The M3 deposit records sedimentation during periods of variable climate during mid-MIS 3 (See Fig. 2.3 for paleoclimate record references).

age as tributary S3y terraces (~50-34 ka) in Grand Canyon (Anders et al., 2005). Importantly, that deposit is interpreted as having been formed under increased contributions from tributary hillslopes during a period of variable climate.

Regional sedimentation also occurred ~75-65 ka (latest MIS 5/MIS 4), represented by the eastern Grand Canyon M3 (Anders et al., 2005), the M3 at Lee's Ferry (Pederson et al., 2013), the study area M6-M4 deposits, and the Qag4 deposit of Aslan and Hanson (2009) in Grand Valley, CO (Fig. 2.10). Again, these time-correlative deposits are found at varying positions in the landscape, from 15-20 m to 64 m above modern grade in Grand Valley and the study area, respectively. Although other age-based correlations are difficult to identify across the major river systems of the Colorado Plateau, there are generally more terrace deposits dated to <160 ka in the upper plateau than at Lee's Ferry and eastern Grand Canyon.

Although it is not possible to directly date incision, episodes of downcutting can be inferred between periods of sedimentation. Thus, the Colorado River above Moab appears to have been vertically incising ~80 ka, ~75-70 ka, ~50 ka, ~40-35 ka, and after ~25 ka (Fig. 2.10).

Sedimentation of the ~30 ka M2 terrace upstream of Moab, within error of all M2 OSL ages, can be compared to local paleoclimate records. Late M2 deposition may coincided with relatively moist local conditions as indicated by the Cowboy Cave pollen record and Colorado Plateau packrat midden data (Lindsay, 1980; Spaulding and Petersen, 1980; Betancourt, 1990). However, these records only extend to ~25 ka and offer no comparison to older terraces upstream of Moab.

At the regional scale, late Pleistocene Colorado River terrace sedimentation can be compared to lake cycles of pluvial Lake Bonneville (Fig. 2.3E; Benson et al., 2011). The timing of M4 sedimentation may overlap with the highstand of the Cutler Dam lake cycle ~60-55 ka, and M2 deposits correlate to the rising limb of the Lake Bonneville hydrograph prior to 25 ka during the onset of the Pinedale glaciation. Colorado River incision above Moab generally correlates with increases in ostracode $\delta^{18}O$ from Bear Lake cores (Fig. 2.10G), implying a linkage between fluvial erosion and decreasing ice volume in the Rocky Mountains. Sedimentation of the M3 deposit correlates to millennial variability in MIS 3 climate as indicated by the Cave of the Bells, AZ, speleothem record (Fig. 2.10H; Wagner et al., 2010). Globally, our chronostratigraphy shows weak relation with the SPECMAP oxygen-isotope curve (Fig. 2.3B).

Overall, study area terraces moderately correlate with other upstream terrace records in the Colorado Plateau but poorly with mainstem records in the southern plateau. Their relation to local, regional, and global paleoclimate records is similarly difficult to discern.

Bedload provenance

We performed lithologic clast counts to test for relative proportion of distal versus locally-sourced sediment. An abundance of mafic and basement clasts derived from the Rocky Mountains should reflect sediment loading from glaciated areas in the Colorado River headwaters. Terrace gravels dominated instead by Mesozoic sedimentary and Tertiary porphyritic lithologies from the nearby La Sal Mountains imply local sediment loading from Onion, Professor, and Castle creeks (e.g., Doelling et al., 2002).

Clast-count results define clear distinctions between the bedload rock types carried by the modern mainstem Colorado River as it enters the study area versus that carried by tributaries (Fig. 2.11; Appendix B). The modern channel of the Colorado River upstream of its confluence with the Dolores River carries 52% resistant lithologies such as quartzite, basement metamorphics, and intrusive rocks. The Dolores River also carries 52% of these lithologies, as well as 11% distantly-sourced Paleozoic sedimentary rocks. The bedloads of the Onion, Professor, and Castle drainages are characterized by 93-98% locally-derived Mesozoic sedimentary and Tertiary porphyritic clasts. Paleozoic carbonate makes up 26% of the Onion Creek bedload and is derived from the Pennsylvanian Honaker Trail Formation, which is not exposed in the Professor and Castle creek drainages.

Provenance results are used to interpret temporal changes in gravel composition as recorded in terraces. In general, deposits formed during MIS 4/early MIS 3 and latest MIS 3 (i.e. M4 and M2 gravels) contain higher percentages of distantly-sourced sediment than those formed during MIS 5 and mid-MIS 3 (Table 2.3). However, these trends are based on averages of $\leq$3 deposits, and more specific trends of mainstem terrace gravels appear equivocal. For instance, terrace gravels in the Dewey Bridge reach are alternately dominated by basement (M4), quartzite (M3), or local igneous sources (M2 below Dolores), or otherwise an overall balance of all lithologies as with the M2 above the Dolores confluence (Fig. 2.11). The quartzite-rich (45%) bedload of the Dolores River is not reflected in the composition of Dewey Bridge M2 gravels below its confluence and, paradoxically, the M2 there contains many igneous clasts that are mostly absent in the bedload of the modern Dolores. However, when distal versus local compositions are

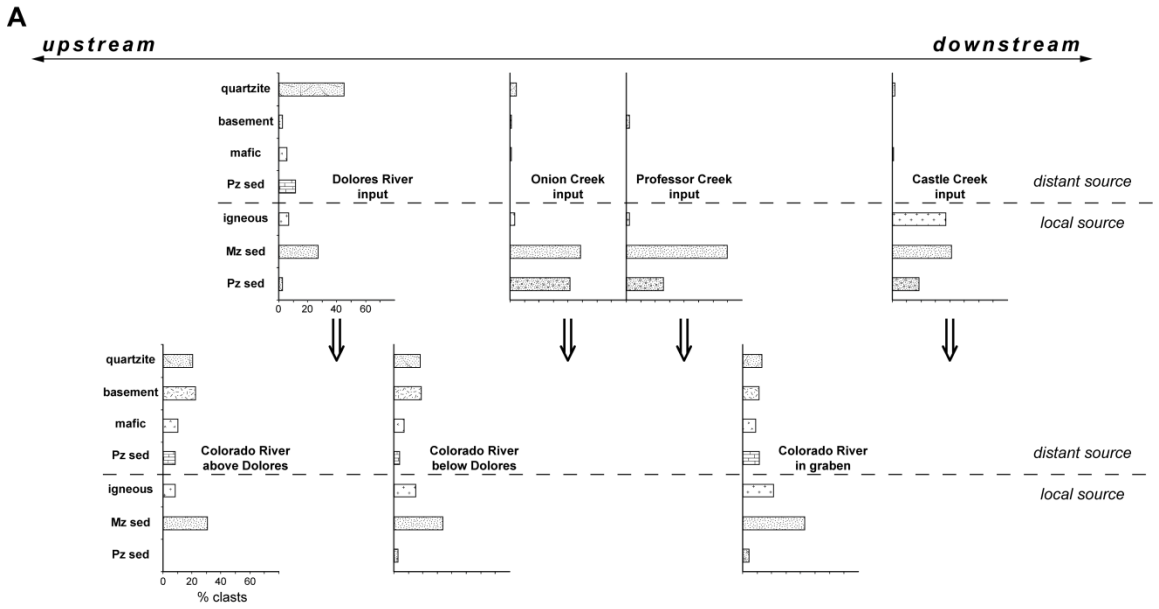

Figure 2.11. Lithologic counts of ~100 randomly sampled clasts each. (A) Data documenting the composition of modern inputs to the Colorado River and the mainstem channel in select locations. The Colorado River above the Dolores lacks distinct lithologic fingerprints, whereas the Dolores includes more distantly traveled quartzite. Onion, Professor, and Castle Creeks are dominated by local Mesozoic sedimentary and Tertiary porphyritic lithologies. (B) Data for late Pleistocene terrace gravels in the study corridor. Professor Valley deposits contain notably higher percentages of local igneous lithologies. The Cache Valley graben M6, and Ida Gulch M6 and M3 deposits are dominated by locally sourced igneous and sedimentary lithologies.

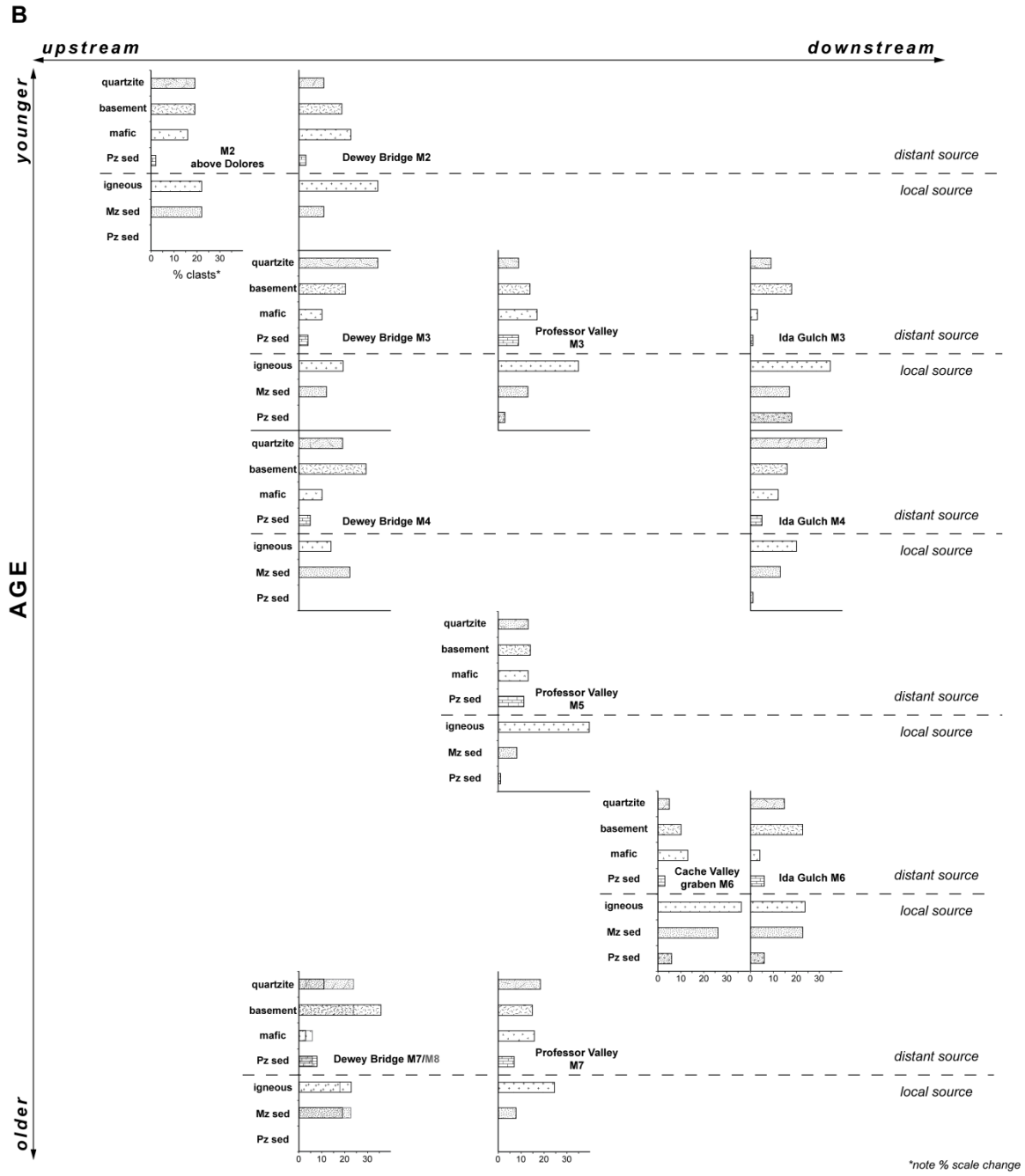

Figure 2.11. *Continued*.

averaged for all clast counts, balanced or distant-deficient compositions (~50-60% locally-sourced) are observed in the M6, M5, and M3 terrace gravels whereas all other deposits contain at least 55% distantly-sourced clasts (Table 2.3). These patterns reflect periods of greater tributary input to the mainstem system during MIS 5 and 3.

TABLE 2.3 SUMMARY OF DISTAL VERSUS LOCAL SEDIMENT SOURCES

	% distantly-sourced sediment	% locally-sourced sediment	n[a]
modern	49.7	50.3	3
M2	55	45	2
M3	49.7	50.3	3
M4	65	35	2
M5	51	49	1
M6	40	60	2
M7	60.5	39.5	2
M8	59	41	1

[a] Number of clast counts averaged.

Spatial variations in terrace form

To test for the influence of canyon/valley-bottom geometry on terrace type and form, we performed spatial analyses of channel width and valley-bottom width at 5 and 50 m above the modern channel. We also calculated gradient and stream power to observe whether these parameters change with valley geometry. Figure 2.12 highlights changes in terrace form in longitudinal profile along the Colorado River upstream of Moab. Mainstem gravel deposits thicken downstream, particularly the younger M4-M2 deposits (Table 2.2; Appendix C). The M7 thickens somewhat from Dewey Bridge to its

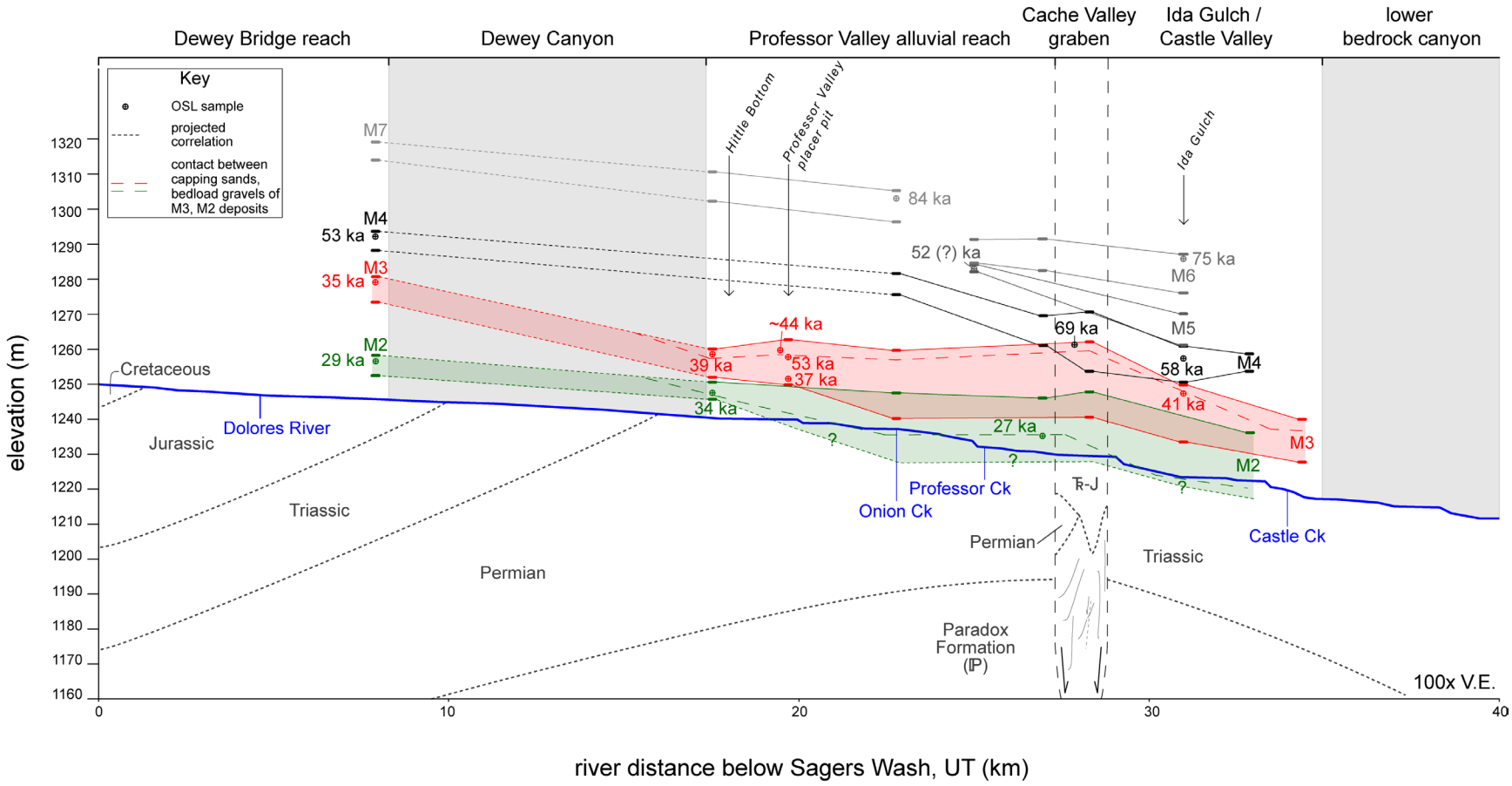

Figure 2.12. Longitudinal profile of the Colorado River. Surveyed late Pleistocene terraces through the study area are shown with bedrock exposed at river level and schematic subsurface geology (modern profile modified from USGS, 1948). Elevation of terrace treads (upper bars) and straths (lower bars) are maximum and minimum values, respectively, giving preserved deposit thickness. Thick, long dashes separate lower bedload gravels from upper overbank sands in M3 and M2 deposits. Strath elevations of M2 in Professor Valley reach and downstream are estimates of basal surfaces below grade.

isolated deposit near the confluence of Onion Creek, and the M6 and M5 deposits display some thickness variations in the vicinity of the graben; poor preservation of these older deposits precludes more specific observation. The M4-M2 terraces are better preserved and show dramatic thickening toward Cache Valley graben and Ida Gulch. The M3 thickens over 15 m between Dewey Bridge and Onion Creek (Table 2.2); its strath diverges from grade above the graben before converging toward the modern river profile in Ida Gulch (Fig. 2.12). Importantly, changes in mainstem gravel thicknesses are coincident with greater interfingering of piedmont and mainstem deposits in the broader reaches of the study area, where deposits are better preserved and strath surfaces are more complex. This is particularly true of the M4, M3, and M2 deposits (Fig. 2.6, 2.8, and 2.9).

Another notable change from upstream to downstream is the variability of basal strath elevations above grade (Table 2.2). Dewey Bridge terraces have planar straths (Fig. 2.5), but these surfaces become highly irregular in the Professor Valley and Cache Valley graben reaches downstream. The straths of the M7 and M6 are quite variable in the Professor Valley reach (Fig. 2.6), whereas the straths of the M4 and M3 display the greatest irregularity in the graben (Fig. 2.8, 2.9).

Topographic analyses demonstrate that valley-bottom width also varies greatly throughout the study area (Fig. 2.13). Channel width tracks the valley-bottom widths taken at 5 and 50 m above the modern channel in the Dewey and lower canyon reaches, but this relationship is not consistent elsewhere. Modern channel width is greatest in the Cache Valley graben reach, and the average 5 m valley-bottom width is greatest in the Dewey Bridge and Cache Valley graben reaches. However, the average 50 m valley-bottom width is by far greatest in the Professor Valley reach. It is intuitive that narrower

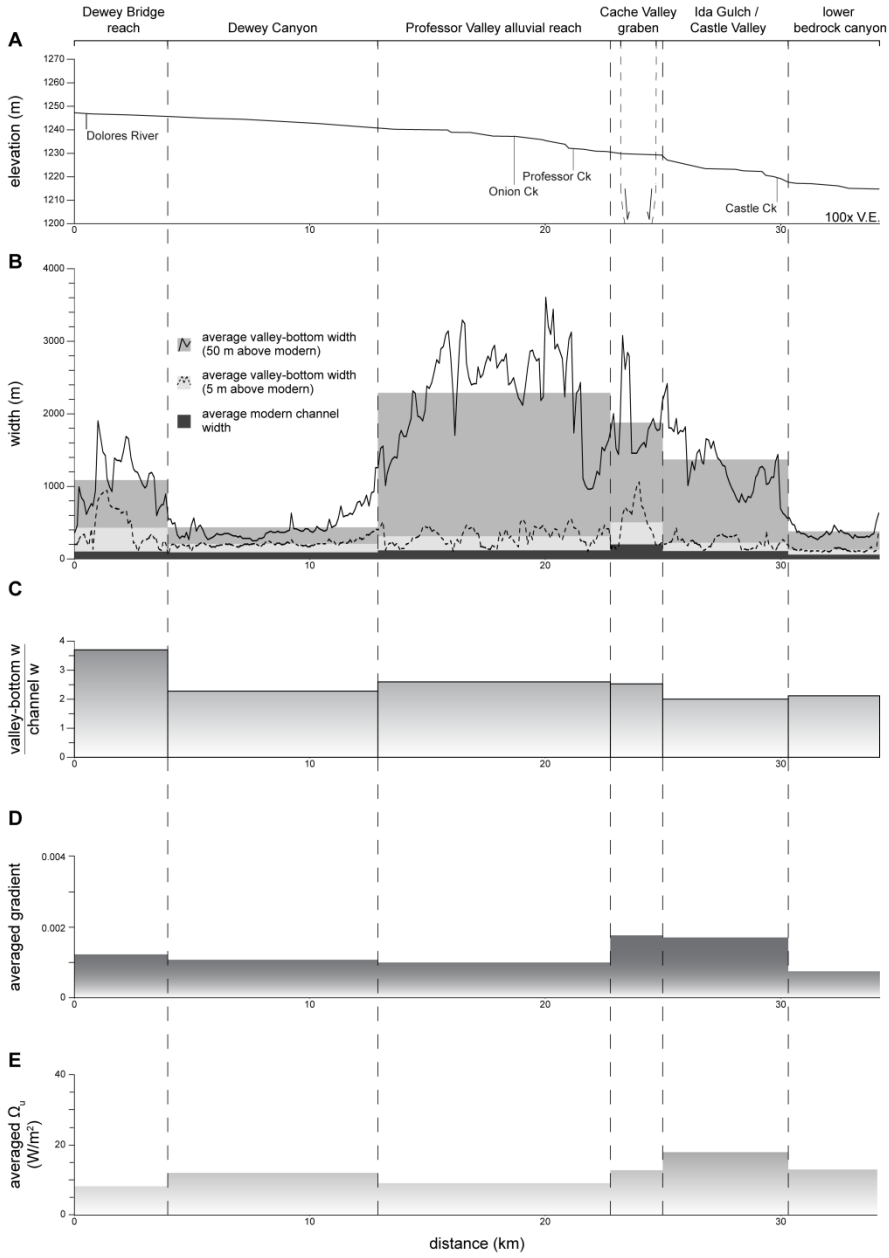

Figure 2.13. Average width, gradient, and stream power by reach. Longitudinal profile view (A) of (B) reach-averaged widths, (C) the ratio of valley-bottom to channel width, (D) reach-averaged gradient, and (E) reach-averaged stream power calculated using 5 m valley-bottom width. Greatest modern channel width is found in Cache Valley graben, whereas greatest valley-bottom width at 50 m above modern is found in the broad Professor Valley reach, where the highly erodible Cutler Formation is exposed. Lower widths in the canyons reflect constriction by bedrock walls of Mesozoic cliff-forming units and the talus below them. Reach-averaged gradient is lower in the upstream reaches, with higher gradient in Cache Valley graben and Ida Gulch. Stream power is lowest in the Dewey Bridge reach and highest in the Ida Gulch reach.

valley-bottoms (e.g., in Dewey Canyon) may reduce the preservation of fluvial terrace deposits, but the relation between terrace preservation and accommodation space is more ambiguous when considering the suites of terraces across the study reaches. On one hand, the increase in deposit thickness in the Professor Valley, Cache Valley graben, and Ida Gulch/Castle Valley reaches coincides with high average valley-bottom widths at 50 m above the modern channel in these segments. On the other hand, the Dewey Bridge reach has a wide valley-bottom at 5 m above the modern channel yet features thin strath terrace deposits.

Reach-averaged gradient and stream power vary throughout the study area, with overall increases in the Cache Valley graben and Ida Gulch/Castle Valley reaches (Fig. 2.13D, E). Peaks in gradient and stream power generally correspond with rapids.

DISCUSSION

Timing and climate controls of sedimentation versus incision

Based on our chronostratigraphy and field observations, we hypothesize that there are two primary conditions under which incision abates and sediment storage occurs along the Colorado River upstream of Moab. The first condition relates to headwater glaciation, particularly the crescendo to and height of glacial advances (Fig 2.14B). This connection is illustrated by the chronostratigraphy of study area M4 and M2 deposits. These deposits aggraded ~70-50 ka and ~35-25 ka, respectively, tracking the build-up to glacial maxima during MIS 4/early MIS 3 and latest MIS 3/MIS 2. In the case of the M2, sedimentation had largely ended before the local LGM observed after ~22 ka in the Colorado Front Range (Young et al., 2011). This chronostratigraphy suggests that the

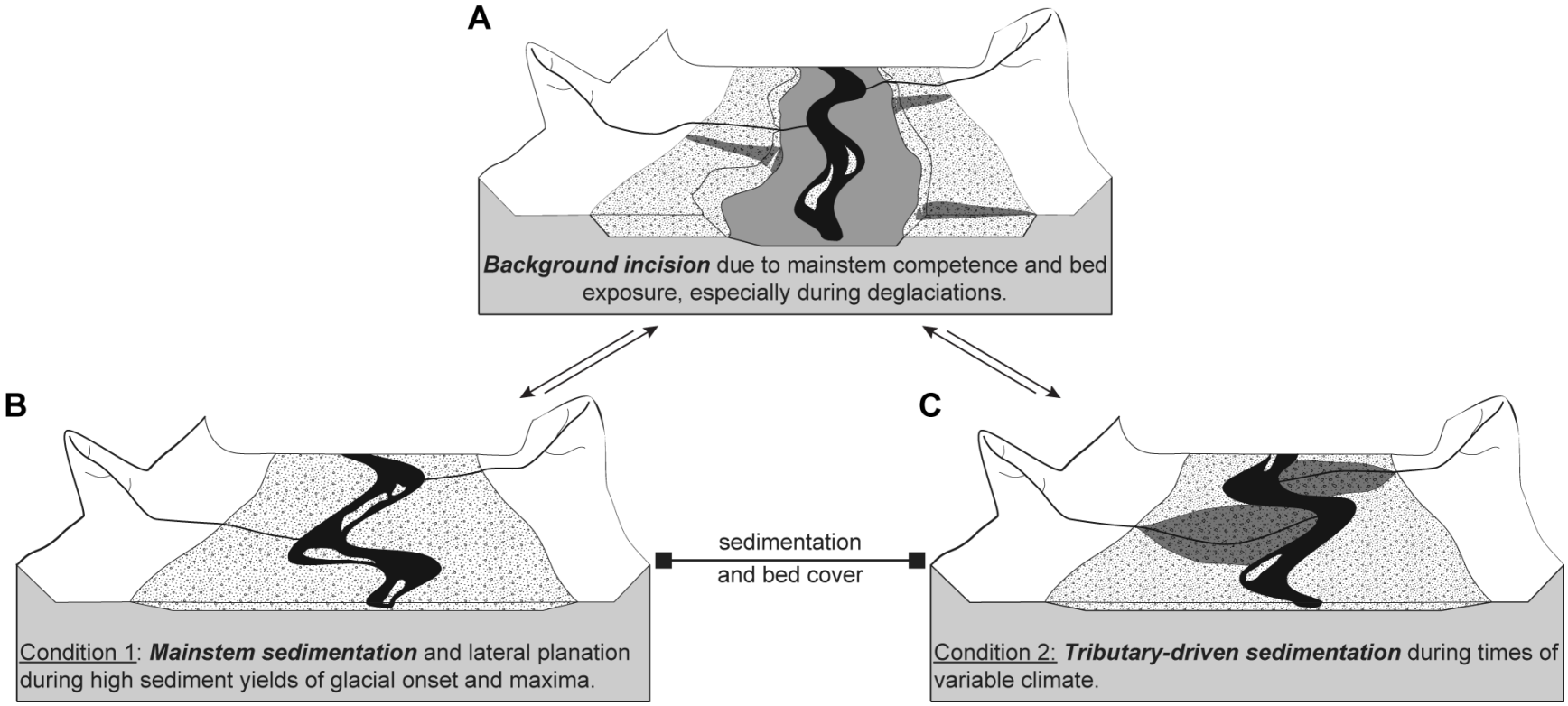

Figure 2.14. Conceptual models of Colorado River terrace formation upstream of Moab, showing two distinct modes of sediment storage and intervening incision. (A) Typical mode of fluvial activity with vertical incision occurring during conditions of high transport capacity, causing floodplain abandonment and terrace formation. (B) Condition 1 represents greater trunk system sediment flux relative to tributary contributions, perhaps coupled with low peak discharges. (C) Condition 2 represents mainstem system overwhelmed with local sediment delivery at tributary junctions.

formation of the M4 and M2 deposits is climatically-induced by hydraulic changes related to the generation of sediment load by glacial erosion in Rocky Mountain headwaters, and perhaps the amount of water trapped in these ice bodies (Fig. 2.4). Thus, the formation of these terraces fits the conceptual model of Hancock and Anderson (2002) in that storage of terrace sediment occurs during the build-up to glacial maxima, and ends when incision and terrace abandonment occur during deglaciations. The M2 is temporally consistent with the oxygen-isotope record from Bear Lake, UT demonstrating $\delta^{18}O$-enriched hydrologic input during late MIS 3/MIS 2 (Bright et al., 2006). Though this pattern results in part from a cyclical hydrologic regime under which the lake alters between a topographically closed and open basin, it may also relate to cooler, wetter conditions in the Rocky Mountains.

The second sedimentation condition results in terrace deposits formed instead during periods of subdued Rocky Mountain ice extent (Fig. 2.14C). We suggest that aggradation of the well-dated M3 deposit may be linked to increased sediment contributions from local tributaries when alpine ice volume is low. The M3 deposit was formed during mid-MIS 3, an interval lacking obvious global trends toward warming or cooling (Imbrie et al., 1984). Although not necessarily tied to broader glacial-interglacial cycles, this second mode of sedimentation requires periods of climate variability that disturb local sediment production and transport dynamics, resulting in increased sediment yield to the mainstem Colorado River from its local tributaries (described below). Indeed, the $\delta^{18}O$ record from Cave of the Bells, AZ, demonstrates millennial fluctuations between overall cooler/wetter and warmer/drier climate conditions in the southwestern US during MIS 3 (Wagner et al., 2010). In this case, the Hancock and Anderson (2002) model

matches neither the timing nor the hydrologic conditions behind the formation of these deposits. Tributary-driven sedimentation may be supported by a greater proportion of locally-derived gravel in M3 deposits than in M4 and M2 deposits (Table 2.3).

The enhanced tributary contributions implied by the second condition of sedimentation may have resulted from millennial-scale climate shifts in the drylands of the Colorado Plateau that drive weathering and transport processes. Colluvium derived from weathering-limited hillslopes accumulates during cooler, wetter periods when self-enhancing feedbacks such as vegetation density prevent the stripping of hillslope sediment to tributary channels (Bull, 1991; Anders et al., 2005). As climate shifts to more arid conditions, high magnitude but low frequency runoff events result in debris flows that remove sediment stored on hillslopes. Such shifts toward stronger monsoons and resulting hydrologic changes have been recorded during the latest Pleistocene/early Holocene on the Colorado Plateau based on soil production and vegetation communities (Weng and Jackson, 1999; Reheis et al., 2005). We suggest that similar climate dynamics could have been at work throughout MIS 3, given the millennial-scale trends in climatic variability and westerly storm patterns observed in the southwestern United States during that time (Wagner et al., 2010). Once sediment is removed from hillslope storage by intense precipitation, it is delivered to and transported down tributary channels (e.g., Clapp et al., 2000). Hydroclimatic models of geomorphic processes indicate that the distribution of precipitation is indeed more important than mean precipitation over time in regards to runoff (Tucker and Slingerland, 1997). A return to evenly distributed rainfall results in temporary storage of sediment in tributary deposits, which are eventually reworked when conditions again favor intense but infrequent flushing

episodes. These cycles of weathering, storage, and transport are repeated until hillslope sediment is delivered through the tributary system to the mainstem Colorado River (cf. Anders et al., 2005), where it is then mixed and aggraded with the sediment load of the trunk system. This model of sediment delivery is corroborated by Schmidt (1985), who found that mechanical denudation in Colorado River tributaries results in high suspended load delivery during high magnitude, low frequency events based on gage data from across the Colorado Plateau. Thus, highly variable climate results in complex, millennial cycles of weathering, transport, and storage of tributary sediment that is gradually conveyed to the Colorado River during periods of suppressed glacial signals from its headwaters. Terraces are formed once vertical incision is renewed.

Salt tectonism as an alternative control on terrace formation

The high number of terraces formed in the study area since ~100 ka implies that factors other than climate may promote terrace formation. Upstream of Moab, the influence of salt tectonism may affect fluvial activity with episodic, syn-depositional deformation creating accommodation space for the thick fill packages of terrace deposits observed in Professor Valley and the Cache Valley graben. Such deformation could occur during wetter periods, with enhanced dissolution of subsurface evaporite facies resulting in subsidence and/or localized collapse where fluvial deposition is concentrated. However, no connection is observed between sustained periods of increased moisture and the timing of aggradation of the M3 deposit (Fig. 2.10). Instead, salt tectonism may simply be a function of differential pressure in the subsurface causing episodic diapirism and ensuing collapse when salt flows into or out of structures such as the Fisher-Salt

Valley salt wall (e.g., Gutiérrez, 2004). Rapid incision could then occur when deformation wanes, as the river returns to its equilibrium profile. Thus, pulses of salt-related deformation may promote the aggradation of Colorado River sediment when climatic controls are not a dominating factor, contributing to the large suite of young (<100 ka) terraces observed in the study area today.

Reach changes in terrace form

Spatial results show great thickening of Colorado River terrace deposits over a reach of ~30 km between Dewey Bridge and Castle Valley, which change from thin (≤7 m) strath terraces in upstream canyon reaches to thick (≤20 m) fill terraces in downstream valley reaches (Fig. 2.12). Additionally , the basal straths of the M4 and M3 deposits converge with the modern Colorado River profile in the Professor Valley alluvial reach before diverging from the modern profile in and upstream of Cache Valley graben. Below, we consider the effects of valley geometry, bedrock lithology, and local salt tectonism on these patterns in terrace form.

Changes in terrace thickness and type correspond to changes in canyon/valley-bottom geometry, with thin strath terraces in the restricted Dewey Bridge reach and thick fill terraces in the broader Professor Valley, Cache Valley graben, and Ida Gulch/Castle Valley reaches (Fig. 2.13). These width patterns are also evident at the 5 and 50 m valley-bottom levels, although the 5 m valley-bottom width at Dewey Bridge is anomalously high due to the presence of a wide, well-preserved M1 terrace in that short (~4 km) reach, as well as the lack of talus debris in the river.

Valley geometry can be explained by lithologic changes in some fluvial settings. Although tensile strength measurements have not been made in the study area, nearby outcrops of the Permian Cutler and Jurassic Glen Canyon (Wingate and Navajo sandstones) groups have been measured in the Moab area (Tressler, 2011). These rocks have similar strength properties, with tensile strengths (σ_t) of the cliff-forming units of the Glen Canyon Group (0.70 MPa $\leq \sigma_t \leq$ 2.06 MPa) closely approximating those of the valley-forming Cedar Mesa Formation of the Cutler Group (0.73 MPa $\leq \sigma_t \leq$ 2.18 MPa) (Tressler, 2011). Thus, lithology does not clearly explain the presence of fill terraces in broad valley reaches. We suggest instead that fill terraces are formed in wider downstream reaches due to bolstered sediment contributions from tributaries as well as an increase in both vertical and lateral accommodation space for the accumulation of mainstem fluvial deposits.

Local neotectonism of Paradox Formation salts drives the creation of accommodation space in the study area. Impressive thickening of the M4 and M3 deposits by over 10 m occurs throughout the Professor Valley reach and in the Cache Valley graben (Fig. 2.12). The basal strath of the M4 converges with the modern profile (drops toward modern grade) in the graben before diverging, whereas the basal strath of the M3 deposit begins to converge near the head of the Professor Valley reach. Local thickening of these deposits through the graben is indicative of salt-related collapse (Fig. 2.8), but reach-scale thickening and strath convergence imply broader subsidence. We suggest that active diapirism in the Onion Creek drainage leads to subsidence in overburden rocks of the Cutler Group at the distant margins of the structure. This activity results in increased vertical accommodation space up to ~8 km away from the Onion

Creek diapir ascension point and results in thickening of Colorado River terraces and convergence of basal straths in the Professor Valley reach, which otherwise lacks surficial expressions of salt-related structures.

Implications

Colorado River terraces upstream of Moab are among the best preserved in the Colorado Plateau, and the younger suite of these landforms (M4, M3, M2) can be dated and correlated along ~30 m of river. Some deposits here correlate to known cycles of sedimentation and incision elsewhere in the plateau, whereas others appear to have unique histories.

The formation of Colorado River terraces cannot be tied to a simplified, bimodal glacial-interglacial climate driver, as has been suggested by numerous studies in other settings. We suggest instead that periods of variable, millennial-scale climate fluctuations such as mid-MIS 3 may drive terrace sedimentation through cycles of hillslope weathering, tributary transport and storage, and sediment delivery to the mainstem Colorado River.

Terrace type and form are controlled by valley geometry and salt tectonism. Thin strath terraces and thick fill terraces of the Colorado River correspond to canyon and valley reaches, respectively. The thickening of deposits and convergence of basal straths toward the modern river profile in the Professor Valley and Cache Valley graben reaches indicate increased accommodation space due to salt-related collapse/subsidence at both local and reach scales, resulting in fill packages aggrading in a valley geometry that would have otherwise favored the formation of strath terraces.

Future work on the Colorado River upstream of Moab should focus on further geochronologic constraints for the suite of six preserved terrace deposits. Poor OSL constraints on older deposits (e.g., M6/M5) could be refined by additional luminescence sampling and/or alternative dating techniques such as the use of terrestrial cosmogenic nuclides. These efforts may reveal that older deposits are genetically identical, yielding a dataset that could more easily be compared and contrasted with other mainstem terrace deposits across the Colorado Plateau in terms of the timing and drivers of their formation.

REFERENCES CITED

Anders, M.D., Pederson, J.L., Rittenour, T.M., Sharp, W.D., Gosse, J.C., Karlstrom, K.E., Crossey, L.J., Goble, R.J., Stockli, L., and Yang, G., 2005, Pleistocene geomorphology and geochronology of eastern Grand Canyon: Linkages of landscape components during climate changes: Quaternary Science Reviews, v. 24, no. 23-24, p. 2428-2448.

Aslan, A., and Hanson, P., 2009, Late Pleistocene Colorado River terraces, western Colorado: A test of the stream power model: Geological Society of America Abstracts with Programs, v. 41, no. 7, p. 622.

Aslan, A., Karlstrom, K.E., Crossey, L.J., Kelley, S., Cole, R., Lazear, G., and Darling, A., 2010, Late Cenozoic evolution of the Colorado Rockies: Evidence for Neogene uplift and drainage integration, *in* Morgan, L.A., and Quane, S.L., eds., Through the generations: Geologic and anthropogenic field excursion in the Rocky Mountains from modern to ancient: Geological Society of America Field Guide 18, p. 21-54, doi:10.1130/2010.0018(02).

Benson, L., Madole, R., Landis, G., and Gosse, J., 2005, New data for Late Pleistocene Pinedale alpine glaciation from southwestern Colorado: Quaternary Science Reviews, v. 24, p. 49-65.

Benson, L.V., Lund, S.P., Smoot, J.P., Rhode, D.E., Spencer , R.J., Verosub, K.L., Louderback, L.A., Johnson, C.A., Rye, R.O., and Negrini, R.M., 2011, The rise and fall of Lake Bonneville between 45 and 10.5 ka: Quaternary International, v. 235, no. 1-2, p. 57-69.

Berger, A., and Loutre, M.F., 1991, Insolation values for the climate of the last 10 million years: Quaternary Science Reviews, v. 10, p. 297-317.

Betancourt, J.L., 1990, Late Quaternary biogeography of the Colorado Plateau, *in* Betancourt, J.L., et al., eds., Packrat middens: The last 40,000 years of biotic change: Tucson, University of Arizona Press, p. 259-292.

Bright, J., Kaufman, D.S., Forester, R.M., and Dean, W.E., 2006, A continuous 250,000 yr record of oxygen and carbon isotopes in ostracode and bulk-sediment carbonate from Bear Lake, Utah–Idaho: Quaternary Science Reviews, v. 25, p. 2258-2270.

Bull, W.B., 1990, Stream-terrace genesis: Implications for soil development: Geomorphology, v. 3, p. 351-367.

Bull, W.B., 1991, Geomorphic responses to climatic change: New York, Oxford University Press, 326 p.

Burbank, D.W., and Anderson, R.S., 2011, Tectonic geomorphology: Oxford, Wiley -Blackwell, 454 p.

Chadwick, O.A., Hall, R.D., and Phillips, F.M., 1997, Chronology of Pleistocene glacial advances in the central Rocky Mountains: Geological Society of America Bulletin, v. 109, no. 11, p. 1443-1452.

Cheng, H., Edwards, R.L., Broecker, W.S., Denton, G.H., Kong, X., Wang, Y., Zhang, R., and Wang, X., 2009, Ice age terminations: Science, v. 326, p. 248-252.

Clark, P.U., Dyke, A.S., Shakun, J.D., Carlson, A.E., Clark, J., Wohlfarth, B., Mitrovica, J.X., Hostetler, S.W., and McCabe, A.M., 2009, The last glacial maximum: Science, v. 325, p. 710-714.

Clapp, E.M., Bierman, P.R., Schick, A.P., Lekach, J., Enzel, Y., and Caffee, M., 2000, Sediment yield exceeds sediment production in arid region drainage basin: Geology, v. 28, no. 11, p. 995-998.

Colman, S.M., 1983, Influence of the Onion Creek salt diapir on the late Cenozoic history of Fisher Valley, southeastern Utah: Geology, v. 11, no. 4, p. 240-243.

Colman, S.M., and Hawkins, F.F., 1985, Surficial geologic map of the Fisher Valley -Professor Valley area, southeastern Utah: U.S. Geological Survey Miscellaneous Investigations Series Map I-1596, scale 1:24 000, 1 sheet.

Darling, A.L., Karlstrom, K.E., Granger, D.E., Aslan, A., Kirby, E., Ouimet, W.B., Lazear, G.D., Coblentz, D.D., and Cole, R.D., 2012, New incision rates along the

Colorado River system based on cosmogenic burial dating of terraces: Implications for regional controls on Quaternary incision: Geosphere, v. 8., no. 5, p. 1020-1041.

Davis, W.M., 1902, Base-level, grade, and peneplain: Journal of Geology, v. 10, p. 77 -111.

DeVecchio, D.E., Heermance, R.V., Fuchs, M., and Owen, L.A., 2012, Climate -controlled landscape evolution in the Western Transverse Ranges, California: Insights from Quaternary geochronology of the Saugus Formation and strath terrace flights: Lithosphere, v. 4, no. 2, p. 110-130.

Doelling, H.H., 1996, Geologic map of the Dewey quadrangle, Grand County, Utah: Utah Geological Survey Map 169, scale 1:24 000, 2 sheets, 21 p. text.

Doelling, H.H., 2001, Geologic map of the Moab and eastern part of the San Rafael Desert 30' by 60' quadrangles, Grand and Emery Counties, Utah, and Mesa County, Colorado: Utah Geological Survey Map 180, scale 1:100 000, 3 sheets.

Doelling, H.H., and Ross, M.L., 1998, Geologic map of the Big Bend quadrangle, Grand County, Utah: Utah Geological Survey Map 171, scale 1:24 000, 2 sheets, 29 p. text.

Doelling, H.H., Oviatt, C.G., and Huntoon, P.W., 1988, Salt deformation in the Paradox Basin: Utah Geological and Mineral Survey Bulletin 122, 93 p.

Doelling, H.H., Ross, M.L., and Mulvey, W.E., 2002, Geologic map of the Moab 7.5' quadrangle, Grand County, Utah: Utah Geological Survey Map 181, scale 1:24000, 2 sheets, 34 p. text.

ESRI, 2011, ArcGIS Desktop: Release 10, Redlands, CA: Environmental Systems Research Institute.

Finnegan, N.J., and Balco, G., 2013, Sediment supply, base level, braiding, and bedrock river terrace formation: Arroyo Seco, California, USA: Geological Society of America Bulletin, doi:10.1130/B30727.1.

Finnegan, N.J., and Dietrich, W.E., 2011, Episodic bedrock strath terrace formation due to meander migration and cutoff: Geology, v. 39, no. 2, p. 143-146.

Fuller, T.K., Perg, L.A., Willenbring, J.K., and Lepper, K., 2009, Field evidence for climate-driven changes in sediment supply leading to strath terrace formation: Geology, v. 37, no. 5, p. 467-470.

Galbraith, R.F., Roberts, R.G., Laslett, G.M., Yoshida, H., and Olley, J.M., 1999, Optical dating of single and multiple grains of quartz from Jinmium Rock Shelter, Northern Australia: Part I experimental design and statistical models: Archaeometry, v. 41, no. 2, p. 339-364.

Gilbert, G.K., 1877, Report on the geology of the Henry Mountains: Geographical and geological survey of the Rocky Mountain region: Washington, D.C., Government Printing Office, 106 p.

Gosse, J.C., Klein, J., Evenson, E.B., Lawn, B., and Middleton, R., 1995, Beryllium-10 dating of the duration and retreat of the last Pinedale glacial sequence: Science, v. 268, p. 1329-1333.

Guérin, G., Mercier, N., and Adamiec, G., 2011, Dose-rate conversion factors: Update: Ancient TL, v. 29, n. 1, p. 5-8.

Gutiérrez, F., 2004, Origin of the salt valleys in the Canyonlands section of the Colorado Plateau: Geomorphology, v. 57, no. 3-4, p. 423-435.

Hancock, G.S., and Anderson, R.S., 2002, Numerical modeling of fluvial strath-terrace formation in response to oscillating climate: Geological Society of America Bulletin, v. 114, no. 9, p. 1131-1142.

Harden, D.R., Biggar, N.E., and Gillam, M.L., 1985, Quaternary deposits and soils in and around Spanish Valley, Utah: Geological Society of America Special Paper 203, p. 43-64.

Hays, J.D., Imbrie, J., and Shackleton, N.J., 1976, Variations in the Earth's orbit: Pacemaker of the ice ages: Science, v. 194, p. 1121-1132.

Hereford, R., Thompson, K.S., Burke, K.J., and Fairley, H.C., 1996, Tributary debris fans and the late Holocene alluvial chronology of the Colorado River, eastern Grand Canyon, Arizona: Geological Society of America Bulletin, v. 108, p. 3-19.

Huntley, D.J., Godfrey-Smith, D.I., and Thewalt, M.L.W., 1985, Optical dating of sediments: Nature, v. 313, p. 105-107.

Imbrie, J., Hays, J.D., Martinson, D.G., McIntyre, A., Mix, A.C., Morley, J.J., Pisias, N.G., Prell, W.L., and Shackleton, N.J., 1984, The orbital theory of Pleistocene climate: Support from a revised chronology of the marine $\delta^{18}O$ record, *in* Berger, A., Imbrie, J., Hays, J., Kukla, G., Saltzmann, B., eds., Milankovitch and climate, part 1: Reidel Publishing Company, Boston, p. 269-305.

Jiménez-Moreno, G., Anderson, R., and Fawcett, P., 2007, Orbital- and millennial-scale vegetation and climate changes of the past 225 ka from Bear Lake, Utah–Idaho (USA): Quaternary Science Reviews, v. 26, no. 13-14, p. 1713-1724.

Karlstrom, K., Coblentz, D., Dueker, K., Ouimet, W., Kirby, E., Van Wijk, J., Schmandt, B., Kelley, S., Lazear, G., Crossey, L., and 15 others, 2012, Mantle-driven dynamic uplift of the Rocky Mountains and Colorado Plateau and its surface response: Toward a unified hypothesis: Lithosphere, v. 4, no. 1, p. 3-22.

Laabs, B.J.C., Marchetti, D.W., Munroe, J.S., Refsnider, K.A., Gosse, J.C., Lips, E.W., Becker, R.A., Mickelson, D.M., and Singer, B.S., 2011, Chronology of latest Pleistocene mountain glaciation in the western Wasatch Mountains, Utah, U.S.A.: Quaternary Research, v. 76, no. 2, p. 272-284.

Lane, E.W., 1955, The importance of fluvial morphology in river hydraulic engineering: American Society of Civil Engineers, v. 81, p. 1-17.

Leopold, L. B., and Maddock, T., Jr., 1953, The hydraulic geometry of stream channels and some physiographic implications: U.S. Geological Survey Professional Paper 252, 57 p.

Licciardi, J.M., and Pierce, K.L., 2008, Cosmogenic exposure-age chronologies of Pinedale and Bull Lake glaciations in greater Yellowstone and the Teton Range, USA: Quaternary Science Reviews, v. 27, no. 7-8, p. 814-831.

Lindsay, L.M.W., 1980, Pollen analysis of Cowboy Cave cultural deposits, *in* Jennings, J.D., ed., Cowboy Cave: Salt Lake City, University of Utah Press, Anthropological Paper 104, p. 213-224.

Lips, E.W., Marchetti, D.W., and Gosse, J.C., 2005, Revised chronology of late Pleistocene glaciers, Wasatch Mountains, Utah: Geological Society of America Abstracts with Programs, v.37, no. 7, p. 41.

Lucchitta, I., 1979, Late Cenozoic uplift of the southwestern Colorado Plateau and lower Colorado River region: Tectonophysics, v. 61, p. 63-95.

Lyle, M., Heusser, L., Ravelo, C., Yamamoto, M., Barron, J., Diffenbaugh, N.S., Herbert, T., and Andreasen, D., 2012, Out of the tropics: The Pacific, Great Basin lakes, and late Pleistocene water cycle in the western United States: Science, v. 337, p. 1629-1633.

Madole, R.F., 1986, Lake Devlin and Pinedale glacial history, Front Range, Colorado: Quaternary Research, v. 25, p. 43-54.

Martinson, D.G., Pisias, N.G., Hays, J.D., Imbrie, J., Moore, T.C., and Shackleton, N.J., 1987, Age dating and the orbital theory of the ice ages: Development of a high -resolution 0 to 300,000-year chronostratigraphy: Quaternary Research, v. 27, no. 1, p. 1-29.

Merritts, D.J., Vincent, K.R., and Wohl, E.E., 1994, Long river profiles, tectonism, and eustasy: A guide to interpreting fluvial terraces: Journal of Geophysical Research, v. 99, p. 14031-14050.

Molnar, P., Erik Thorson, B., Burchfiel, B.C., Deng, Q., Feng, X., Li, J., Raisbeck, G.M., Shi, J., Zhangming, W., Yiou, F., and You, H., 1994, Quaternary climate change and the formation of river terraces across growing anticlines on the north flank of the Tien Shan, China: Journal of Geology, v. 102, p. 583-602, doi:10.1086/629700.

Montgomery, D.R., 2001, Slope distributions, threshold hillslopes, and steady-state topography: American Journal of Science, v. 301, p. 432-454.

Munroe, J.S., Laabs, B.J., Shakun, J.D., Singer, B.S., Mickelson, D.M., Refsnider, K.A., and Caffee, M.W., 2006, Latest Pleistocene advance of alpine glaciers in the southwestern Uinta Mountains, Utah, USA: Evidence for the influence of local moisture sources: Geology, v. 34, no. 10, p. 841-844.

Murray, A.S., and Olley, J.M., 2002, Precision and accuracy in the optically stimulated luminescence dating of sedimentary quartz: A status review: Geochronometria, v. 21, p. 1-16.

Murray, A.S., and Wintle, A.G., 2000, Luminescence dating of quartz using an improved single- aliquot regenerative-dose protocol: Radiation Measurements, v. 32, p. 57 -73.

Pan, B., Burbank, D., Wang, Y., Wu, G., Li, J., and Guan, Q., 2003, A 900 ky record of strath terrace formation during glacial-interglacial transitions in northwest China: Geology, v. 31, no. 11, p. 957-960.

Patton, P.C., and Boison, P.L., 1986, Processes and rates of formation of Holocene alluvial terraces in Harris Wash, Escalante River basin, south-central Utah: Geological Society of America Bulletin, v. 97, p. 369-378.

Pazzaglia, F.J., 2013, Fluvial terraces, *in* Wohl, E.E., ed., Treatise on geomorphology: Elsevier, New York (in press).

Pazzaglia, F.J., and Brandon, M.T., 2001, A fluvial record of rock uplift and shortening across the Cascadia forearc high: American Journal of Science, v. 301, p. 385 -431.

Pazzaglia, F.J., and Gardner, T.W., 1993, Fluvial terraces of the lower Susquehanna River: Geomorphology, v. 8, p. 83-113.

Pederson, J.L., Mackley, R.D., and Eddleman, J.L., 2002, Colorado Plateau uplift and erosion evaluated using GIS: GSA Today, v. 12, no. 8, p. 4-10.

Pederson, J.L., Anders, M.D., Rittenour, T.M., Sharp, W.D., Gosse, J.C., and Karlstrom, K.E., 2006, Using fill terraces to understand incision rates and evolution of the Colorado River in eastern Grand Canyon: Journal of Geophysical Research, v. 111, F02003, doi:10.1029/2004JF000201.

Pederson, J.L., Cragun, W.S., Hidy, H.J., Rittenour, T.M., and Gosse, J.C., 2013, Colorado River chronostratigraphy at Lee's Ferry, Arizona and the central Colorado Plateau bull's-eye of incision: Geology, v. 40, doi:10.1130/G34051.1.

Phillips, F.M., Zreda, M.G., Gosse, J.C., Klein, J., Evenson, E.B., Hall, R.D., Chadwick, O.A., and Sharma, P., 1997, Cosmogenic ^{36}Cl and ^{10}Be ages of Quaternary glacial and fluvial deposits of the Wind River Range, Wyoming: Geological Society of America Bulletin, v. 109, no. 11, p. 1453-1463.

Pierce, K.L., 1979, History and dynamics of glaciation in the northern Yellowstone National Park area: US Geological Survey Professional Paper 729-F, 90 p.

Refsnider, K.A., Laabs, B.J.C., Plummer, M.A., Mickelson, D.M., Singer, B.S., and Caffee, M.W., 2008, Last glacial maximum climate inferences from cosmogenic dating and glacier modeling of the western Uinta ice field, Uinta Mountains, Utah: Quaternary Research, v. 69, p. 130-144.

Reheis, M.C., Reynolds, R.L., Goldstein, H., Roberts, H.M., Yount, J.C., Axford, Y., Cummings, L.S., and Shearin, N., 2005, Late Quaternary eolian and alluvial response to paleoclimate, Canyonlands, southeastern Utah: Geological Society of America Bulletin, v. 117, no. 7-8, p. 1051-1069.

Richmond, G.M., 1962, Quaternary stratigraphy of the La Sal Mountains, Utah: U.S. Geological Survey Professional Paper 324, 135 p.

Riihimaki, C.A., Anderson, R.S., and Safran, E.B., 2007, Impact of rock uplift on rates of late Cenozoic Rocky Mountain river incision: Journal of Geophysical Research, v. 112, F03S02, doi:10.1029/2006JF000557.

Rittenour, T.M., 2008, Luminescence dating of fluvial deposits: Applications to geomorphic, palaeoseismic and archaeological research: Boreas, v. 37, p. 613 -635, doi:10.1111/j.1502-3885.2008.00056.x.

Ritter, D.F., Kochel, R.S., and Miller, J.R, 2002, Process geomorphology: McGraw-Hill, New York: 540 p.

Schmidt, K.H., 1985, Regional variation of mechanical and chemical denudation, upper Colorado River basin, USA: Earth Surface Processes and Landforms, v. 10, p. 497-508.

Schumm, S.A., and Hadley, R.F., 1957, Arroyos and the semiarid cycle of erosion: American Journal of Science, v. 255, p. 161-174.

Schumm, S.A., and Parker, R.S., 1973, Implications of complex response of drainage systems for Quaternary alluvial stratigraphy: Nature, v. 243, p. 99-100.

Shafer, D.S., 1989, The timing of late Quaternary monsoon precipitation maxima in the southwest United States [Ph.D. dissertation]: Tucson, University of Arizona, 234 p.

Sharp, W.D., Ludwig, K.R., Chadwick, O.A., Amundson, R., and Glaser, L.L., 2003, Dating fluvial terraces by ^{230}Th/U on pedogenic carbonate, Wind River Basin, Wyoming: Quaternary Research, v. 59, no. 2, p. 139-150.

Sharpe, S.E., 1991, Late-Pleistocene and Holocene vegetation change in Arches National Park, Grand County, Utah and Dinosaur National Monument, Moffat County, Colorado [M.S. thesis]: Flagstaff, Northern Arizona University, 95 p.

Sklar, L.S., and Dietrich, W.E., 2001, Sediment and rock strength controls on river incision into bedrock: Geology, v. 29, no. 12, p. 1087-1090.

Spaulding, W.G., and Petersen, K.L., 1980, Late Pleistocene and early Holocene paleoecology of Cowboy Cave, *in* Jennings, J.D., ed., Cowboy Cave: Salt Lake City, University of Utah Press, Anthropological Paper 104, p. 163-177.

Sturchio, N.C., Pierce, K.L., Murrell, M.T., and Sorey, M.L., 1994, Uranium series ages of travertines and timing of the last glaciation in the northern Yellowstone area, Wyoming-Montana: Quaternary Research, v. 41, p. 265-277.

Thompson, R.S., Whitlock, C., Bartlein, P.J., Harrison, S.P., and Spaulding, W.G., 1993, Climatic changes in the western United States since 18,000 yr B.P., *in* Wright, H.E., Jr., et al., eds., Global climates since the last glacial maximum: Minneapolis, University of Minnesota Press, p. 468-513.

Tressler, C., 2011, From hillslope to canyons, studies of erosion at differing time and spatial scales within the Colorado River drainage [MS Thesis]: Logan, Utah State University, 109 p.

Trudgill, B.D., 2011, Evolution of salt structures in the northern Paradox Basin: Controls on evaporite deposition, salt wall growth and supra-salt stratigraphic architecture: Basin Research, v. 23, no. 2, p. 208-238.

Tucker, G.E., and Slingerland, R., 1997, Drainage basin response to climate change: Water Resources Research, v. 33, no. 8, p. 2031-2047.

USDA, 2011, NRCS Web Soil Survey: http://websoilsurvey.nrcs.usda.gov/ (accessed October 2011).

USGS, 1948, Plan and profile Colorado River, mile 987 to mile 1076, Colorado and Utah; Dolores River to mile 22: U.S. Geological Survey, Utah Dam Sites Surveyed in 1944.

Wagner, J.D.M., Cole, J.E., Beck. J.W., Patchett, P.J., Henderson, G.M., and Barnett, H.R., 2010, Moisture availability in the southwestern United States linked to abrupt glacial climate change: Nature Geoscience, v. 3, p. 110-113.

Wallinga, J., Murray, A., and Wintle, A., 2000, The single-aliquot regenerative-dose (SAR) protocol applied to coarse-grain feldspar: Radiation Measurements, v. 32, p. 529-533.

Ward, D.J., Anderson, R.S., Guido, Z.S., and Briner, J.P., 2009, Numerical modeling of cosmogenic deglaciation records, Front Range and San Juan mountains, Colorado: Journal of Geophysical Research, v. 114, F01026, doi:10.1029/2008JF001057.

Wegmann, K.W., and Pazzaglia, F.J., 2002, Holocene strath terraces, climate change, and active tectonics: The Clearwater River basin, Olympic Peninsula, Washington State: Geological Society of America Bulletin, v. 114, no. 6, p. 731-744.

Weng, C., and Jackson, S.T., 1999, Late glacial and Holocene vegetation history and paleoclimate of the Kaibab Plateau, Arizona: Palaeogeography, Palaeoclimatology, Palaeoecology, v. 153, p. 179-201.

Whipple, K.X., and Tucker, G.E., 1999, Dynamics of the stream-power river incision model: Implications for height limits of mountain ranges, landscape response timescales, and research needs: Journal of Geophysical Research, v. 104, p. 17661-17674.

Winograd, I.J., Coplen, T.B., Landwehr, J.M., Riggs, A.C., Ludwig, K.R., Szabo, B.J., Kolesar, P.T., and Revesz, K.M., 1992, Continuous 500,000-year climate record from vein calcite in Devils Hole, Nevada: Science, v. 258, p. 255-260.

Winograd, I.J., Landwehr, J.M., Coplen, T.B., Sharpe, W.D., Riggs, A.C., Ludwig, K.R., and Kolesar, P.T., 2006, Devils Hole, Nevada, $\delta^{18}O$ record extended to mid -Holocene: Quaternary Research, v. 66, p. 202-212.

Wolman, M.G., 1954, A method of sampling coarse river-bed material: Transactions of the American Geophysical Union, v. 35, no. 6, p. 951-956.

Young, N.E., Briner, J.P., Leonard, E.M., Licciardi, J.M., and Lee, K., 2011, Assessing climatic and nonclimatic forcing of Pinedale glaciation and deglaciation in the western United States: Geology, v. 39, no. 2, p. 171-174.

CHAPTER 3

QUATERNARY SALT DEFORMATION AND INCISION ALONG THE COLORADO RIVER NEAR MOAB, UTAH

ABSTRACT

River terraces can serve as markers of tectonic deformation and incision. We use terraces and terrain analysis to assess recent salt deformation in the northern Paradox Basin, Utah, USA, as well as patterns in regional incision of the Colorado Plateau. Luminescence-based chronostratigraphy of Colorado River terraces upstream of Moab reveals a correlative suite of deposits, with three deposits well-constrained to <70 ka in age. Previous speculation over active salt deformation in this part of the Paradox Basin is now confirmed by alluvial deposits tilted by localized collapse in the Cache Valley graben, as well as evidence for up to 15 m of subsidence in the Professor Valley area, perhaps related to salt diapirism. We calculate a surprisingly rapid incision rate over the past ~70 ka of ~900 m/Ma in an upstream reach unaffected by salt tectonism. Additionally, concavity and knickzone distributions in tributary profiles are discordant and signal that salt tectonism is expressed differently in local Colorado River tributaries. These results suggest that salt tectonism has recently perturbed fluvial activity upstream of Moab, and rapid incision rates imply that the Colorado River may be responding to flexural rebound in the central plateau that is consistent with a bull's-eye pattern of regional incision. Rapid local incision may also reflect an increase in Colorado Plateau incision rates during the late Pleistocene based on similar trends observed downstream.

INTRODUCTION

Researchers have investigated the architecture of ancient fluvial deposits deformed by salt tectonism (e.g., Hazel, 1994), but the use of river terraces as markers of Quaternary salt deformation is limited or nonexistent. Such salt-related activity in the Paradox Basin of southeastern Utah has been suggested by previous workers based on the warping of alluvial basin fill and apparent tilting of fluvial terraces where the Colorado River and its tributaries bisect salt-cored grabens and collapsed anticlines of the Fisher-Salt Valley salt wall (Colman, 1983; Doelling et al., 1988). However, this activity remains unconstrained.

Widespread use of fluvial terraces as markers of tectonic deformation has instead focused on constraining faulting and folding in other real world and experimental settings (e.g., Ouchi, 1985; Merritts et al., 1994; Keller et al., 1998; Lavé and Avouac, 2000; Burbank and Anderson, 2011). The major challenge of geomorphology-based investigations of deformation has been the correlation of remnant terraces over distances sufficient to identify meaningful spatial patterns. Additionally, achieving age control through radiocarbon, cosmogenic nuclide, and luminescence dating can be problematic.

More broadly, regional tectonism can be evaluated through the study of fluvial incision rates in response to changes in baselevel, the fundamental driver of incision in river systems (Powell, 1876; Hack, 1957). Incision rates integrated over timescales of 10^4-10^6 yr and the upstream migration of knickzones (oversteepened segments of stream profiles) represent observable perturbations to the otherwise graded profiles of rivers in dynamic equilibrium (e.g., Mackin, 1948; Gasparini et al., 2007; Cook et al., 2009).

Tectonic activity can also be explored through spatial analysis of topography using a geographic information system (GIS). Computational analyses include the use of spatial metrics to distinguish actively uplifting drainage basins from those that are inactive (e.g., Frankel and Pazzaglia, 2005; Wolinsky and Pratson, 2005). Other studies assess uplift through analysis of stream-profile concavity and channel gradient indices (e.g., Kirby and Whipple, 2001; Wobus et al., 2006; Kirby and Whipple, 2012). When coupled with field observations, these efforts can be used to compare relative tectonic activity between tributary catchments and to identify transient responses to baselevel changes originating in trunk river systems.

Southeastern Utah provides an ideal setting in which to use terraces as markers of salt-related deformation, evaluate the effect of salt tectonism on tributary catchments, and calculate late Pleistocene incision rates. A ~30 km segment of the Colorado River above Moab features well-preserved, correlative river terraces and traverses two major structures cored by salt deposits of the Pennsylvanian Paradox Formation: the Fisher-Salt Valley and Castle Valley salt walls (Fig. 3.1). The dynamics of Paradox Basin salt movement and deformation are well-documented in this area through geophysical and field-based studies (Case and Joesting, 1972; Gutiérrez, 2004; Trudgill, 2011), but their manifestation in the fluvial geomorphology of the Colorado River and its local tributaries has not been well documented. The goals of this study are to determine whether Colorado River terraces are warped by salt tectonism and whether such activity is manifested in tributary basin morphology. We then use luminescence dates to constrain both potential salt-related deformation as well as overall late Pleistocene incision rates. We provide evidence of both localized collapse and reach-scale subsidence related to salt tectonism

during the late Pleistocene, as well as unexpectedly rapid incision rates of the mainstem Colorado River in this area.

BACKGROUND

Salt tectonism of the Paradox Basin

Late Paleozoic strata of the Paradox Basin in southeast Utah and southwest Colorado (Fig. 3.1A) are dominated by great thicknesses of evaporites. These deposits accumulated in the foreland basin of the Uncompahgre uplift (ancestral Rocky Mountains), and passive diapirism induced by subsequent sedimentation and unloading has resulted in elongate salt walls up to 4500 m thick (Trudgill, 2011). The deepest portion of the Paradox Basin abuts the Uncompahgre front in the northeast (Case and Joesting, 1972). Salt structures here include diapirs, NW-SE trending collapsed salt-cored anticlines, salt-cored grabens, and ring-faulted collapse centers. Many of these features are intersected by the Colorado River and/or its tributaries (Fig. 3.1B).

Generally NW-SE trending faults (including the Moab Fault) and folds developed in multiple episodes over the late Mesozoic and into the Eocene in response to salt movement in the subsurface (Doelling et al., 1988; Pevear et al., 1997; Foxford et al., 1998). Younger salt destabilization resulting in deformation is commonly attributed to dissolution and transport by groundwater and unloading from Colorado River incision (Gutiérrez, 2004). For example, the Meander anticline and the Needles fault zone/grabens district of Canyonlands ~125 km downstream of the study area (Fig. 3.1A) are interpreted as gravity-driven structures with free boundaries where the Colorado River is removing subsurface salts (Huntoon, 1982; Furuya et al., 2007; Trudgill, 2011).The primary salt-

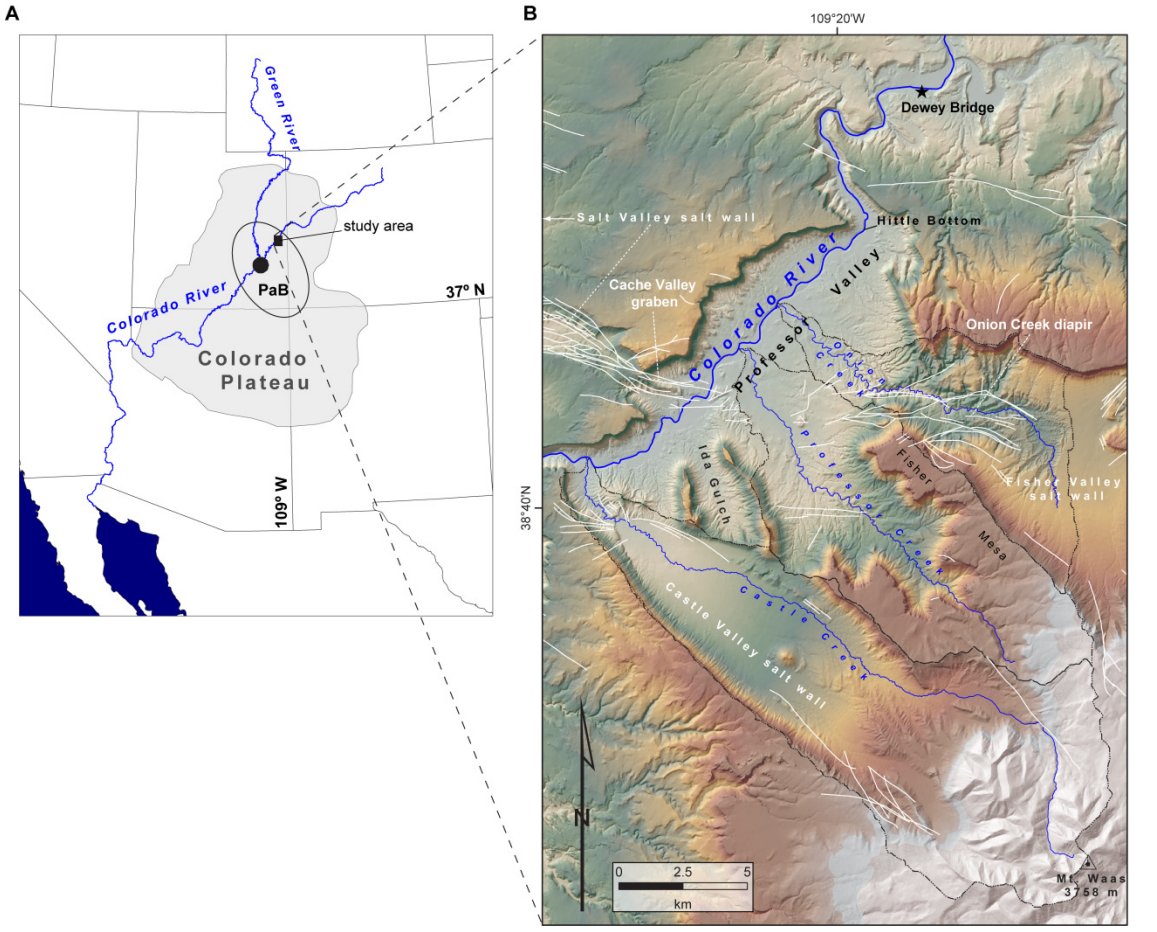

Figure 3.1. Maps of Colorado Plateau and Colorado River study area. (A) Colorado Plateau and Paradox Basin (PaB). Dark circle is Needles fault zone and grabens formed by gravity-driven salt flow in Canyonlands National Park. (B) Map of study area tributary watersheds and major salt structures. White lines represent faults and folds (Doelling, 2001).

tectonic structures underlying the study area are genetically distinct from these southern features, and include the Fisher-Salt Valley and Castle Valley salt walls and their overlying grabens. The Cache Valley graben intersects the Colorado River and represents a roughly E-W trending segment of the Fisher-Salt Valley structure that is a lateral deflection between the Fisher and Salt Valley anticlines (Fig. 3.1; Trudgill, 2011). The Onion Creek diapir to the east is an ascension point of the Fisher Valley salt wall and is cut by its namesake stream.

There are no constraints on the rates of activity and the effects of salt tectonism in the study area. The slip rate of faults in Salt and Cache valleys is estimated to be <0.2 m/ka (Black and Hecker, 1999). Workers have previously suggested warping of Colorado River terraces within and on the margins of Cache Valley based on topographic observations (Colman, 1983; Doelling et al., 1988). Drainage reorganization and Pleistocene sedimentation due to salt activity in the Onion Creek catchment has been well documented (Colman, 1983; Balco and Stone, 2005). However, salt activity resulting in deformed Quaternary deposits is purely speculative and has not been quantitatively constrained.

Uplift and incision patterns in the Colorado Plateau

The Colorado Plateau's high elevation (~1.9-2 km) and minor internal deformation stem from an unclear history of uplift and erosion throughout the Cenozoic (Pederson et al., 2002; Levander et al., 2011). Workers formerly believed that Colorado Plateau uplift was inherited from the Laramide orogeny, but this may only be true at the extreme southwestern margin of the plateau (e.g., Smith and Levy, 1976; Lucchitta,

1979; Flowers et al., 2008). Five sources of rock uplift have been proposed and include (a) crustal injection/thickening (McQuarrie and Chase, 2000), (b) warming of heterogeneous lithosphere (Roy et al., 2009), (c) lithospheric delamination (Spencer, 1996; Levander et al., 2011), (d) dynamic mantle flow and topography (Moucha et al., 2009; Liu and Gurnis, 2010; Karlstrom et al., 2012), and (e) flexural rebound in response to erosional unloading (Pederson et al., 2002). Each of these hypotheses has different implications for the timing of Cenozoic uplift, and each contains significant implications for the patterns of fluvial incision of the Colorado River and its tributaries.

Recent debate has focused on spatial and temporal patterns of incision in the Colorado Plateau. Pederson et al. (2013) identify a bull's-eye pattern of late Pleistocene (≤150 ka) incision centered over the Canyonlands district, and Pederson and Tressler (2012) suggested potential transient knickzones upstream of Canyonlands. Younger-towards-center patterns revealed by thermochronologic data collected from central and southern portions of the plateau also reveal a bull's-eye pattern of overall exhumation during the late Cenozoic (Flowers et al., 2008; Hoffman, 2009; Lee et al., 2013).

Other researchers have uncovered similar erosional patterns in the plateau, but with temporally variable incision rates. Darling et al. (2012) determined an increase in incision rates of the Colorado River through Glen Canyon, UT, between 500 and 250 ka from ~60 m/Ma to ~400 m/Ma. This pulse of recent rapid incision has been attributed to a transient wave of incision migrating past the Paleozoic-Mesozoic contact/knickpoint at Lee's Ferry, AZ, sometime after 500 ka (Cook et al., 2009; Darling et al., 2012).

METHODS

Terrace chronostratigraphy and correlation

Determining whether a terrace chronostratigraphy reveals patterns of neotectonic deformation requires age constraints and accurate spatial information. We dated mainstem Colorado River terrace sediment using optically stimulated luminescence (OSL), a technique that measures the amount of time elapsed since quartz grains were exposed to light prior to deposition (Huntley et al., 1985). Luminescence samples from sand lenses in terrace deposits were collected and equivalent doses were determined in the USU Luminescence Laboratory using the single-aliquot regenerative (SAR) protocol. Environmental dose rates were determined from bulk sediment elemental analyses. Ages are calculated as the equivalent dose divided by the dose rate, and were determined using the central age model of Galbraith et al. (1999) and dose rate conversion factors of Guérin et al. (2011).

High-resolution topographic data were obtained for the elevations of terrace straths, risers, treads, and piedmont deposits in the study area using a real-time kinematic (RTK) TopCon HiPer GA GPS, with vertical and lateral spatial errors of ≤3 cm and ≤1.5 cm, respectively. Terrace correlation was based on physical tracing, landscape position, and OSL ages.

Spatial analyses

All spatial analyses were performed on 10 m digital elevation models (DEMs) in ArcGIS (ESRI, 2011). The following metrics were analyzed: basin topography (gradient

and relief), hypsometric integral (HI), volume to area ratio (R_{VA}), and normalized steepness index (k_{sn}).

The topographic metrics of hypsometry (HI) and ratio of catchment volume to area (R_{VA}) were calculated to assess the tectonic activity of the study catchments. Hypsometry is the distribution of elevation in a catchment and indicates the relative maturity of a landscape (Strahler, 1952). The hypsometric distribution and integral for the three study area tributary drainages were determined from raw DEMs. The HI value is calculated as:

$$HI = \frac{(z_{ave} - z_{min})}{(z_{max} - z_{min})}, \quad (1)$$

where z is elevation, and the denominator is simply total basin relief.

R_{VA} represents the change in mean basin depth through time and is related to the erosional response of a catchment to baselevel fall, particularly in fault-bounded catchments (Frankel and Pazzaglia, 2005). This metric is calculated as:

$$R_{VA} = \frac{V}{A}, \quad (2)$$

where V is catchment volume and A is planimetric area. These values are derived from DEMs and triangulated irregular network surfaces "capping" the basins. R_{VA} values typically exceed 100 in basins with high uplift rates (Frankel and Pazzaglia, 2005).

The normalized steepness index (k_{sn}) is a generalized form of the stream-gradient index of Hack (1973). The calculation of profile concavity and k_{sn} assumes that the river profile is in steady state with respect to uplift and climate, and that uplift rate and erosivity are uniform throughout each reach (Snyder et al., 2000). The calculation of k_{sn}

is based on "Flint's law" (Flint, 1974), but uses a uniform reference concavity to identify steepness anomalies in different tributary profiles:

$$S = k_{sn} A^{-\theta_{ref}}, \quad (3)$$

where A is contributing area and θ_{ref} is reference concavity (Whipple and Tucker, 1999; Snyder et al., 2000). Thus, θ_{ref} permits comparisons between drainages. Using an ArcGIS add-on and associated MATLAB scripts (Kirby et al., 2003; Wobus et al., 2006), the longitudinal profiles of raster flow paths were extracted and smoothed with a moving-average window of 250 m. Elevation values were extracted at 10 m contours along each profile, and steepness indices were calculated at each interval using θ_{ref} = 0.35, gradient, and contributing area. Our reference concavity was based on the approximate average concavity of the upper segments of each profile, reaches we hypothesize to be insulated from baselevel fall.

RESULTS

Terrace chronostratigraphy

Seven late Pleistocene terraces are documented in the study area; our focus is on the flight of younger terraces (M4, M3, and M2) with the best-constrained ages. These terraces span the last ~70 ka, with central OSL ages ranging from ~70-50 ka for the M4, ~50-40 ka for the M3, and ~35-25 ka for the M2 (Table 3.1). These deposits thicken greatly between the upstream reach at Dewey Bridge and the lower valley reaches where the Colorado River traverses salt structures, including the Cache Valley graben (Fig. 3.2A). The M4-M2 terraces are poorly preserved in the canyon upstream of the Professor Valley reach, except at Dewey Bridge. These deposits feature thicker fill packages of

TABLE 3.1 SUMMARY OF PRELIMINARY OSL AGE CONTROL FOR COLORADO RIVER M4-M2 DEPOSITS

Deposit[a]	Sample[b]	USU Sample #	Depth (m)	# Aliquots	Dose Rate, Gy/ka	Equivalent Dose (D_e), Gy (overdispersion, %)	OSL Age, ka[c]
M2	AJ-DB-T2A	USU-1075	1.7	13 (29)	3.42 ± 0.18	98.63 ± 15.54 (22.5)	29 ± 5
M2	AJ-HB-M2	USU-1195	2.8	16 (19)	3.56 ± 0.20	121.82 ± 15.83 (23.4)	34 ± 6
M2	AJ-CVG-T2Au	USU-1073	2.5	23 (30)	2.81 ± 0.15	75.04 ± 13.73 (39.7)	27 ± 6
M3	AJ-DB-T3	USU-1078	1.8	12 (31)	3.54 ± 0.19	124.85 ± 13.08 (0.0)	35 ± 5[d]
M3	AJ-HB-M3	USU-1196	1.5	5 (5)	5.07 ± 0.29[e]	197.55 ± 20.33 (5.5)	39 ± 5[e]
M3	AJ-PV-T3usAu	USU-1072	3.0	17 (30)	3.12 ± 0.14[f]	137.10 ± 24.00 (33.5)	~44[f]
M3	AJ-PV-T3uAu	USU-1076	3.0	20 (28)	3.21 ± 0.17	170.34 ± 26.76 (32.5)	53 ± 10
M3	AJ-PV-T3lAu	USU-1077	8.0	4 (5)	2.62 ± 0.64	114.70 ± 18.66 (8.8)	37 ± 6
M3	AJ-IG-T3g	USU-1074	1.5	19 (25)	3.25 ± 0.17	133.92 ± 20.87 (31.0)	41 ± 8
M4	AJ-DB-M4	USU-1336	1.5	18 (31)	3.12 ± 0.16	164.44 ± 32.98 (40.0)	53 ± 12
M4	AJ-CVG-M3o	USU-1200	9.4	12 (28)	3.15 ± 0.17	218.59 ± 48.76 (34.1)	69 ± 17
M4	AJ-IG-M3	USU-1280	8.0	18 (35)	3.40 ± 0.19	197.86 ± 21.90 (20.3)	58 ± 9

[a] Organized by stratigraphic position; "M" is mainstem Colorado River deposit.

[b] DB = Dewey Bridge, HB = Hittle Bottom, PV = Professor Valley, CVG = Cache Valley graben, IG = Ida Gulch.

[c] Reported ages with 2σ error.

[d] Sample corrected for falling $D_e(t)$ using early background subtraction.

[e] Age calculated from infrared luminescence performed on feldspar grains.

[f] Mean dose rate of other samples used due to erroneously high chemistry results (see Chapter 2); age is only an estimate.

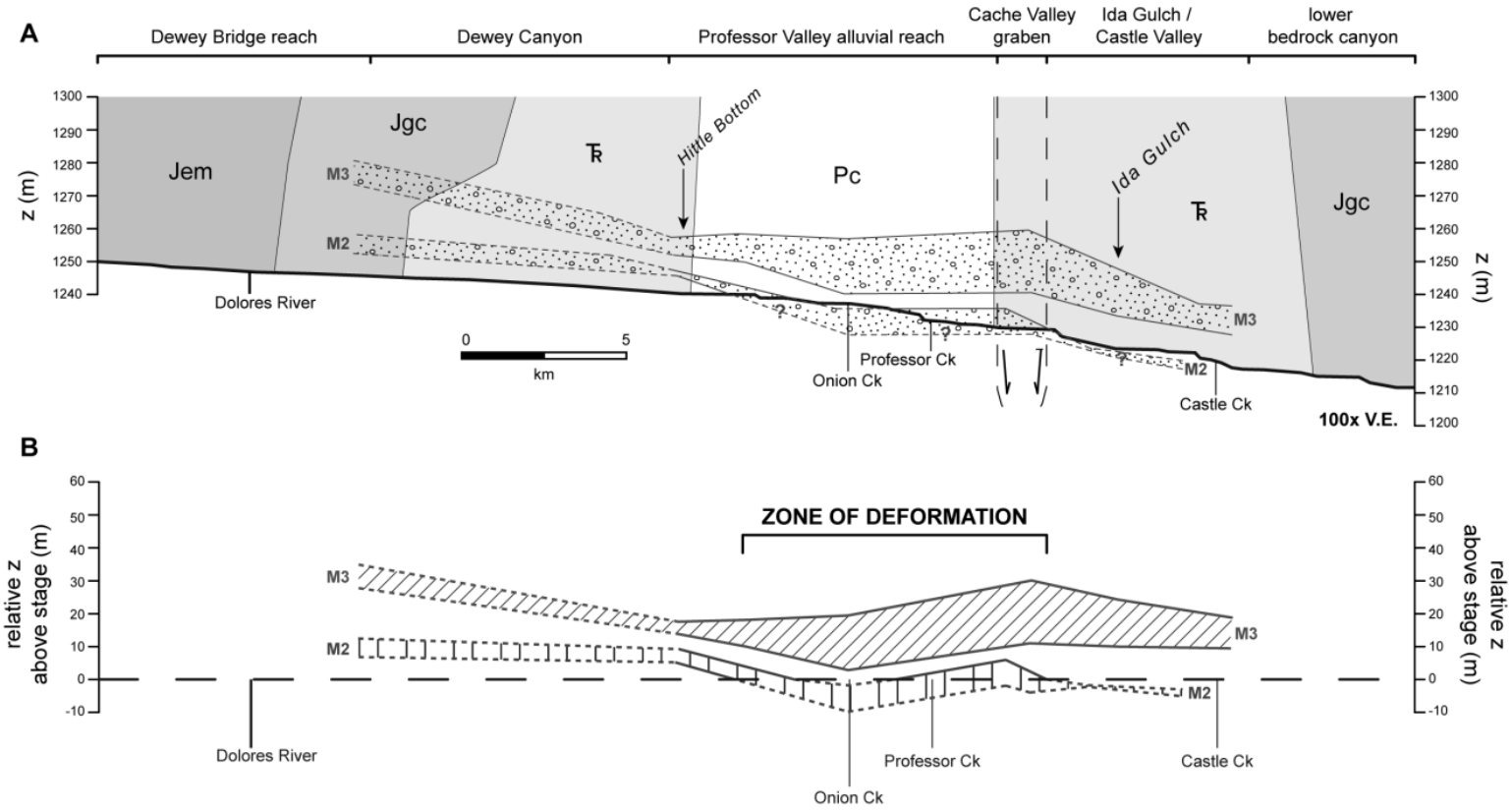

Figure 3.2. Deformation of study area M3 and M2 deposits. (A) Longitudinal profile of Colorado River in study area showing exposed bedrock along canyons/valley bottoms, Cache Valley graben, and patterns in basal gravels and thickness of M3 and M2 terrace deposits. Jem - Jurassic Morrison and Entrada formations, Jgc - Jurassic Glen Canyon Group, T_R - Triassic Chinle and Moenkopi formations, Pc - Permian Cutler Group. (B) M3 and M2 profiles normalized relative to local river level (= 0 m), showing thickness changes and irregularity in thickness of basal straths from upstream to downstream. M3 basal gravels increase up to ~15 m in thickness in Professor Valley and Cache Valley graben reaches before tapering downstream.

mainstem sediment (up to 22 m) and greater basal strath irregularity in the graben and surrounding reaches. The M4 thickens by ~12 m between Dewey Bridge and Ida Gulch. The M3 displays pronounced thickening of ~15 m, and the M2 thickens by a minimum of 8 m, as its basal strath drops below grade in Professor Valley (Fig. 3.2B). The M3 begins to thicken at the head of the Professor Valley reach near Hittle Bottom, and thins somewhat in Ida Gulch.

The M4 and interfingering piedmont deposits within the Cache Valley graben display evidence of localized collapse (Fig. 3.3). This includes asymmetric deformation of the M4 basal strath and piedmont gravels tilted opposite to their transport gradient into a circular depression ~100 m in diameter. M4 stratigraphy here is marked by cobble gravel ringed by capping overbank sediment. The relief of the M4 strath in this small collapse center is ~4 m. Piedmont deposits dip 11-13° NE, whereas graded piedmonts of Professor Valley and Ida Gulch dip no more than 1-2° and grade evenly into their associated mainstem deposits (e.g., P3 graded to M3). Thus, total deformation has occurred through an arc of ~12-15°.

Spatial metrics and k_{sn}

Topographic metrics are shown in Table 3.2 and Appendix D for the three study area tributaries. The high relief of the study area is not necessarily observed in the hypsometric integral and R_{VA} metrics of Onion, Professor, and Castle Creek. All three tributaries feature similar, low HI values of 0.36-0.40. Other basin topography measurements are shown in Appendix D. Castle Creek has a much higher R_{VA} than Onion and Professor creeks. The normalized steepness index (k_{sn}) varies across two

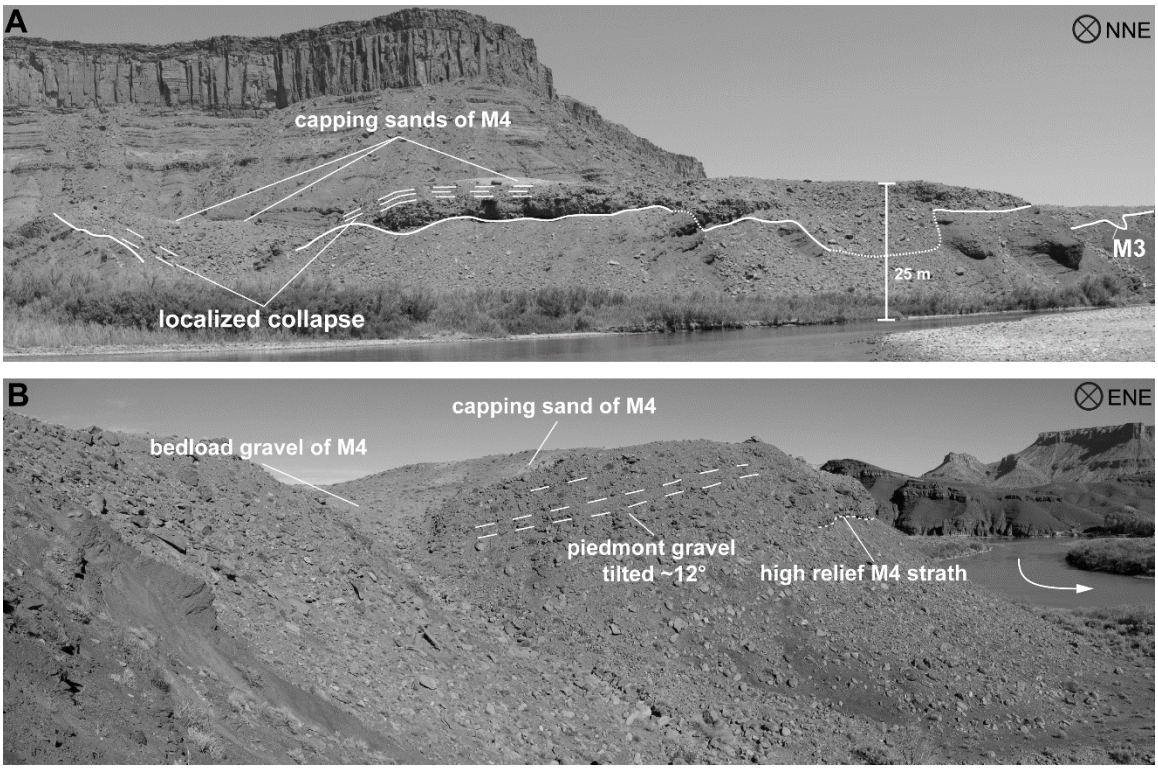

Figure 3.3. Annotated photographs of terrace stratigraphy and warping in Cache Valley graben. (A) Looking upstream from river level, illustrating irregular strath and collapsed gravels at left. (B) Looking upstream from level of M4 bedload gravels, showing warping of piedmont gravels in relation to M4 deposits. White arrow indicates direction of flow.

orders of magnitude in tributary channels, with the mean k_{sn} of Professor Creek double that of Onion Creek (Table 3.2). Knickzones are found in the upper and lower reaches of all three tributaries (Fig. 3.4). Average profile concavities vary, though the Professor Creek profile is notably straighter ($\theta = 0.15$) than the profiles of Onion and Castle creeks.

Incision rates

We calculate an unexpectedly rapid late Pleistocene incision rate of ~900 m/Ma for the mainstem Colorado River at Dewey Bridge by integrating three cycles of terrace formation since ~70 ka (Fig. 3.5). The Dewey Bridge reach is interpreted as being unaffected by salt tectonism because of its distance upstream from known salt structures (>15 km). The rate was determined from the best-fit line through central OSL ages from the entire dataset for each correlative terrace deposit versus survey data of their elevations above modern grade at Dewey Bridge.

TABLE 3.2 TOPOGRAPHIC METRICS OF STUDY AREA AND TRIBUTARY DRAINAGES

			slope (°)	steepness index (k_{sn})	
relief (m)	HI	R_{VA} (m)	mean	mean[a]	θ[b]
1232	0.37	190	26.4	9	0.41
1469	0.40	193	17.9	18	0.15
2535	0.36	226	19.8	21	0.33

[a] Calculated using reference concavity (θ_{ref}) of 0.35.
[b] Regressed concavity over entire tributary length.

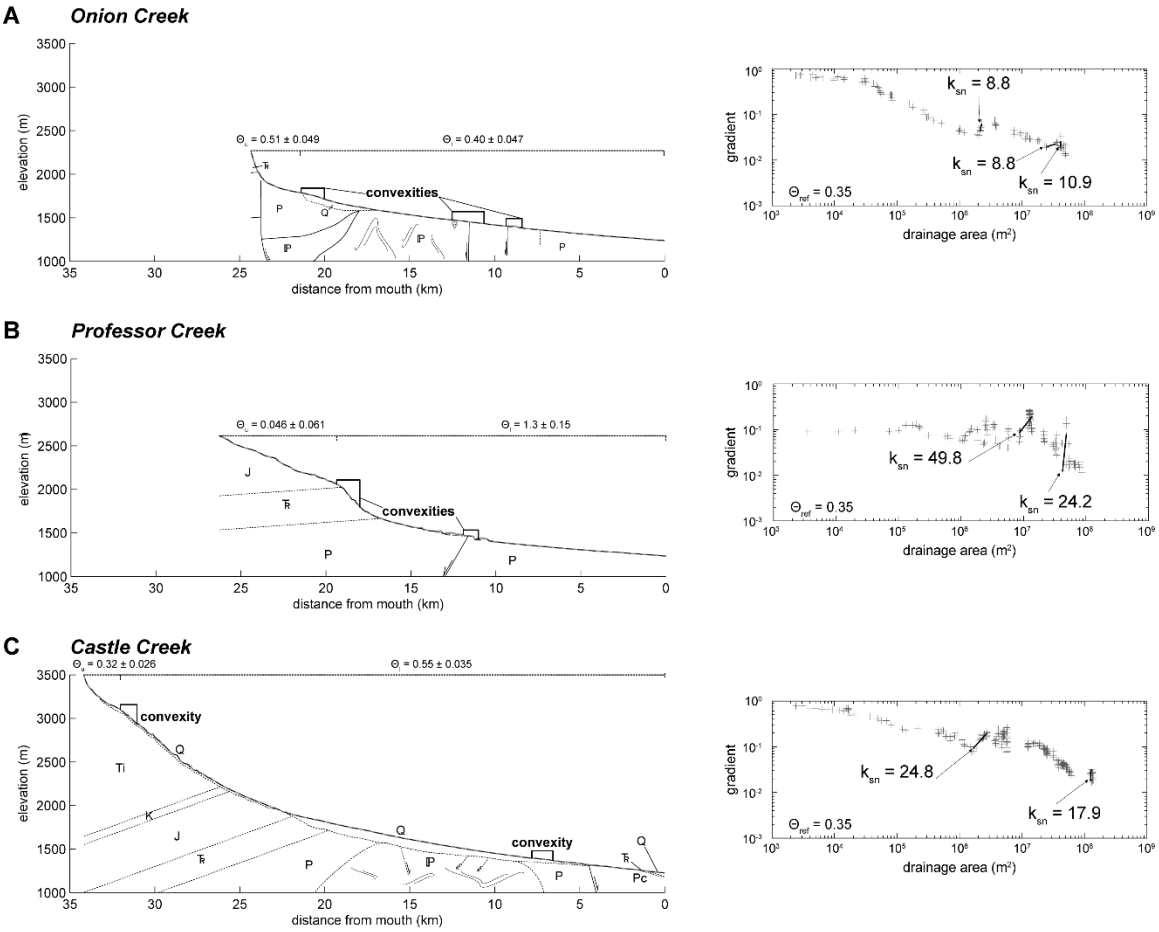

Figure 3.4. Longitudinal profiles of study area tributaries showing underlying geologic units. Slope-area diagrams (right) show select steepness indices (k_{sn}) and convexities (heavy black lines) associated with major knickzones labeled on profiles. Gray lines are raw profiles, dashed black lines are profiles predicted by best-fit regressions using reference concavity (θ_{ref}) of 0.35. Upper and lower profile concavities shown for each profile. Geologic units: Q - Quaternary surficial cover, Ti - Tertiary intrusive, K - Cretaceous, J - Jurassic, T_R - Triassic, P - Permian, lP - Pennsylvanian. (A) Onion Creek profile. The steepness indices of major knickzones in this drainage are an order of magnitude less than those of other study area tributary drainages. (B) Professor Creek profile, showing high steepness indices associated with transient signal or structural changes. (C) Castle Creek profile, showing knickzone in upper drainage associated with proglacial sediment-choked channel and concave lower reach overlying salt wall.

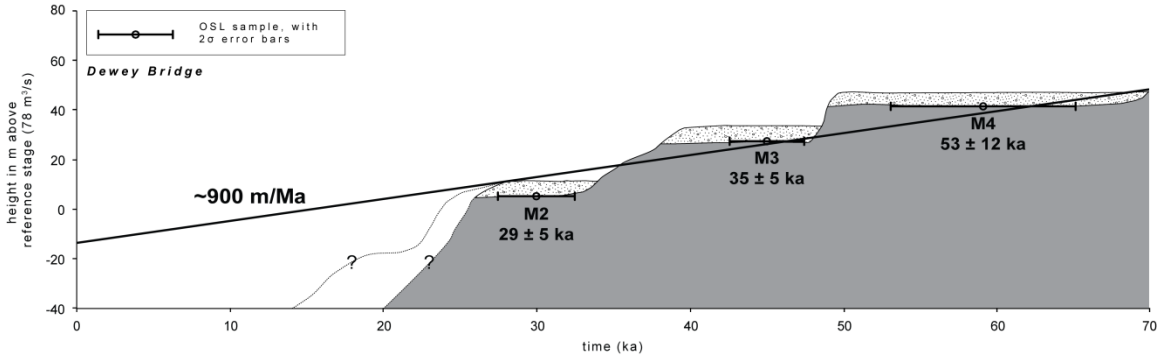

Figure 3.5. Integrated incision rate calculated from age and position of Dewey Bridge terraces. Thick bold line is best-fit to central OSL ages. Error bars are 2σ uncertainties for OSL ages of Dewey Bridge terrace deposits. Lateral extent of terraces is equivalent to the duration of time spent at a given grade based on the range of central ages from all OSL data for each correlative deposit. Dashed lines indicate uncertainties in extent of M2 deposit and depth to bedrock below modern channel.

DISCUSSION

Salt activity revealed by terrace markers

The impressive thickening of the youngest terrace deposits by ~15 m through Professor Valley and the Cache Valley graben is an expression of the apparent subsidence and deformation of their basal straths. A likely explanation for this pattern is salt activity that has occurred since ~70 ka, the OSL age obtained for the M4 deposit in the Cache Valley graben (Table 3.1). On a local scale, the back-tilted alluvium of the M4 deposit and its collapsed basal strath imply salt deformation due to dissolution of subsurface evaporites. Highly localized collapse is observed elsewhere in the northern Paradox Basin, where ring-faulted depressions are associated with thick basin fill deposits found in flanking drainages (Doelling, 2002; Gutiérrez, 2004).

We interpret broader, reach-scale subsidence as creating accommodation space in and on the flanks of the Cache Valley graben and Onion Creek diapir. Active diapirism in the Onion Creek drainage leads to subsidence of overburden rocks of the Permian Cutler Group at the distal margins of the structure. This activity results in increased vertical accommodation space up to ~8 km away from surface exposures of the Onion Creek diapir, as well as attendant thickening of Colorado River terraces and convergence of basal straths with the modern profile in the Professor Valley reach. This reach otherwise lacks surficial expressions of salt-related structures. Such subsidence could occur syn- and/or post-depositionally with regards to Colorado River sedimentation, though terrace deposits will develop an "inflated" geometry (Fig. 3.2) only if subsidence is syn-depositional. Thus, deformation likely occurred after deposition of the relatively thin M4 deposit and was ongoing during deposition of the M3 and M2 deposits.

Localized collapse deforms basal gravels of the M4-M2 terrace deposits in the Cache Valley graben. In this case, salt-related deformation is driven by dissolution of subsurface salts. Karstification occurs due to groundwater infiltration and removal of subsurface salts by the Colorado River. This results in deposition of terrace gravels into small ($\leq$3 km^2) collapse centers. Such local deformation is likely syn-depositional, given the thickness of mainstem gravel deposits here. Intriguingly, the normalized profile of the M3 deposit in Cache Valley graben diverges sharply from modern grade (Fig. 3.2). This could be due to localized upwarping and doming, such as that observed in the Onion Creek diapir, where salt flow is concentrated due to density and pressure differences on the flanks of the structure (e.g., Vendeville and Jackson, 1992).

Salt tectonism and other geomorphic controls in tributary drainages

The distribution of knickzones and k_{sn} values throughout the three tributary drainages suggests that each basin has undergone its own unique history with respect to movement of subsurface Paradox Basin evaporites. Onion Creek has experienced stream piracy and recapture spurred by localized uplift of the Onion Creek diapir (Colman, 1983; Balco and Stone, 2005), and the channel may have yet to completely respond to upwarping. Minor knickzones with k_{sn} = 9-11 are located at the downstream end of the diapir (Fig. 3.4A), with lower k_{sn} throughout the upstream profile. Low steepness indices along nearly the entire Onion Creek profile suggest ongoing adjustment of the drainage to salt activity at the surface.

Professor Creek has two knickzones (Fig. 3.4B), with the upper knickzone coinciding with weak shale of the Triassic Chinle Formation where it underlies the more resistant, cliff-forming Jurassic Wingate Sandstone. This knickzone could represent excavation of erodible Chinle sediments, creating a steep profile. Alternatively, it may be a transient signal related to Colorado River baselevel fall. The lower Professor Creek knickzone occurs at the intersection of the stream with a minor down-to-the-south normal fault, in the transfer zone between the Fisher Valley salt wall and the Cache Valley graben (Fig. 3.1). The origin and activity of this structure likely relates to halokinetic movement or folding (Doelling, 2002), though the knickzone could also be attributed to the juxtaposition of more resistant facies of the Cutler Group in the hanging wall against less resistant facies in the footwall.

To the south, Castle Creek features a knickzone in its upper drainage (Fig. 3.4C) that corresponds to a coarse, sediment-choked reach just below the Pleistocene glacial

terminus of ~2800 m (Doelling, 2001). Here, post-glacial mass movements and talus overload the channel with sediment. Any activity in the salt wall over which Castle Valley lies is not well-expressed, with moderate k_{sn} values (10-30) found in the middle and lower Castle Creek drainage. However, a comparatively high concavity ($\theta = 0.55$; Fig. 3.4C) of the lower profile may signal a response to subsidence along the northeast flank of the Castle Valley salt wall.

In summary, knickzones correspond to different lithologic and structural controls in each of the three study catchments, including salt activity. Importantly, although knickzones ultimately result from baselevel fall along the trunk Colorado River, they cannot be explicitly assigned to upstream migration of a distinct, ancient baselevel fall pulse on the trunk Colorado River (cf. Cook et al., 2009; Darling et al., 2012). During the upstream migration of baselevel fall through the Onion, Professor, and Castle profiles, these signals may have been differentially altered by drainage reorganization, salt tectonism, adjustment to varying bedrock lithologies and/or sediment loading, or some combination of these factors.

Incision and regional tectonism

The fast integrated incision rate calculated for the Dewey Bridge terrace suite of 900 m/Ma exceeds that predicted by the bull's-eye hypothesis (~400 m/Ma; Pederson et al., 2013). To address error associated with luminescence ages, we considered minimum and maximum ages of correlative deposits throughout the study area to constrain our incision rate to 750-1000 m/Ma. Regardless of this disparity with the bull's-eye prediction, the high rate may generally reflect flexural rebound of the central Colorado

Plateau due to erosional unloading. If this locally high rate represented a response to an upstream migrating pulse of incision due to salt-related subsidence in the Professor Valley and Cache Valley graben reaches below, we may expect to see concordant knickzones in tributary drainages. However, as alluded to above, knickzones are discordant in tributary drainages and can be explained by local geologic and/or geomorphic controls. If subsidence occurred only recently, we would expect the attendant accommodation space to be quickly filled, dampening an upstream migrating signal. Additionally, the hypothesis of an upstream migrating pulse of salt-related incision would require lower incision rates at Ida Gulch. However, preliminary rates there are estimated to be 750-900 m/Ma. Thus, rapid incision at Dewey Bridge does not appear to be salt-related.

The high incision rate at Dewey Bridge may result from a locally incomplete suite of terraces, as well as the relatively short timescale over which it is calculated. Poor age control on the M7 deposit and the absence of the M6 and M5 deposits are key data points missing in our calculation of an integrated late Pleistocene incision rate. Thus, our younger dataset does not resolve the hypothesized increase in Colorado Plateau incision rates after ~500 ka. Nevertheless, sedimentation of Dewey Bridge terraces spans two climate cycles (MIS 4/3, 3/2) and incision rates calculated from them can reasonably be expected to capture Milankovitch-scale oscillations of deposition and incision (Pederson et al., 2006). We therefore argue that the incision rate of ~900 m/Ma at Dewey Bridge is an accurate late Pleistocene rate for the Colorado River upstream of Moab.

It should be noted that there is an apparent increase in incision rates between the deposition of the M3 and M2 deposits at Dewey Bridge (Fig. 3.5). This increase results in

a rate of ~1650 m/Ma, and may be superimposed on the late Pleistocene increase in Colorado Plateau incision rates observed by Darling et al. (2012). Alternatively, the high rate may reflect particularly low sediment supply during late MIS 3, facilitating incision over the <10 ka interval.

Implications

Deformation resulting from tectonism of Paradox Basin salts has occurred over at least the past ~70 ka and is manifested in ~15 m of subsidence observed in the Professor Valley M3 strath, as well as an example of a locally deformed M4 strath and tilted deposits within the Cache Valley graben. Tributary profiles and topography indicate unique histories related to Quaternary salt dynamics and local bedrock or sediment loading controls. Finally, an integrated incision rate of ~900 m/Ma at Dewey Bridge is the fastest rate recorded in the Colorado Plateau and much greater than that hypothesized to accompany erosion-driven flexural rebound in the central plateau.

REFERENCES CITED

Balco, G., and Stone, J.O.H., 2005, Measuring middle Pleistocene erosion rates with cosmic-ray-produced nuclides in buried alluvial sediment, Fisher Valley, southeastern Utah: Earth Surface Processes and Landforms, v. 30, no. 8, p. 1051 -1067.

Black, B.D., and Hecker, S., compilers, 1999, Fault number 2474, Salt and Cache Valleys faults, *in* Quaternary fault and fold database of the United States: U.S. Geological Survey website, http://earthquake.usgs.gov/regional/qfaults, accessed Aug. 11, 2011.

Burbank, D.W., and Anderson, R.S., 2011, Tectonic geomorphology: Oxford, Wiley -Blackwell, 454 p.

Case, J.E., and Joesting, H.R., 1972, Regional geophysical investigations in the central Colorado Plateau: U.S. Geological Survey Professional Paper 736, 31 p.

Colman, S.M., 1983, Influence of the Onion Creek salt diapir on the late Cenozoic history of Fisher Valley, southeastern Utah: Geology, v. 11, no. 4, p. 240-243.

Cook, K.L., Whipple, K.X., Heimsath, A.M., and Hanks, T.C., 2009, Rapid incision of the Colorado River in Glen Canyon: Insights from channel profiles, local incision rates, and modeling of lithologic controls: Earth Surface Processes and Landforms, v. 34, p. 994-1010.

Darling, A.L., Karlstrom, K.E., Granger, D.E., Aslan, A., Kirby, E., Ouimet, W.B., Lazear, G.D., Coblentz, D.D., and Cole, R.D., 2012, New incision rates along the Colorado River system based on cosmogenic burial dating of terraces: Implications for regional controls on Quaternary incision: Geosphere, v. 8., no. 5, p. 1020-1041.

Doelling, H.H., 2001, Geologic map of the Moab and eastern part of the San Rafael Desert 30' by 60' quadrangles, Grand and Emery Counties, Utah, and Mesa County, Colorado: Utah Geological Survey Map 180, scale 1:100 000, 3 sheets.

Doelling, H.H., 2002, Geologic map of the Fisher Towers 7.5' quadrangle, Grand County, Utah: Utah Geological Survey Map 183, scale 1:24 000, 2 sheets, 22 p. text.

Doelling, H.H., Oviatt, C.G., and Huntoon, P.W., 1988, Salt deformation in the Paradox Basin: Utah Geological and Mineral Survey Bulletin 122, 93 p.

ESRI, 2011, ArcGIS Desktop: Release 10, Redlands, CA: Environmental Systems Research Institute.

Flint, J.J., 1974, Stream gradient as a function of order, magnitude, and discharge: Water Resources Research, v. 10, no. 5, p. 969-973.

Flowers, R.M., Wernicke, B.P., and Farley, K.A., 2008, Unroofing, incision, and uplift history of the southwestern Colorado Plateau from apatite (U-Th)/He thermochronometry: Geological Society of America Bulletin, v. 120, no. 5-6, p. 571-587.

Foxford, K.A., Walsh, J.J., Watterson, J., Garden, I.R., Guscott, S.C., and Burley, S.D., 1998, Structure and content of the Moab fault zone, Utah, USA, and its implications for fault seal prediction: *in* Jones, G., Fisher, Q.J., and Knipe, R.J., eds., Faulting, fault sealing and fluid flow in hydrocarbon reservoirs: London, Geological Society, Special Publication, v. 147, p. 87-103.

Frankel, K.L., and Pazzaglia, F.J., 2005, Tectonic geomorphology, drainage basin metrics, and active mountain fronts: Geografia Fisica e Dinamica Quaternaria (Testo stampato), v. 28, no. 1, p. 7-21.

Furuya, M., Mueller, K., and Wahr, J., 2007 Active salt tectonics in the Needles District, Canyonlands (Utah) as detected by interferometric synthetic aperture radar and point target analysis: 1992-2002: Journal of Geophysical Research, v. 112, B06418, doi:10.1029/2006JB004302.

Galbraith, R.F., Roberts, R.G., Laslett, G.M., Yoshida, H., and Olley, J.M., 1999, Optical dating of single and multiple grains of quartz from Jinmium Rock Shelter, Northern Australia: Part I experimental design and statistical models: Archaeometry, v. 41, no. 2, p. 339-364.

Gasparini, N.M., Whipple, K.X., and Bras, R.L., 2007, Predictions of steady state and transient landscape morphology using sediment-flux-dependent river incision models: Journal of Geophysical Research, v. 112, F03S09, doi:10.1029/2006JF000567.

Guérin, G., Mercier, N., and Adamiec, G., 2011, Dose-rate conversion factors: Update: Ancient TL, v. 29, n. 1, p. 5-8.

Gutiérrez, F., 2004, Origin of the salt valleys in the Canyonlands section of the Colorado Plateau: Geomorphology, v. 57, no. 3-4, p. 423-435.

Hack, J.T., 1957, Studies of longitudinal profiles in Virginia and Maryland: U.S. Geological Survey Professional Paper 294-B, 97 p.

Hack, J.T., 1973, Stream-profile analysis and stream-gradient index: Journal of Research of the U. S. Geological Survey, v. 1, p. 421-429.

Hazel Jr., J.E., 1994, Sedimentary response to intrabasinal salt tectonism in the Upper Triassic Chinle Formation, Paradox Basin, Utah: U.S. Geological Survey Bulletin 2000-F, 34 p.

Hoffman, M.D., 2009, Mio-Pliocene erosional exhumation of the central Colorado Plateau, eastern Utah: New insights from apatite (U-Th)/He thermochronometry [MS Thesis]: Lawrence, University of Kansas, 185 p.

Huntley, D.J., Godfrey-Smith, D.I., and Thewalt, M.L.W., 1985, Optical dating of sediments: Nature, v. 313, p. 105-107.

Huntoon, P.W., 1982, The Meander anticline, Canyonlands, Utah: An unloading structure resulting from horizontal gliding on salt: Geological Society of America Bulletin, v. 93, p. 941-950.

Karlstrom, K., and 24 others, 2012, Mantle-driven dynamic uplift of the Rocky Mountains and Colorado Plateau and its surface response: Toward a unified hypothesis: Lithosphere, v. 4, no. 1, p. 3-22.

Keller, E.A., Zepeda, R.L., Rockwell, T.K., Ku, T.L., and Dinklage, W.S., 1998, Active tectonics at Wheeler Ridge, southern San Joaquin Valley, California: Geological Society of America Bulletin, v. 110, no. 3, p. 298-310.

Kirby, E., and Whipple, K., 2001, Quantifying differential rock-uplift rates via stream profile analysis: Geology, v. 29, no. 5, p. 415-418.

Kirby, E., and Whipple, K.X., 2012, Expression of active tectonics in erosional landscapes: Journal of Structural Geology, v. 44, p. 54-75.

Kirby, E., Whipple, K., Tang, W., Cheng, Z., 2003, Distribution of rock uplift along the eastern margin of the Tibetan Plateau: inferences from bedrock channel longitudinal profiles: Journal of Geophysical Research, v. 108, no. B4, 2217, doi:10.1029/2001JB000861.

Lavé, J., and Avouac, J.P., 2000, Active folding of fluvial terraces across the Siwaliks Hills, Himalayas of central Nepal: Journal of Geophysical Research, v. 105, no. B3, p. 5735-5770.

Lee, J.P., Stockli, D.F., Kelley, S.A., Pederson, J.L., Karlstrom, K.E., and Ehlers, T.A., 2013, New thermochronometric constraints on the Tertiary landscape evolution of the central and eastern Grand Canyon, Arizona: Geosphere, v. 9, no. 2, p. 1-13.

Levander, A., Schmandt, B., Miller, M.S., Liu, K., Karlstrom, K.E., Crow, R.S., Lee, C. -T.A., and Humphreys, E.D., 2011, Continuing Colorado plateau uplift by delamination-style convective lithospheric downwelling: Nature, v. 472, p. 461 -465.

Liu, L., and Gurnis, M., 2010, Dynamic subsidence and uplift of the Colorado Plateau: Geology, v. 38, no. 7, p. 663-666, doi:10.1130/G30624.1.

Lucchitta, I., 1979, Late Cenozoic uplift of the southwestern Colorado Plateau and lower Colorado River region: Tectonophysics, v. 61, p. 63-95.

Mackin, J.H., 1948, Concept of the graded river: Geological Society of America Bulletin, v. 59, no. 5, p. 463-512.

McQuarrie, N., and Chase, C.G., 2000, Raising the Colorado Plateau: Geology, v. 28, no. 1, p. 91-94.

Merritts, D.J., Vincent, K.R., and Wohl, E.E., 1994, Long river profiles, tectonism, and eustasy: A guide to interpreting fluvial terraces: Journal of Geophysical Research, v. 99, p. 14031-14050.

Moucha, R., Forte, A.M., Rowley, D.B., Mitrovica, J.X., Simmons, N.A., and Grand S.P., 2009, Deep mantle forces and the uplift of the Colorado Plateau: Geophysical Research Letters, v. 36, L19310, doi:10.1029/2009GL039778.

Ouchi, S., 1985, Response of alluvial rivers to slow active tectonic movement: Geological Society of America Bulletin, v. 96, p. 504-515.

Pederson, J.L., and Tressler, C., 2012, Colorado River long-profile metrics, knickzones and their meaning: Earth and Planetary Science Letters, v. 345-348, p. 171-179.

Pederson, J.L., Mackley, R.D., and Eddleman, J.L., 2002, Colorado Plateau uplift and erosion evaluated using GIS: GSA Today, v. 12, no. 8, p. 4-10.

Pederson, J.L., Anders, M.D., Rittenour, T.M., Sharp, W.D., Gosse, J.C., and Karlstrom, K.E., 2006, Using fill terraces to understand incision rates and evolution of the Colorado River in eastern Grand Canyon: Journal of Geophysical Research, v. 111, F02003, doi:10.1029/2004JF000201.

Pederson, J.L., Cragun, W.S., Hidy, H.J., Rittenour, T.M., and Gosse, J.C., 2013, Colorado River chronostratigraphy at Lees Ferry, Arizona and the central Colorado Plateau bull's-eye of incision: Geology, v. 40, doi:10.1130/G34051.1.

Pevear, D.R., Vrolijk, P.J., and Longstaffe, F.J., 1997, Timing of Moab Fault displacement and fluid movement integrated with burial history using radiogenic and stable isotopes: *in* Hendry, J., Carey, P., Parnell, J., Ruffell, A., Worden, R., eds., Geofluids II '97: Contributions to the second international conference on fluid evolution, migration and interaction in sedimentary basins and orogenic belts: Belfast, p. 42-45.

Powell, J.W., 1876, Exploration of the Colorado River of the West: Smithsonian Institution, Washington, D.C., 291 p.

Roy, M., Jordan, T.H., and Pederson, J., 2009, Colorado Plateau magmatism and uplift by warming of heterogeneous lithosphere: Nature, v. 459, no. 7249, p. 978-982, doi:10.1038/nature08052.

Smith, D., and Levy, S., 1976, Petrology of Green Knobs diatreme, New Mexico, and implications for the mantle below the Colorado Plateau: Earth and Planetary Science Letters, v. 19, p. 107-125.

Snyder, N.P., Whipple, K.X., Tucker, G.E., and Merritts, D.J., 2000, Landscape response to tectonic forcing: Digital elevation model analysis of stream profiles in the Mendocino triple junction region, northern California: Geological Society of America Bulletin, v. 112, no. 8, p. 1250-1263.

Spencer, J. E., 1996, Uplift of the Colorado Plateau due to lithospheric attenuation during Laramide low-angle subduction: Journal of Geophysical Research, v. 101, p. 13595-13609.

Strahler, A.N., 1952, Hypsometric (area-altitude) analysis of erosional topography: Geological Society of America Bulletin, v. 63, p. 1117-1142.

Trudgill, B.D., 2011, Evolution of salt structures in the northern Paradox Basin: controls on evaporite deposition, salt wall growth and supra-salt stratigraphic architecture: Basin Research, v. 23, no. 2, p. 208-238.

Vendeville, B.C., and Jackson, M.P.A., 1992, The rise of diapirs during thin-skinned extension: Marine and Petroleum Geology, v. 9, p. 331-353.

Whipple, K.X., and Tucker, G.E., 1999, Dynamics of the stream-power river incision model: Implications for height limits of mountain ranges, landscape response timescales, and research needs: Journal of Geophysical Research, v. 104, p. 17661-17674.

Wobus, C., Whipple, K.X., Kirby, E., Snyder, N., Johnson, J., Spyropolou, K., Crosby, B., and Sheehan, D., 2006, Tectonics from topography: Procedures, promise, and pitfalls: *in* Willett, S.D., Hovius, N., Brandon, M.T., Fisher, D.M., eds., Tectonics, climate, and landscape evolution: Geological Society of America Special Paper, v. 398, p. 55-74.

Wolinsky, M.A., and Pratson, L.F., 2005, Constraints on landscape evolution from slope histograms: Geology, v. 33, no. 6, p. 477-480.

CHAPTER 4

SUMMARY

This thesis includes two core chapters representing related studies centered on late Pleistocene Colorado River terraces and the geomorphologic implications of salt tectonism upstream of Moab, Utah, USA. These chapters are summarized below.

Controls on the formation of Colorado River terraces

Mainstem terrace deposits in the study area represent one of the best-preserved suites of Colorado River terraces that have been intensively studied in the Colorado Plateau. Study area terrace gravels were deposited during MIS 5-3. Terraces formed during MIS 4/early MIS 3 (M4 deposit) and mid-MIS 3 (M3) are time-correlative across the plateau, although they exhibit varying landscape position. Older deposits formed during MIS 5 and latest MIS 3/MIS 2 have no clear correlative deposits across the plateau. These results suggest the possibility of transient sedimentation in the Colorado River system over the late Pleistocene.

Our chronostratigraphy of Colorado River terraces reveals two modes of sedimentation that interrupt the background mode of incision. The first condition results in sedimentation linked to the build-up to and height of major glaciations (e.g., MIS 4, latest MIS 3/MIS 2) in the Rocky Mountain headwaters. The second condition results in sedimentation during intervals of highly variable climate (e.g., mid-MIS 3), when sediment delivery from local tributaries of the plateau drylands and canyons is enhanced by high intensity, low frequency runoff and disturbance to hillslope vegetation maintaining sediment. These intervals are marked by concordant increases in the

proportion of locally-derived gravel clasts, and coincide with millennial-scale climate variability. Climate controls are the ultimate drivers of terrace formation in the study area, but local salt tectonism may partly account for the high number (6) of late Pleistocene terraces observed upstream of Moab.

Terrace type and form are controlled by valley-bottom geometry and salt tectonism in the study area. Restricted upstream canyon reaches feature thin strath terrace deposits, whereas broad, downstream valley reaches feature thick packages of fill terrace deposits. We suggest that the greater local thickness of downstream deposits results from an increase in accommodation space formed in response to salt-related subsidence and localized collapse occurring both syn- and post-depositionally.

Quaternary salt deformation and incision along the Colorado River

Using the chronostratigraphy for the youngest flight of terraces as well as spatial analyses of tributary catchment morphology, we document evidence of salt-related deformation in the study area during the late Quaternary. Unexpectedly thick terrace deposits with irregular basal strath elevations signal deformation since ~70 ka by both reach-scale subsidence and local collapse related ultimately to the movement or dissolution of late Paleozoic Paradox Basin evaporites. Salt-related deformation has resulted in ~15 m of deformation of Colorado River terrace deposits in Professor Valley, and 11-13º of tilting of piedmont deposits associated with the M4 gravel in the Cache Valley graben.

The k_{sn} steepness index and profile concavity were calculated for stream-profiles of three study area tributaries. Along with the distribution of knickzones within each

catchment, these metrics demonstrate distinct patterns of topographic development in response to salt tectonism, as well as bedrock, drainage reorganization, and other controls. Disparate mean k_{sn} values and concavities reflect the relative adjustment of each tributary to these factors, with recent salt-related activity apparent in the k_{sn} values and knickzones distributions of Onion and Professor creeks, as well as the comparatively high concavity of the lower Castle Creek profile.

Finally, an unexpectedly rapid incision rate of ~900 m/Ma was determined for the mainstem Colorado River at Dewey Bridge. This is the highest rate calculated in the Colorado Plateau, if not the interior western United States. It significantly exceeds values predicted by the hypothesized bull's-eye pattern of regional incision, though it is still consistent with the strong positive feedback of erosion-driven flexural rebound. It may also reflect an increase in mainstem incision during the late Pleistocene as interpreted elsewhere in the Colorado Plateau.

Future work

Further efforts toward resolving the formation of Colorado River terraces above Moab should focus on a refined geochronology of these deposits. Additional luminescence dating paired with terrestrial cosmogenic dating of terrace gravels would clarify the timing of formation of older deposits such as the M7, M6, and M5 gravels, some or all of which may belong to the same overall aggradation event sometime ~100-75 ka. Single-grain luminescence dating could enhance the precision of OSL dates for older deposits, and the recently developed technique of isochron cosmogenic dating is particularly useful for terrace gravels in dryland settings. Improved geochronology will

permit accurate, updated mapping of late Pleistocene terrace landforms and associated piedmont deposits in this area. Additionally, the identification of glacial-interglacial climate drivers of terrace formation would greatly benefit from the use of cosmogenic nuclides to calculate paleo-erosion rates and sediment yield in the headwaters of the Colorado River.

The influence of salt tectonism on fluvial activity in the Paradox Basin can be further illuminated through the use of geophysical techniques such as reflection seismology and the use of remote sensing methods such as light detection and ranging (LIDAR) or interferometric synthetic aperture radar (InSAR). Seismology should resolve the exact location of salt bodies, corroborating or updating gravity surveys completed in the 1970s. Remote sensing will reveal precise ground movement related to subsurface salt dynamics, as has already been accomplished in the Canyonlands area using InSAR.

Together, further geochronologic and geophysical efforts will allow researchers to develop analogues for terrace formation and the influence of salt activity upstream of Moab over the late Pleistocene and perhaps earlier in the Quaternary. Future research in this area is critical to understanding the geomorphic evolution of large river systems that are subject to both climatic and tectonic drivers throughout their profiles.

APPENDICES

Appendix A. Optically stimulated luminescence (OSL) data

TABLE A.1 SUMMARY OF PRELIMINARY OSL AGE CONTROL FOR COLORADO RIVER TERRACE DEPOSITS

Deposit[a]	Sample[b]	USU Sample #	Lat/Long	Elev. (m)	Depth (m)	# Aliquots	Dose Rate, Gy/ka	Equivalent Dose (D_e), Gy (overdispersion, %)	OSL Age, ka[c]
M2	AJ-DB-T2A	USU-1075	38.81°N, 109.31°W	1260	1.7	13 (29)	3.42 ± 0.18	98.63 ± 15.54 (22.5)	29 ± 5
M2	AJ-HB-M2	USU-1195	38.76°N, 109.32°W	1253	2.8	16 (19)	3.56 ± 0.20	121.82 ± 15.83 (23.4)	34 ± 6
M2	AJ-CVG-T2Au	USU-1073	38.71°N, 109.39°W	1237	2.5	23 (30)	2.81 ± 0.15	75.04 ± 13.73 (39.7)	27 ± 6
M3	AJ-DB-T3	USU-1078	38.81°N, 109.30°W	1273	1.8	12 (31)	3.54 ± 0.19	124.85 ± 13.08 (0.0)	35 ± 5[d]
M3	AJ-HB-M3	USU-1196	38.76°N, 109.32°W	1265	1.5	5 (5)	5.07 ± 0.29[e]	197.55 ± 20.33 (5.5)	39 ± 5[e]
M3	AJ-PV-T3usAu	USU-1072	38.76°N, 109.34°W	1262	3.0	17 (30)	3.12 ± 0.14[f]	137.10 ± 24.00 (33.5)	~44[f]
M3	AJ-PV-T3uAu	USU-1076	38.75°N, 109.34°W	1258	3.0	20 (28)	3.21 ± 0.17	170.34 ± 26.76 (32.5)	53 ± 10
M3	AJ-PV-T3lAu	USU-1077	38.75°N, 109.34°W	1256	8.0	4 (5)	2.62 ± 0.64	114.70 ± 18.66 (8.8)	37 ± 6
M3	AJ-IG-T3g	USU-1074	38.69°N, 109.41°W	1251	1.5	19 (25)	3.25 ± 0.17	133.92 ± 20.87 (31.0)	41 ± 8
M4	AJ-DB-M4	USU-1336	38.82°N, 109.31°W	1288	1.5	18 (31)	3.12 ± 0.16	164.44 ± 32.98 (40.0)	53 ± 12
M4	AJ-CVG-M3o	USU-1200	38.71°N, 109.40°W	1273	9.4	12 (28)	3.15 ± 0.17	218.59 ± 48.76 (34.1)	69 ± 17
M4	AJ-IG-M3	USU-1280	38.69°N, 109.41°W	1264	8.0	18 (35)	3.40 ± 0.19	197.86 ± 21.90 (20.3)	58 ± 9
M5	AJ-PV-M4B	USU-1198	38.73°N, 109.37°W	1284	2.0	16 (26)	2.88 ± 0.15	142.16 ± 28.38 (35.6)	52 ± 12[d]
M6	AJ-IG-M5	USU-1279	38.69°N, 109.41°W	1294	1.5	19 (33)	2.64 ± 0.14	196.80 ± 43.43 (45.4)	75 ± 18
M7	AJ-PV-M4	USU-1197	38.75°N, 109.36°W	1307	2.3	10 (15)	2.71 ± 0.14	222.46 ± 78.02 (49.7)	84 ± 31

[a] Organized by stratigraphic position; "M" is mainstem Colorado River deposit.
[b] DB = Dewey Bridge, HB = Hittle Bottom, PV = Professor Valley, CVG = Cache Valley graben, IG = Ida Gulch.
[c] Reported ages with 2σ error.
[d] Sample corrected for falling $D_e(t)$ using early background subtraction.
[e] Age calculated from infrared luminescence performed on feldspar grains.
[f] Mean dose rate of other samples used due to erroneously high chemistry results (see Chapter 2); age is only an estimate.

TABLE A.2 SUMMARY OF OSL DOSE RATE INFORMATION FOR COLORADO RIVER TERRACE DEPOSITS[a]

Deposit	Sample	USU Sample #	Grain size fraction (μm)	U (ppm)[b]	Th (ppm)[b]	%K[b]	Rb (ppm)[b]	Cosmic (Gy/ka)[c]	Dose Rate, (Gy/ka)[d]
M2	AJ-DB-T2A	USU-1075	150-250	2.4 ± 0.2	8.2 ± 0.7	2.22 ± 0.06	91.9 ± 3.7	0.21 ± 0.02	3.42 ± 0.18
M2	AJ-HB-M2	USU-1195	75-125	5.0 ± 0.4	8.6 ± 0.8	1.74 ± 0.04	69.0 ± 2.8	0.18 ± 0.02	3.56 ± 0.20
M2	AJ-CVG-T2Au	USU-1073	150-250	2.5 ± 0.2	8.0 ± 0.7	1.59 ± 0.04	69.3 ± 2.8	0.19 ± 0.02	2.81 ± 0.15
M3	AJ-DB-T3	USU-1078	90-150	3.6 ± 0.3	9.3 ± 0.8	1.90 ± 0.05	67.2 ± 2.7	0.21 ± 0.02	3.54 ± 0.19
M3	AJ-HB-M3	USU-1196	90-180	2.5 ± 0.2	9.5 ± 0.9	1.90 ± 0.05	80.1 ± 3.2	0.22 ± 0.02	5.07 ± 0.29[e]
M3	AJ-PV-T3usAu	USU-1072	90-150	20.9 ± 1.5[f]	9.9 ± 0.9	2.26 ± 0.06	88.0 ± 3.5	0.18 ± 0.02	3.12 ± 0.14
M3	AJ-PV-T3uAu	USU-1076	75-150	2.8 ± 0.2	10.4 ± 0.9	1.69 ± 0.04	74.0 ± 3.0	0.18 ± 0.02	3.21 ± 0.17
M3	AJ-PV-T3lAu	USU-1077	180-250	2.3 ± 0.2	9.8 ± 0.9	1.96 ± 0.05	79.1 ± 3.2	0.10 ± 0.01	2.62 ± 0.64[g]
M3	AJ-IG-T3g	USU-1074	150-250	2.9 ± 0.2	6.5 ± 0.6	2.04 ± 0.05	68.9 ± 2.8	0.22 ± 0.02	3.25 ± 0.17
M4	AJ-DB-M4	USU-1336	125-250	2.6 ± 0.2	6.7 ± 0.6	1.94 ± 0.05	76.7 ± 3.1	0.22 ± 0.02	3.12 ± 0.16
M4	AJ-CVG-M3o	USU-1200	75-150	3.2 ± 0.2	8.8 ± 0.8	1.74 ± 0.04	73.6 ± 2.9	0.09 ± 0.01	3.15 ± 0.17
M4	AJ-IG-M3	USU-1280	75-125	3.7 ± 0.3	11.0 ± 1.0	1.71 ± 0.04	69.1 ± 2.8	0.10 ± 0.01	3.40 ± 0.19
M5	AJ-PV-M4B	USU-1198	150-250	2.6 ± 0.2	6.8 ± 0.6	1.71 ± 0.04	62.9 ± 2.5	0.20 ± 0.02	2.88 ± 0.15
M6	AJ-IG-M5	USU-1279	150-250	2.5 ± 0.2	5.4 ± 0.5	1.57 ± 0.04	56.9 ± 2.3	0.22 ± 0.02	2.64 ± 0.14
M7	AJ-PV-M4	USU-1197	180-250	2.5 ± 0.2	5.8 ± 0.5	1.64 ± 0.04	57.2 ± 2.3	0.20 ± 0.02	2.71 ± 0.14

[a] Radioelemental concentrations by ICP-MS and ICP-AES at ALS Chemex, dose rate using conversion factors in Aitken (1985), Adamiec and Aitken (1998).
[b] Errors on concentration values are based on detection limits and follow those described in Rittenour et al. (2005).
[c] Contribution of cosmic radiation to dose rate is calculated using sample depth, elevation, and lat/long following Prescott and Hutton (1994).
[d] Dose rate was calculated assuming a 2.0 g/cm3 sample density, 3 ± 3% water content (except USU-1077; see footnote g), and reported grain size.
[e] Age calculated from infrared luminescence performed on feldspar grains.
[f] Uranium content averaged from ALS Chemex analyses and additional analyses at USGS Luminescence Dating Laboratory, Denver, CO.
[g] Saturated water content of 20% assumed due to local reduction.

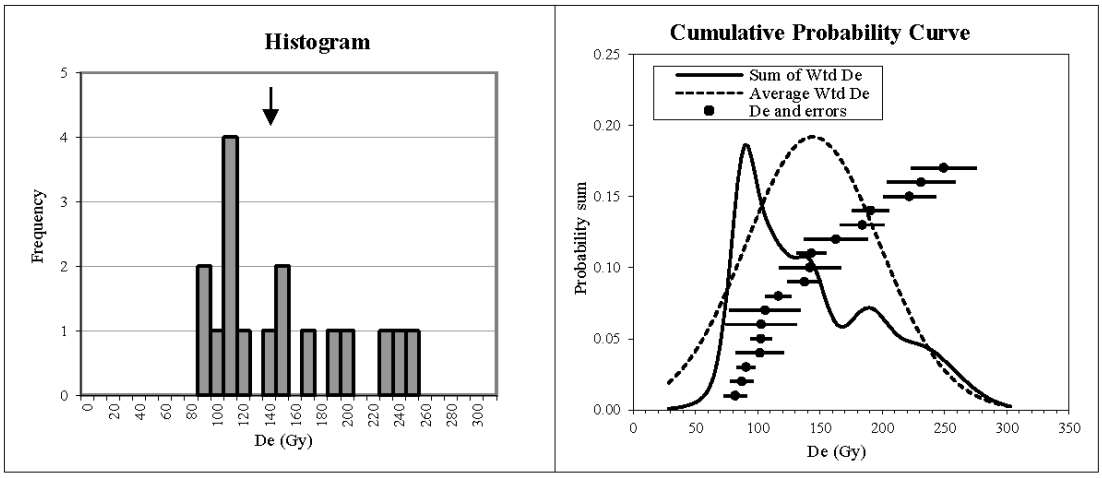

Sample #	Sample Location				Individual Aliquot Data			
USU-1072	Professor Valley, UT							
	De (Gy)	±	Age (ka)	±	De (Gy)	±	Age (ka)	±
CAM =	**137.10**	**53.78**	**17.29**	**3.54**	81.90	9.34	10.33	2.11
					87.19	9.07	10.99	2.25
					90.51	7.33	11.41	2.33
Median =	137.52		17.3	3.5	101.73	19.21	12.83	2.62
Min =	81.90		10.3	2.1	102.43	8.49	12.92	2.64
Max =	249.26		31.4	6.4	102.77	28.60	12.96	2.65
					105.85	28.40	13.35	2.73
n =	**17**	**Aliquots**			116.51	10.12	14.69	3.01
					137.52	13.76	17.34	3.55
S.D. =	53.78				142.00	25.06	17.91	3.66
Standard error =	13.04				142.92	11.85	18.02	3.69
Random Errors=	17.88	%			162.68	25.42	20.51	4.20
Systematic Error=	9.94	%			184.02	17.80	23.20	4.75
Total Error=	20.46	%			190.66	14.79	24.04	4.92
					221.81	21.11	27.97	5.72
Bin Width =	10.00	**Gy**			231.17	27.15	29.15	5.96
					249.26	26.28	31.43	6.43
Overdispersion (%) =	33.5	±	6.6					

		+/-	
dose rate=	**7.93**	**0.47**	**Gy/ka**
U =	20.87	1.5	**ppm**
Th =	9.90	0.9	**ppm**
K2O =	2.26	0.06	**wt. %**
Rb2O=	88.0	3.5	**ppm**
H2O=	3.0	3.0	**wt. %**
Cosmic=	0.18	**Gy/ka**	
depth =	3.0	**m**	
latitude=	38.76	**degrees (north positive)**	
longitude=	-109.34	**degrees (east positive)**	
elevation=	1.26	**km asl**	

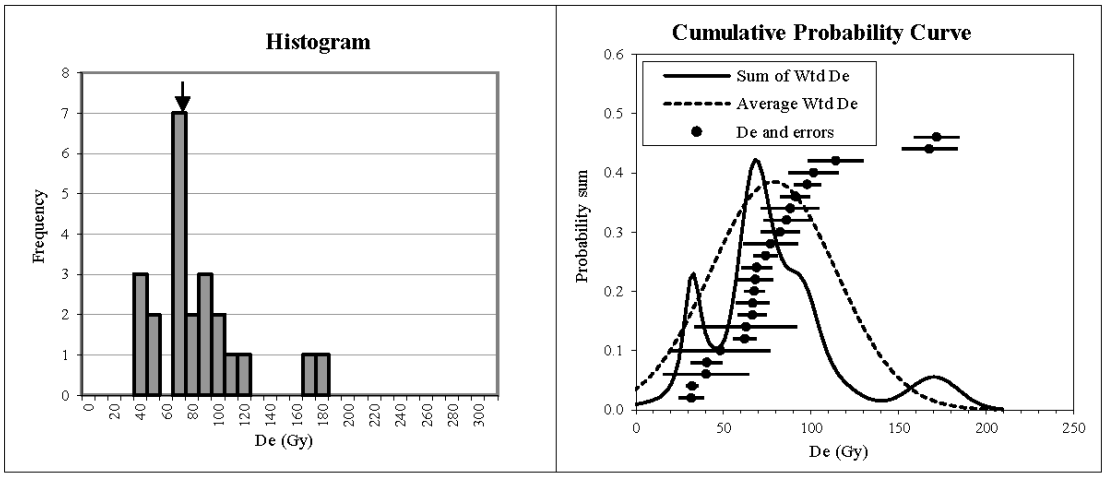

Sample #	Sample Location				Individual Aliquot Data			
USU-1073	Cache Valley graben, UT							
	De (Gy)	±	Age (ka)	±	De (Gy)	±	Age (ka)	±
CAM =	**75.04**	**35.98**	**26.72**	**5.57**	31.46	6.98	11.20	2.34
					32.02	3.64	11.40	2.38
					39.92	24.68	14.22	2.96
Median =	68.92		24.5	5.1	40.40	8.97	14.39	3.00
Min =	31.46		11.2	2.3	47.99	28.48	17.09	3.56
Max =	171.71		61.1	12.7	62.14	6.47	22.13	4.61
					62.82	29.30	22.37	4.66
n =	**23**	**Aliquots**			66.53	8.21	23.69	4.94
					66.67	9.46	23.74	4.95
S.D. =	35.98				67.53	5.75	24.05	5.01
Standard error =	7.50				68.08	10.04	24.24	5.05
Random Errors=	18.48	%			68.92	8.66	24.54	5.11
Systematic Error=	9.64	%			74.07	6.87	26.37	5.50
Total Error=	20.84	%			76.81	15.38	27.35	5.70
					82.24	11.10	29.29	6.10
Bin Width =	10.00	**Gy**			86.06	13.06	30.64	6.39
					88.05	16.68	31.35	6.53
Overdispersion (%) =	39.7	±	6.9		91.02	8.39	32.41	6.76
					97.72	7.64	34.80	7.25
		+/-			101.44	14.40	36.12	7.53
dose rate=	**2.81**	**0.15**	**Gy/ka**		114.06	15.75	40.62	8.47
U =	2.50	0.2	**ppm**		167.54	15.79	59.66	12.43
Th =	8.00	0.7	**ppm**		171.71	12.96	61.14	12.74
K2O =	1.59	0.04	**wt. %**					
Rb2O=	69.3	2.8	**ppm**					
H2O=	3.0	3.0	**wt. %**					
Cosmic=	0.19	**Gy/ka**						
depth =	2.5	**m**						
latitude=	38.71	**degrees (north positive)**						
longitude=	-109.39	**degrees (east positive)**						
elevation=	1.24	**km asl**						

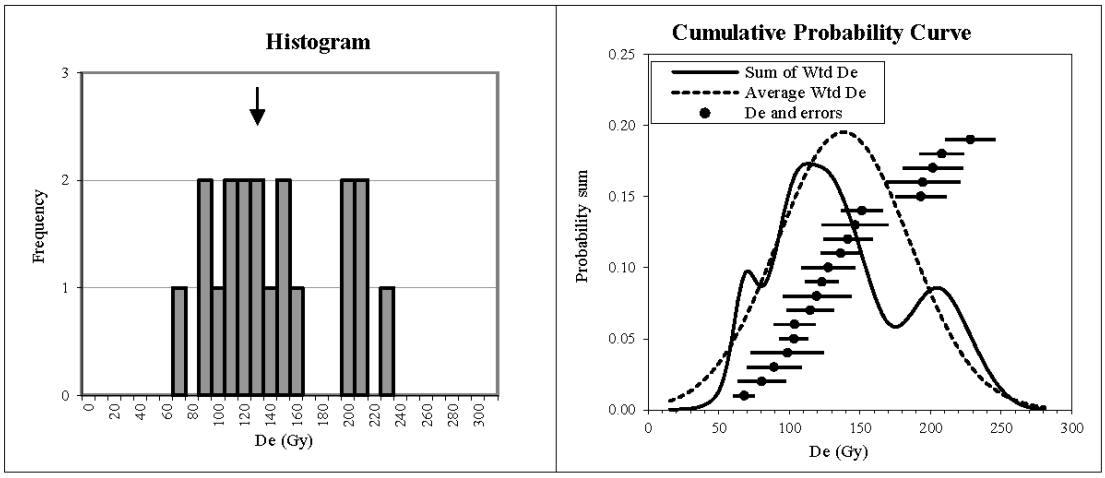

Sample #	Sample Location				Individual Aliquot Data			
USU-1074	Ida Gulch, UT							
	De (Gy)	±	Age (ka)	±	De (Gy)	±	Age (ka)	±
CAM =	**133.92**	**46.80**	**41.17**	**7.62**	67.84	7.35	20.86	3.86
					80.31	17.02	24.69	4.57
					89.08	19.19	27.39	5.07
Median =	127.38		39.2	7.2	98.66	25.90	30.33	5.61
Min =	67.84		20.9	3.9	103.25	10.12	31.74	5.87
Max =	228.26		70.2	13.0	103.60	14.94	31.85	5.89
					114.78	16.47	35.29	6.53
n =	**19**	**Aliquots**			119.38	24.20	36.70	6.79
					123.07	11.91	37.84	7.00
S.D. =	46.80				127.38	18.76	39.16	7.25
Standard error =	10.74				136.24	14.25	41.89	7.75
Random Errors=	15.76	%			141.39	17.21	43.47	8.04
Systematic Error=	9.70	%			146.46	23.66	45.03	8.33
Total Error=	18.51	%			151.44	14.53	46.56	8.62
					193.24	18.06	59.41	10.99
Bin Width =	10.00	Gy			194.61	26.24	59.83	11.07
					201.61	21.15	61.98	11.47
Overdispersion (%) =	31.0	±	6.0		208.07	15.69	63.97	11.84
					228.26	17.82	70.18	12.99

		+/-	
dose rate=	**3.25**	**0.17**	**Gy/ka**
U =	2.90	0.2	**ppm**
Th =	6.50	0.6	**ppm**
K2O =	2.04	0.05	**wt. %**
Rb2O=	68.9	2.8	**ppm**
H2O=	3.0	3.0	**wt. %**
Cosmic=	0.22	**Gy/ka**	
depth =	1.5	**m**	
latitude=	38.69	**degrees (north positive)**	
longitude=	-109.41	**degrees (east positive)**	
elevation=	1.25	**km asl**	

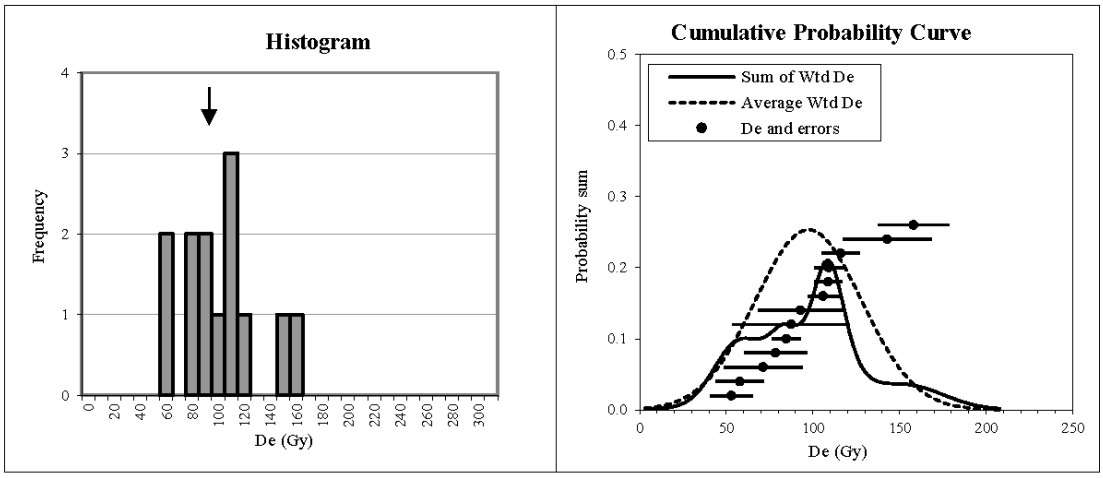

Sample #	Sample Location				Individual Aliquot Data			
USU-1075	Dewey Bridge, UT							
	De (Gy)	±	Age (ka)	±	De (Gy)	±	Age (ka)	±
CAM =	**98.63**	**30.73**	**28.81**	**5.38**	52.87	12.06	15.44	2.88
					57.70	13.97	16.86	3.15
					71.28	22.70	20.82	3.89
Median =	92.82		27.1	5.1	78.36	18.01	22.89	4.27
Min =	52.87		15.4	2.9	84.67	8.38	24.73	4.62
Max =	158.18		46.2	8.6	87.40	33.80	25.53	4.77
					92.82	24.65	27.12	5.06
n =	**13**	**Aliquots**			105.96	9.03	30.95	5.78
					108.75	7.96	31.77	5.93
S.D. =	30.73				109.13	8.29	31.88	5.95
Standard error =	8.52				116.02	10.83	33.89	6.33
Random Errors=	15.93	%			142.85	25.57	41.73	7.79
Systematic Error=	9.74	%			158.18	20.48	46.21	8.63
Total Error=	18.67	%						
Bin Width =	10.00	**Gy**						
Overdispersion (%) =	22.5	±	6.6					

		+/-	
dose rate=	**3.42**	**0.18**	**Gy/ka**
U =	2.40	0.2	**ppm**
Th =	8.20	0.7	**ppm**
K2O =	2.22	0.06	**wt. %**
Rb2O=	91.9	3.7	**ppm**
H2O=	3.0	3.0	**wt. %**
Cosmic=	0.21	**Gy/ka**	
depth =	1.7	**m**	
latitude=	38.81	**degrees (north positive)**	
longitude=	-109.31	**degrees (east positive)**	
elevation=	1.26	**km asl**	

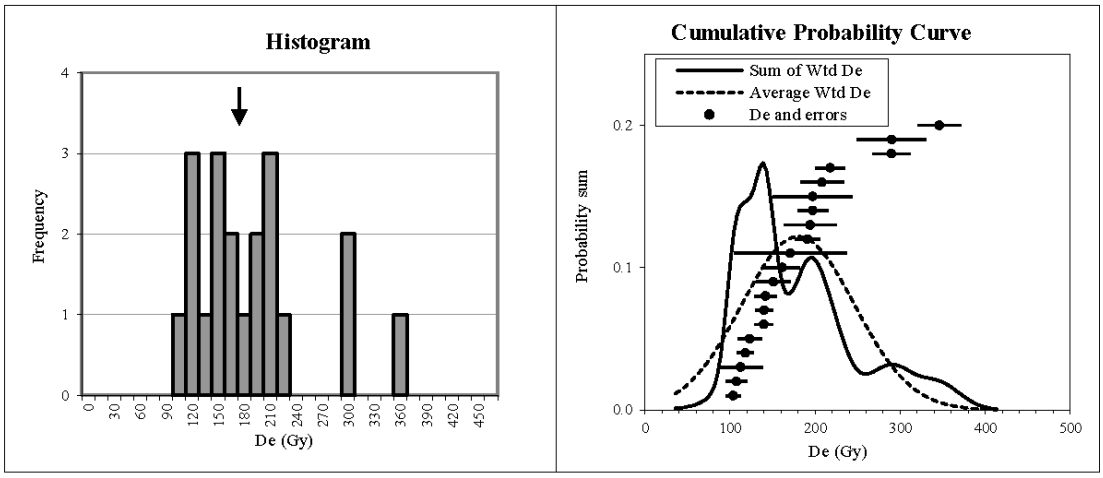

Sample #	Sample Location				Individual Aliquot Data			
USU-1076	Professor Valley, UT							
	De (Gy)	±	Age (ka)	±	De (Gy)	±	Age (ka)	±
CAM =	**170.34**	**66.32**	**53.08**	**9.89**	103.44	8.76	32.23	6.01
					107.49	12.53	33.49	6.24
					112.15	26.68	34.95	6.51
Median =	166.15		51.8	9.7	117.99	9.54	36.77	6.85
Min =	103.44		32.2	6.0	123.05	14.30	38.35	7.15
Max =	345.89		107.8	20.1	139.49	10.91	43.47	8.10
					139.85	10.34	43.58	8.12
n =	**20**	**Aliquots**			141.55	13.29	44.11	8.22
					150.79	19.75	46.99	8.76
S.D. =	66.32				161.39	20.47	50.29	9.37
Standard error =	14.83				170.91	66.23	53.26	9.93
Random Errors=	15.95	%			190.98	14.47	59.51	11.09
Systematic Error=	9.64	%			194.12	30.54	60.49	11.28
Total Error=	18.64	%			197.22	17.65	61.46	11.46
					197.29	46.63	61.48	11.46
Bin Width =	15.00	**Gy**			208.12	25.54	64.85	12.09
					217.56	17.34	67.80	12.64
Overdispersion (%) =	32.5	±	5.9		289.64	21.88	90.26	16.82
					289.98	40.65	90.36	16.84
		+/-			345.89	25.41	107.79	20.09
dose rate=	**3.21**	**0.17**	**Gy/ka**					
U =	2.80	0.2	**ppm**					
Th =	10.40	0.9	**ppm**					
K2O =	1.69	0.04	**wt. %**					
Rb2O=	74.0	3.0	**ppm**					
H2O=	3.0	3.0	**wt. %**					
Cosmic=	0.18	**Gy/ka**						
depth =	3.0	**m**						
latitude=	38.75	**degrees (north positive)**						
longitude=	-109.34	**degrees (east positive)**						
elevation=	1.26	**km asl**						

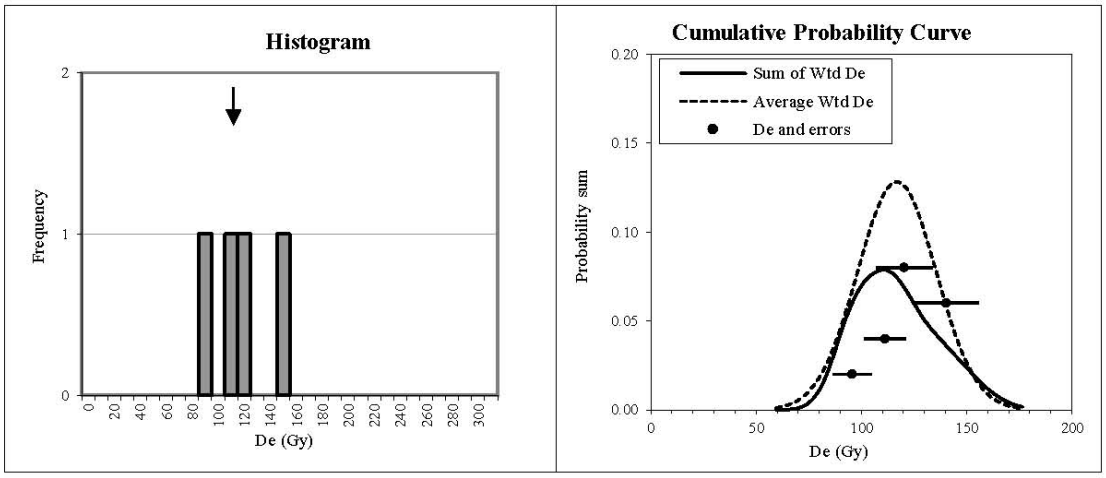

Sample #	Sample Location				Individual Aliquot Data			
USU-1077	Professor Valley, UT							
	De (Gy)	±	Age (ka)	±	De (Gy)	±	Age (ka)	±
CAM =	**114.70**	**18.66**	**43.84**	**12.79**	95.60	9.36	36.54	10.66
					111.15	10.01	42.48	12.40
					120.27	13.30	45.97	13.41
Median =	115.71		44.2	12.9	140.27	15.48	53.61	15.65
Min =	95.60		36.5	10.7				
Max =	140.27		53.6	15.6				

n =	**4**	**Aliquots**
S.D. =	18.66	
Standard error =	9.33	
Random Errors=	13.73	%
Systematic Error=	25.75	%
Total Error=	29.18	%
Bin Width =	10.00	**Gy**
Overdispersion (%) =	8.8 ±	7.2

		+/-	
dose rate=	**2.62**	**0.64**	**Gy/ka**
U =	2.30	0.2	**ppm**
Th =	9.75	0.9	**ppm**
K2O =	1.96	0.05	**wt. %**
Rb2O=	79.1	3.2	**ppm**
H2O=	20.0	20.0	**wt. %**
Cosmic=	0.10	**Gy/ka**	
depth =	8.0	**m**	
latitude=	38.75	**degrees (north positive)**	
longitude=	-109.34	**degrees (east positive)**	
elevation=	1.26	**km asl**	

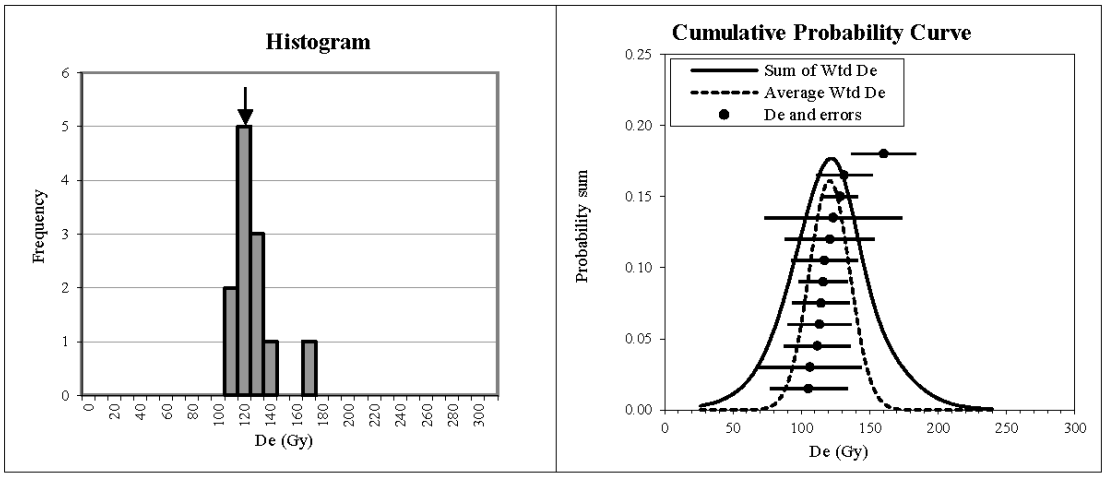

Sample #	Sample Location				Individual Aliquot Data			
USU-1078	Dewey Bridge, UT							
	De (Gy)	±	Age (ka)	±	De (Gy)	±	Age (ka)	±
CAM =	**124.85**	**14.77**	**35.26**	**5.11**	105.29	28.29	29.74	4.31
					106.41	37.65	30.05	4.35
					111.70	24.07	31.55	4.57
Median =	116.33		32.9	4.8	113.23	23.38	31.98	4.63
Min =	105.29		29.7	4.3	114.30	20.89	32.28	4.68
Max =	160.25		45.3	6.6	115.88	17.94	32.73	4.74
					116.78	24.33	32.98	4.78
n =	**12**	**Aliquots**			120.81	32.84	34.12	4.94
					123.28	50.04	34.82	5.04
S.D. =	14.77				128.30	13.08	36.24	5.25
Standard error =	4.26				131.35	20.43	37.10	5.37
Random Errors=	10.81	%			160.25	23.69	45.26	6.56
Systematic Error=	9.64	%						
Total Error=	14.48	%						
Bin Width =	10.00	**Gy**						
Overdispersion (%) =	0.0	±	0.0					

		+/-	
dose rate=	**3.54**	**0.19**	**Gy/ka**
U =	3.58	0.3	**ppm**
Th =	9.28	0.8	**ppm**
K2O =	1.90	0.05	**wt. %**
Rb2O=	67.2	2.7	**ppm**
H2O=	3.0	3.0	**wt. %**
Cosmic=	0.21	**Gy/ka**	
depth =	1.8	**m**	
latitude=	38.81	**degrees (north positive)**	
longitude=	-109.30	**degrees (east positive)**	
elevation=	1.27	**km asl**	

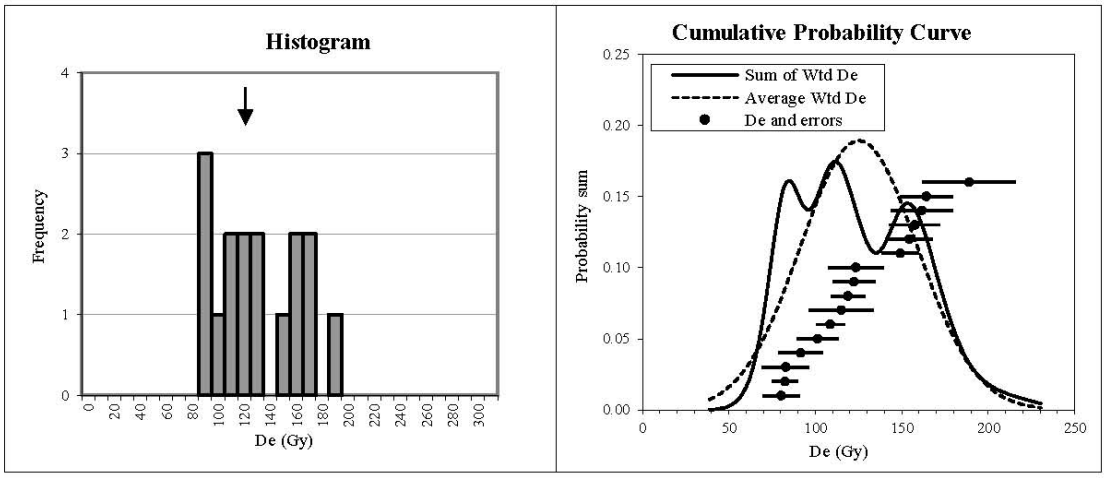

Sample #	Sample Location				Individual Aliquot Data			
USU-1195	Hittle Bottom, UT							
	De (Gy)	±	Age (ka)	±	De (Gy)	±	Age (ka)	±
CAM =	**121.82**	**33.82**	**34.24**	**5.63**	80.13	10.75	22.52	3.70
					82.36	7.55	23.15	3.80
					82.70	13.64	23.25	3.82
Median =	120.57		33.9	5.6	91.55	12.86	25.73	4.23
Min =	80.13		22.5	3.7	101.32	12.05	28.48	4.68
Max =	188.88		53.1	8.7	108.58	8.33	30.52	5.01
					114.88	18.83	32.29	5.31
n =	**16**	**Aliquots**			118.84	9.94	33.41	5.49
					122.30	12.08	34.38	5.65
S.D. =	33.82				123.39	16.21	34.68	5.70
Standard error =	8.45				149.16	10.56	41.93	6.89
Random Errors=	13.30	%			154.18	13.64	43.34	7.12
Systematic Error=	9.65	%			157.39	14.66	44.24	7.27
Total Error=	16.43	%			161.53	17.92	45.40	7.46
					164.19	15.21	46.15	7.58
Bin Width =	10.00	**Gy**			188.88	26.84	53.09	8.72

Overdispersion (%) = 23.4 ± 5.1

		+/-	
dose rate=	**3.56**	**0.20**	**Gy/ka**
U =	4.95	0.4	**ppm**
Th =	8.55	0.8	**ppm**
K2O =	1.74	0.04	**wt. %**
Rb2O=	69.0	2.8	**ppm**
H2O=	5.3	3.0	**wt. %**
Cosmic=	0.18	**Gy/ka**	
depth =	2.8	**m**	
latitude=	38.76	**degrees (north positive)**	
longitude=	-109.32	**degrees (east positive)**	
elevation=	1.25	**km asl**	

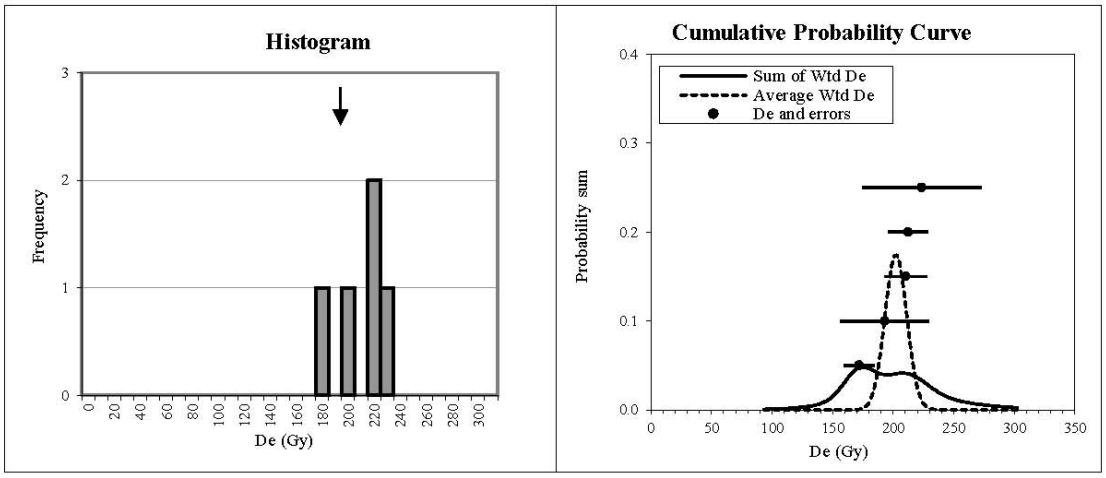

Sample #	Sample Location				Individual Aliquot Data			
USU-1196	Hittle Bottom, UT							
	De (Gy)	±	Age (ka)	±	De (Gy)	±	Age (ka)	±
CAM =	**197.55**	**20.12**	**38.94**	**5.33**	171.97	12.70	33.90	4.64
					193.00	36.49	38.04	5.20
					210.29	17.23	41.45	5.67
Median =	210.29		41.5	5.7	212.24	16.16	41.84	5.72
Min =	171.97		33.9	4.6	223.52	49.01	44.06	6.03
Max =	223.52		44.1	6.0				

n = **5** **Aliquots**

S.D. =	94.25	
Standard error =	42.15	
Random Errors=	10.79	%
Systematic Error=	8.40	%
Total Error=	13.68	%

Bin Width = 10.00 **Gy**

Overdispersion (%) = 5.5 ± 6.6

		+/-	
dose rate=	**5.07**	**0.29**	**Gy/ka**
U =	2.50	0.2	**ppm**
Th =	9.50	0.9	**ppm**
K2O =	1.90	0.05	**wt. %**
Rb2O=	80.1	3.2	**ppm**
H2O=	3.0	3.0	**wt. %**
Cosmic=	0.22	**Gy/ka**	
depth =	1.5	**m**	
latitude=	38.76	**degrees (north positive)**	
longitude=	-109.32	**degrees (east positive)**	
elevation=	1.27	**km asl**	

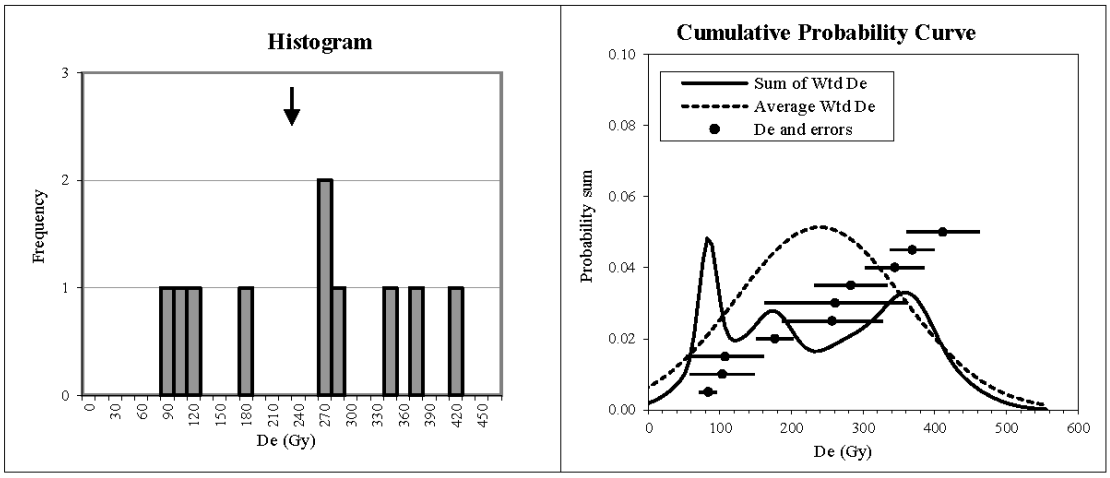

Sample #	Sample Location				Individual Aliquot Data			
USU-1197	Professor Valley, UT							
	De (Gy)	±	Age (ka)	±	De (Gy)	±	Age (ka)	±
CAM =	**222.46**	**117.41**	**83.96**	**30.62**	83.48	12.20	31.51	11.49
					103.20	45.45	38.95	14.21
					107.25	54.24	40.48	14.76
Median =	258.69		97.6	35.6	176.58	25.73	66.64	24.31
Min =	83.48		31.5	11.5	256.73	70.14	96.89	35.34
Max =	411.19		155.2	56.6	260.65	98.75	98.37	35.88
					282.56	51.31	106.64	38.89
n =	**10**	**Aliquots**			344.12	41.24	129.87	47.37
					368.66	30.94	139.14	50.75
S.D. =	117.41				411.19	50.62	155.19	56.60
Standard error =	37.13							
Random Errors=	35.15	%						
Systematic Error=	9.75	%						
Total Error=	36.47	%						
Bin Width =	15.00	**Gy**						
Overdispersion (%) =	49.7	±	13.5					

		+/-	
dose rate=	**2.65**	**0.14**	**Gy/ka**
U =	2.00	0.1	**ppm**
Th =	4.70	0.4	**ppm**
K2O =	1.78	0.04	**wt. %**
Rb2O=	60.8	2.4	**ppm**
H2O=	3.0	3.0	**wt. %**
Cosmic=	0.20	**Gy/ka**	
depth =	2.3	**m**	
latitude=	38.75	**degrees (north positive)**	
longitude=	-109.36	**degrees (east positive)**	
elevation=	1.31	**km asl**	

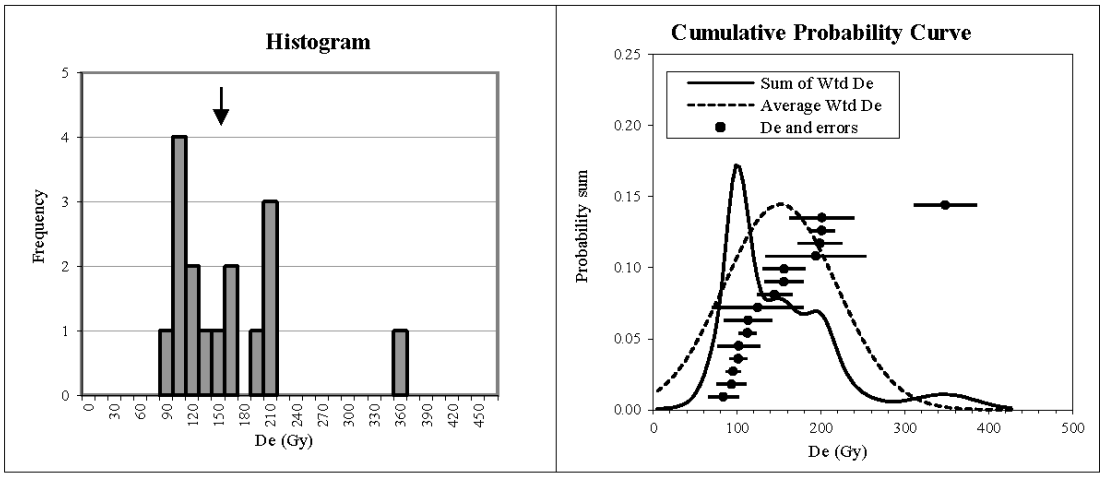

Sample #	Sample Location				Individual Aliquot Data			
USU-1198	Professor Valley, UT							
	De (Gy)	±	Age (ka)	±	De (Gy)	±	Age (ka)	±
CAM =	**142.16**	**67.07**	**52.47**	**11.71**	83.56	17.93	30.84	6.88
					93.39	17.35	34.47	7.69
					95.26	9.16	35.16	7.85
Median =	134.41		49.6	11.1	101.46	10.28	37.45	8.36
Min =	83.56		30.8	6.9	101.89	25.32	37.61	8.39
Max =	348.08		128.5	28.7	112.51	10.31	41.53	9.27
					112.94	28.28	41.69	9.30
n =	**16**	**Aliquots**			124.42	54.27	45.92	10.25
					144.40	20.80	53.30	11.89
S.D. =	67.07				155.69	23.00	57.47	12.82
Standard error =	16.77				156.08	25.16	57.61	12.86
Random Errors=	20.12	%			193.90	60.16	71.57	15.97
Systematic Error=	9.66	%			198.46	26.32	73.25	16.35
Total Error=	22.32	%			200.78	15.20	74.11	16.54
					200.98	38.93	74.19	16.56
Bin Width =	15.00	**Gy**			348.08	37.63	128.48	28.67

Overdispersion (%) = 35.6 ± 7.8

		+/-	
dose rate=	**2.71**	**0.14**	**Gy/ka**
U =	2.45	0.2	**ppm**
Th =	5.80	0.5	**ppm**
K2O =	1.64	0.04	**wt. %**
Rb2O=	57.2	2.3	**ppm**
H2O=	3.0	3.0	**wt. %**
Cosmic=	0.20	**Gy/ka**	
depth =	2.0	**m**	
latitude=	38.73	**degrees (north positive)**	
longitude=	-109.37	**degrees (east positive)**	
elevation=	1.28	**km asl**	

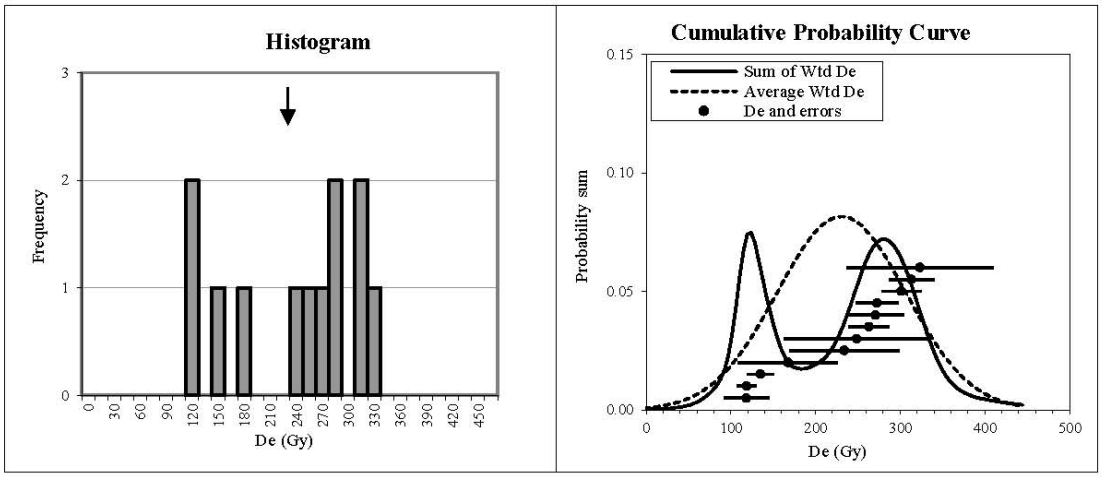

Sample #	Sample Location				Individual Aliquot Data			
USU-1200	Cache Valley graben, UT							
	De (Gy)	±	Age (ka)	±	De (Gy)	±	Age (ka)	±
CAM =	**218.59**	**75.99**	**69.33**	**16.98**	118.24	26.57	37.50	9.18
					118.46	11.14	37.57	9.20
					135.05	15.78	42.83	10.49
Median =	255.85		81.2	19.9	167.51	58.85	53.13	13.01
Min =	118.24		37.5	9.2	234.21	64.74	74.29	18.19
Max =	323.57		102.6	25.1	248.55	86.32	78.84	19.30
					263.16	23.95	83.47	20.44
n =	**12**	**Aliquots**			270.56	33.99	85.82	21.01
					272.60	25.04	86.46	21.17
S.D. =	112.02				301.19	23.34	95.53	23.39
Standard error =	32.34				313.19	26.81	99.34	24.32
Random Errors=	22.47	%			323.57	86.33	102.63	25.13
Systematic Error=	9.72	%						
Total Error=	24.48	%						
Bin Width =	15.00	**Gy**						
Overdispersion (%) =	34.1	±	8.7					

		+/-	
dose rate=	**3.15**	**0.17**	**Gy/ka**
U =	3.20	0.2	**ppm**
Th =	8.80	0.8	**ppm**
K2O =	1.74	0.04	**wt. %**
Rb2O=	73.6	2.9	**ppm**
H2O=	3.0	3.0	**wt. %**
Cosmic=	0.09	**Gy/ka**	
depth =	9.4	**m**	
latitude=	38.71	**degrees (north positive)**	
longitude=	-109.40	**degrees (east positive)**	
elevation=	1.27	**km asl**	

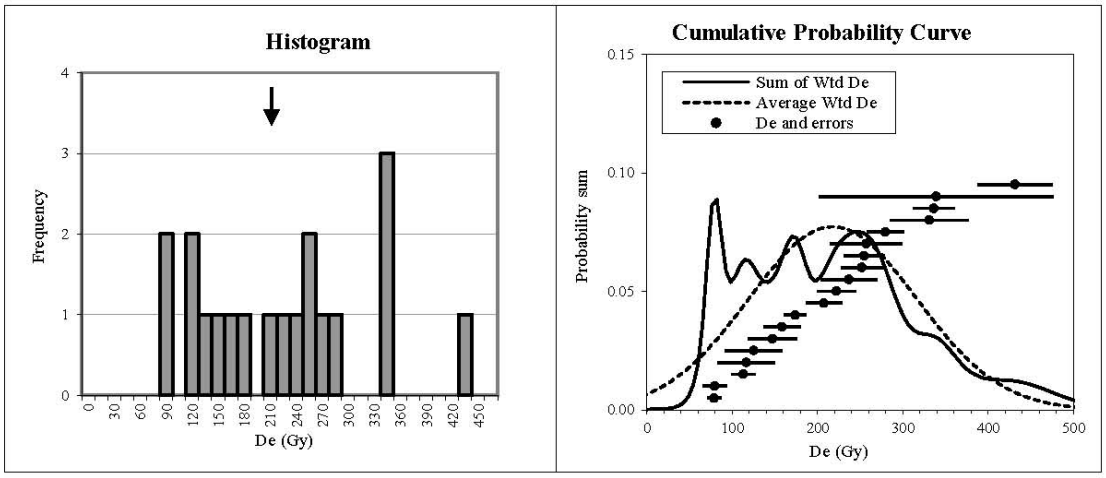

Sample #	Sample Location				Individual Aliquot Data			
USU-1279	Ida Gulch, UT							
	De (Gy)	±	Age (ka)	±	De (Gy)	±	Age (ka)	±
CAM =	**196.80**	**98.42**	**74.51**	**18.04**	78.66	8.12	29.78	7.21
					79.45	14.39	30.08	7.28
					112.99	13.97	42.78	10.35
Median =	222.15		84.1	20.4	116.77	33.37	44.21	10.70
Min =	78.66		29.8	7.2	125.27	33.23	47.42	11.48
Max =	431.50		163.4	39.5	147.24	28.16	55.74	13.49
					158.52	21.37	60.01	14.53
n =	**19**	**Aliquots**			173.93	13.00	65.85	15.94
					207.53	21.29	78.57	19.02
S.D. =	98.42				222.15	22.53	84.11	20.36
Standard error =	22.58				237.14	32.98	89.78	21.73
Random Errors=	22.21	%			251.99	24.66	95.40	23.09
Systematic Error=	9.63	%			254.77	24.25	96.45	23.35
Total Error=	24.21	%			257.24	42.21	97.39	23.57
					279.56	21.63	105.84	25.62
Bin Width =	15.00	**Gy**			331.00	45.81	125.31	30.33
					336.55	24.64	127.41	30.84
Overdispersion (%) =	45.4	±	8.2		339.02	136.99	128.35	31.07
					431.50	44.07	163.36	39.54

		+/-	
dose rate=	**2.64**	**0.14**	**Gy/ka**
U =	2.50	0.2	**ppm**
Th =	5.40	0.5	**ppm**
K2O =	1.57	0.04	**wt. %**
Rb2O=	56.9	2.3	**ppm**
H2O=	3.0	3.0	**wt. %**
Cosmic=	0.22	**Gy/ka**	
depth =	1.5	**m**	
latitude=	38.69	**degrees (north positive)**	
longitude=	-109.41	**degrees (east positive)**	
elevation=	1.29	**km asl**	

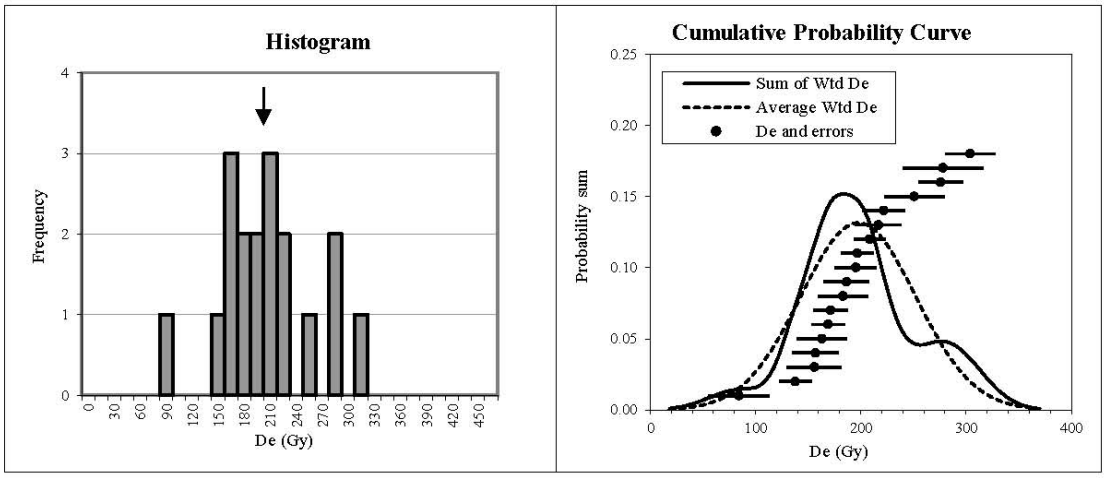

Sample #	Sample Location				Individual Aliquot Data			
USU-1280	Ida Gulch, UT							
	De (Gy)	±	Age (ka)	±	De (Gy)	±	Age (ka)	±
CAM =	**197.86**	**54.62**	**58.13**	**8.72**	84.28	28.65	24.76	3.71
					137.69	15.24	40.45	6.07
					155.91	25.81	45.81	6.87
Median =	190.74		56.0	8.4	156.92	22.02	46.10	6.92
Min =	84.28		24.8	3.7	163.14	23.83	47.93	7.19
Max =	303.98		89.3	13.4	169.09	15.97	49.68	7.45
					171.20	15.97	50.30	7.55
n =	**18**	**Aliquots**			183.03	23.85	53.77	8.07
					186.35	21.31	54.75	8.21
S.D. =	54.62				195.14	19.95	57.33	8.60
Standard error =	12.88				196.77	15.40	57.81	8.67
Random Errors=	11.45	%			208.27	15.02	61.19	9.18
Systematic Error=	9.70	%			216.76	21.85	63.68	9.55
Total Error=	15.00	%			221.83	20.17	65.17	9.78
					250.86	28.71	73.70	11.06
Bin Width =	15.00	**Gy**			275.98	21.09	81.08	12.17
					278.18	37.82	81.73	12.26
Overdispersion (%) =	20.3	±	4.4		303.98	23.31	89.31	13.40

		+/-	
dose rate=	**3.40**	**0.19**	**Gy/ka**
U =	3.65	0.3	**ppm**
Th =	10.95	1.0	**ppm**
K2O =	1.71	0.04	**wt. %**
Rb2O=	69.1	2.8	**ppm**
H2O=	3.0	3.0	**wt. %**
Cosmic=	0.10	**Gy/ka**	
depth =	8.0	**m**	
latitude=	38.69	**degrees (north positive)**	
longitude=	-109.41	**degrees (east positive)**	
elevation=	1.26	**km asl**	

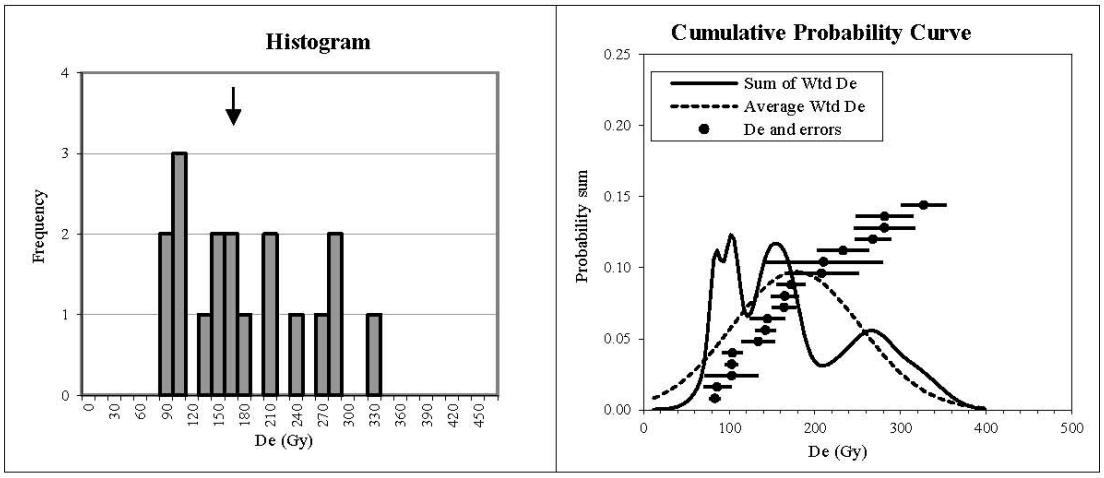

Sample #	Sample Location				Individual Aliquot Data			
USU-1336	Dewey Bridge, UT							
	De (Gy)	±	Age (ka)	±	De (Gy)	±	Age (ka)	±
CAM =	**164.44**	**74.98**	**52.76**	**11.82**	83.27	6.29	26.72	5.98
					85.84	16.21	27.54	6.17
					102.81	31.31	32.99	7.39
Median =	164.47		52.8	11.8	102.83	7.46	32.99	7.39
Min =	83.27		26.7	6.0	103.51	12.31	33.21	7.44
Max =	326.99		104.9	23.5	133.84	19.21	42.94	9.62
					142.14	11.64	45.61	10.22
n =	**18**	**Aliquots**			144.80	20.58	46.46	10.41
					164.13	13.81	52.66	11.80
S.D. =	94.68				164.81	16.26	52.88	11.85
Standard error =	22.32				172.18	16.87	55.24	12.37
Random Errors=	20.20	%			207.75	43.02	66.65	14.93
Systematic Error=	9.69	%			209.98	68.94	67.37	15.09
Total Error=	22.40	%			232.86	29.68	74.71	16.74
					267.72	21.32	85.90	19.24
Bin Width =	15.00	**Gy**			281.22	35.69	90.23	20.21
					281.46	33.26	90.30	20.23
Overdispersion (%) =	40.0	±	7.5		326.99	26.68	104.91	23.50

		+/-	
dose rate=	**3.12**	**0.16**	**Gy/ka**
U =	2.60	0.2	**ppm**
Th =	6.70	0.6	**ppm**
K2O =	1.94	0.05	**wt. %**
Rb2O=	76.7	3.1	**ppm**
H2O=	3.0	3.0	**wt. %**
Cosmic=	0.22	**Gy/ka**	
depth =	1.5	**m**	
latitude=	38.82	**degrees (north positive)**	
longitude=	-109.31	**degrees (east positive)**	
elevation=	1.29	**km asl**	

Appendix B. Clast-count data

TABLE B.1 SUMMARY OF CLAST COUNTS PERFORMED IN STUDY AREA

Location	Deposit[a]	N	E	Elevation (m)	n[b]
Modern Inputs					
Colorado River above Dolores confluence	modern channel alluvium	4299231	648785	1253	98
Dolores River	modern channel alluvium	4297133	649812	1255	89
Colorado River below Dolores confluence	modern channel alluvium	4295444	645228	1246	100
Onion Creek	modern channel alluvium	4286789	644612	1302	94
Professor Creek	modern channel alluvium	4286157	641515	1258	93
Colorado River in Cache Valley graben	modern channel alluvium	4285182	639360	1233	101
Castle Creek	modern channel alluvium	4281468	634859	1256	97
Late Pleistocene Terraces					
above Dewey Bridge	M2	4300830	649004	1258	100
Dewey Bridge	M8	4296004	647985	1396	101
Dewey Bridge	M7	4297443	646373	1318	100
Dewey Bridge	M4	4297570	646656	1291	99
Dewey Bridge	M3	4297583	647222	1273	100
Dewey Bridge	M2	4297547	647597	1261	103
Professor Valley	M7	4289370	642289	1308	101
Professor Valley	M5	4287852	641380	1287	100
Professor Valley	M3 upper gravel	4290819	644055	1260	102
Professor Valley	M3 lower gravel	4290826	644089	1254	100
Cache Valley graben	M6	4286141	640214	1286	98
Ida Gulch	M6	4283437	638280	1294	101
Ida Gulch	M4	4283442	637979	1259	101
Ida Gulch	M3	428653	637891	1250	101

[a]Organized upstream to downstream and by stratigraphic position; "M" is mainstem Colorado River deposit.

[b]Total number of clasts counted.

TABLE B.2 CLAST TYPE AND MEDIAN DIAMETER (cm) FOR THE MODERN CHANNEL OF THE COLORADO RIVER ABOVE DOLORES RIVER CONFLUENCE

	rhy/porph	feld porph	basalt	basement	vf/f Qzt	c Qzt	black vf Oqzt	T_R red f Ss-Sltst	J tan f Ss	Jm Ss	carb	chert	Pz Ls, Ss
	7	4.5	6.4	5.4	4.5	5.2	5	7.7	8	6.5	4	8	4.1
	7		6.1	4.5	3	6	4		4.7	4			7.3
	5.7		6.5	5	9	4.7			6	21			6.5
	6.6		3	5.4	5.5	10.2			7	7			4.4
	4.3		7	8	4.5				3.3	8			5.7
	6.4		7	9	3.5				7.3	4.5			4.5
	5.4		5	4.7	4.5				5	9.5			
			6	6	7.2				7	7.5			
			4.5	6	3.1				3.5	4.1			
			3.1	4.4	6.3				4.8				
				5	4.7				7.6				
				4	8.7				6				
				4	2.9				6.1				
				6.5	6.4				6.2				
				6					4.7				
				6.7					3.8				
				8					6.1				
				6.4					3.2				
				2.8					7.4				
				7					3.6				
				6.4									
				6.4									
n	7	1	10	22	14	4	2	1	20	9	1	1	6
% total	7.1	1.0	10.2	22.4	14.3	4.1	2.0	1.0	20.4	9.2	1.0	1.0	6.1
median d (cm)	6.4	4.5	6.1	6.0	4.6	5.6	4.5	7.7	6.0	7.0	4.0	8.0	5.1

TABLE B.3 CLAST TYPE AND MEDIAN DIAMETER (cm) FOR THE MODERN CHANNEL OF THE DOLORES RIVER

	feld porph	basalt	basement	vf/f Qzt	c Qzt	Pc	T_R red f Ss-Sltst	J tan f Ss	Jm Ss	carb	Pz Ls, Ss
	4	4.8	5.7	2.5	4.5	4.3	2.5	3.5	6.8	5.8	8.1
	5.2	6.1	3.5	4.1	4	3.8	3.1	2.9		2.8	
	8.1	3.1		6	3.6			6		8	
	6.8	3.3		7.6	3.7			4.7		2.4	
	7.1	2.9		3	6			5.3		3.9	
	7.7			4.2	3.1			6.8		5.7	
				5.5	7.5			5.2		3.5	
				6.2	6.5			9.6		4.2	
				4.1	3.4			3.6		4.8	
				5.6	5.7			6.2			
				7.5	6			7			
				4	3.9			6			
				2.6	9.1			6			
				3.7	3.8			5.1			
				2.1	2.5			4.7			
				6	4.5			5.3			
				5.4	4.7			2.5			
				5.3	9.2			8			
				1.4	5.2			4			
				1.3	6.6			3.7			
								10			
n	6	5	2	20	20	2	2	21	1	9	1
% total	6.7	5.6	2.2	22.5	22.5	2.2	2.2	23.6	1.1	10.1	1.1
median d (cm)	7.0	3.3	4.6	4.2	4.6	4.1	2.8	5.3	6.8	4.2	8.1

TABLE B.4 CLAST TYPE AND MEDIAN DIAMETER (cm) FOR THE MODERN CHANNEL OF THE COLORADO RIVER BELOW DOLORES RIVER CONFLUENCE

	rhy/porph	feld porph	basalt	basement	vf/f Qzt	c Qzt	Pc	T_R red f Ss-Sltst	J tan f Ss	Jm Ss	Pz Ls, Ss
	2	4	4.2	7.8	7	7	6.5	6	6	2.5	7.2
	6	7.5	5.5	5	9	7	4.3	6.5	7	3	4
	8	3	7	7	7	5	5.7	3	6	6	6.5
		5	2	7	6.5	3		3.5	6	7	3.5
		4.5	4	5	7	4		3.5	5	6	
		7	4.5	3	1.5	3			3.5	4	
		7.5	4.5	4	10.5	3.5			7	4	
		3.5		6	4	7			2.5	2.8	
		2.5		2.5	5	9			15	4	
		4		2					6.5	8	
		3.2		3.5					2.8		
		4		6.5					2.7		
				2					4.5		
				4.5					4.1		
				6					3		
				5.8					6.5		
				2.5					3.7		
				6					6		
				5					2.2		
n	3	12	7	19	9	9	3	5	19	10	4
% total	3.0	12.0	7.0	19.0	9.0	9.0	3.0	5.0	19.0	10.0	4.0
median d (cm)	6.0	4.0	4.5	5.0	7.0	5.0	5.7	3.5	5.0	4.0	5.3

TABLE B.5 CLAST TYPE AND MEDIAN DIAMETER (cm) FOR THE MODERN CHANNEL OF ONION CREEK

	rhy/porph	feld porph	basalt	basement	vf/f Qzt	Pc	T_R red f Ss-Sltst	J tan f Ss	Jm Ss	Carb
	2.8	2	2.5	3.2	2.5	10	9	5.5	2.3	2
		1.8			1.6	7	3.5	15	2	1.5
					1.3	2.5	3.5	10	2.7	2
					1.5	2	5.5	10.5	1.5	1.5
						4.5	3	2.5		1.5
						5	3.4	2.5		1.4
						6	2.5	4		2.5
						2.8	2.2	2.5		4.5
						2	1.6	4		2.5
						1.3	1.1	4		1.8
						1.4	1.3	5		3.5
						1.5	1.4	6		3.5
						1.4	1.2	4		2
						1.2	1.1	2		2
						1.3	1	2.3		2.5
							1.5	3		2.8
							0.9	2.5		1.7
							1	2.2		1.8
								1.6		1.5
								1.3		1.3
								1.5		1
								1.5		1.3
								1		1.5
								1.3		1.6
n	1	2	1	1	4	15	18	24	4	24
% total	1.1	2.1	1.1	1.1	4.3	16.0	19.1	25.5	4.3	25.5
median d (cm)	2.8	1.9	2.5	3.2	1.6	2.0	1.6	2.5	2.2	1.8

TABLE B.6 CLAST TYPE AND MEDIAN DIAMETER (cm) FOR THE MODERN CHANNEL OF PROFESSOR CREEK

	Hbl porph	rhy/porph	basement	Pc	T_R red f Ss-Sltst	J tan f Ss	Chert
	4.5	4.5	4.5	3	6.5	13	2.5
			4	3	6	8	
				6.5	4.5	12	
				10	3.5	12	
				5.5	4.5	5.5	
				4	3.5	6	
				2	4.5	8	
				3	4.5	3.5	
				1.5	4.5	2	
				1.5	6.5	4	
				2.5	2.5	2	
				2.5	3.5	4.5	
				4.5	1.5	1	
				12	3	18	
				4.5	2.5	6.5	
				3.5	1.5	4	
				6.5	1.5	3	
				3.5	6	5.5	
				3	6.5	2.5	
				2	8.5	15	
				10	4.5	5.5	
				6	4.5	1.5	
				3	3	11.5	
				4.5	3.5	7.5	
					2	5.5	
					6	2	
					10	3	
					3	2.5	
					3.5	6.5	
					3.5	8.5	
					2		
					4.5		
					4.5		
					4.5		
n	1	1	2	24	34	30	1
% total	1.1	1.1	2.2	25.8	36.6	32.3	1.1
median d (cm)	4.5	4.5	4.3	3.5	4.5	5.5	2.5

TABLE B.7 CLAST TYPE AND MEDIAN DIAMETER (cm) FOR THE MODERN CHANNEL OF THE COLORADO RIVER IN CACHE VALLEY GRABEN

	Hbl porph	rhy/porph	feld porph	basalt	basement	vf/f Qzt	c Qzt	Pc	T_R red f Ss-Sltst	J tan f Ss	Jm Ss	Pz Ls, Ss
	4.2	3.5	3	3.8	4.4	8.5	13	5.4	5.1	7.5	5.7	2.1
	6.1	6.6	6.1	4.1	9	3.5	4	6	5.2	6.6	6.8	5.6
	4.7	4.8	3.5	5.8	1	6	12	4.7	9.5	5.7	2.8	3.1
	7.3		6.1	3.7	3	4.5	4.8	15	12	8.6	4	2.6
	4.5			5.1	3.5	5.5			4.5	4.8	3.5	4.6
	7			4.8	3.6	10			6	6.5	6	7
	5.5			3.4	4	14			5.5	6.3	3.9	6.3
	3.5			6.4	5.5	9			7.1	7.1		8.5
	4				7.5				2.2	14		4.1
	3				4.5				5	12		2.5
	11.5								8.2	3.9		
	1.4								10	6.2		
									10.4	14		
										12		
										7.8		
										7		
										3.5		
										3.8		
n	12	3	4	8	10	8	4	4	13	18	7	10
% total	11.9	3.0	4.0	7.9	9.9	7.9	4.0	4.0	12.9	17.8	6.9	9.9
median d (cm)	4.6	4.8	4.8	4.5	4.2	7.3	8.4	5.7	6.0	6.8	4.0	4.4

TABLE B.8 CLAST TYPE AND MEDIAN DIAMETER (cm) FOR THE MODERN CHANNEL OF CASTLE CREEK

	Hbl porph	feld porph	basalt	vf/f Qzt	c Qzt	Pc	T_R red f Ss-Sltst	J tan f Ss
	4	5	3	3	6	5	9	4
	4	1.5				2.5	2	4.5
	5	4				2.5	6	3.5
	1.5	5.5				2	3	6.5
	3.5	2.5				1.5	2.5	3
	1.5	2				5	6.5	2
	4	3				4	2	5
	3.5	3				2	1.5	3
		3				1	4	6
		2				2	3.5	1
		2				1	4.5	8
		2				3	3	8
		9				3.5	2.5	5.5
		3.5				5	3	3.5
		2				4	2	3
		5				3	3	2.5
		6.5				2.5	3	2.5
		5				2	8	2.5
		4					5.5	
		3					2.5	
		3					3	
		4.5					2	
		2						
		3						
		2.5						
		2.5						
		1.5						
		2						
n	8	28	1	1	1	18	22	18
% total	8.2	28.9	1.0	1.0	1.0	18.6	22.7	18.6
median d (cm)	3.8	3.0	3.0	3.0	6.0	2.5	3.0	3.5

TABLE B.9 CLAST TYPE AND MEDIAN DIAMETER (cm) FOR THE DEWEY BRIDGE M2 DEPOSIT (ABOVE DOLORES RIVER CONFLUENCE)

	Hbl porph	rhy/porph	basalt	basement	vf/f Qzt	c Qzt	black vf Oqzt	T_R red f Ss-Sltst	J tan f Ss	chert	Pz Ls, Ss
	1	1	1	1	1	1	1	1	1	1	1
	1	1	1	1	1	1	1	1	1		
	1		1	1	1	1	1	1	1		
	1		1	1	1	1	1	1	1		
	1		1	1	1	1	1	1	1		
	1		1	1	1	1	1		1		
	1		1	1	1				1		
	1		1	1					1		
	1		1	1					1		
	1		1	1					1		
	1		1	1					1		
	1		1	1					1		
	1		1	1					1		
	1		1	1					1		
	1		1	1					1		
	1		1	1					1		
	1			1					1		
	1			1							
	1			1							
	1										
n	20	2	16	19	7	6	6	5	17	1	1
% total	20.0	2.0	16.0	19.0	7.0	6.0	6.0	5.0	17.0	1.0	1.0
median d (cm)[a]	NA	NA	NA	NA	NA	NA	NA	NA	NA	NA	NA

[a] Clast diameters not measured.

TABLE B.10 CLAST TYPE AND MEDIAN DIAMETER (cm) FOR THE DEWEY BRIDGE M8 DEPOSIT

	Hbl porph	rhy/porph	feld porph	basalt	basement	vf/f Qzt	c Qzt	black vf Oqzt	T_R red f Ss-Sltst	J tan f Ss	Jm Ss	chert	Pz Ls, Ss
	4	1.5	1.5	3	4.5	8	3	3	8	2	2	4	2
	9	1.5	2	7.5	8	10	3	5.5	12	1	1.5	1.5	
	4.5		2.5	2	3	11.5	4	3.5	5.5	14.5	5.5	2.5	
	1		7.5	2.5	3	2	9	9	11.5	6.5	1.5	2	
			14.5	4.5	4	10	2		3.5	3.5	1.5	1.5	
			1.5	1.5	3	8	5.5		1.5	4	0.5		
			3		2	1.5			6	15	9		
			1.5		1.5	4.5				10			
			4		2	2.5				12.5			
			5		1	0.5							
			8		3	3							
			15		2	7.5							
					4	2							
					3	5							
					1.5								
					4.5								
					8								
					8								
					3.5								
					1.5								
					6								
					2								
					16.5								
					11								
n	4	2	12	6	24	14	6	4	7	9	7	5	1
% total	4.0	2.0	12.1	6.1	24.2	14.1	6.1	4.0	7.1	9.1	7.1	5.1	1.0
median d (cm)	4.3	1.5	3.5	2.8	3.0	4.8	3.5	4.5	6.0	6.5	1.5	2.0	2.0

TABLE B.11 CLAST TYPE AND MEDIAN DIAMETER (cm) FOR THE DEWEY BRIDGE M7 DEPOSIT

	Hbl porph	rhy/porph	feld porph	basalt	basement	vf/f Qzt	c Qzt	black vf Oqzt	T_R red f Ss-Sltst	J tan f Ss	Jm Ss	chert	Pz Ls, Ss
	7	2	1.5	6.5	1.5	2	7.5	7	5	12	5.5	2	1.5
	5.5	3.5	6	8	5	1	10	4.5	4	11.5	3	1.5	1.5
	2		5.5	3	2.5	1	2.5			2.5	5	1	1
	2.5		3.5		1	4				2	3.5	2	
	4.5		3		16	15.5				9	6.5	1.5	
	6		3.5		3	10.5				10.5	3		
	8		1.5		2					4.5	4		
			3		6					2	4		
			3.5		5.5					19			
			2.5		3.5								
			1.5		1.5								
			4.5		2.5								
			5.5		2.5								
			4.5		2.5								
					2.5								
					2.5								
					3.5								
					1								
					5.5								
					4								
					7								
					3.5								
					6								
					16								
					4.5								
					1.5								
					1.5								
					1								
					3								
					4								
					4.5								
					6.5								
					3.5								
					3.5								
					1.5								
					1.5								
n	7	2	14	3	36	6	3	2	2	9	8	5	3
% total	7.1	2.0	14.1	3.0	36.4	6.1	3.0	2.0	2.0	9.1	8.1	5.1	3.0
median d (cm)	5.5	2.8	3.5	6.5	3.3	3.0	7.5	5.8	4.5	9.0	4.0	1.5	1.5

TABLE B.12 CLAST TYPE AND MEDIAN DIAMETER (cm) FOR THE DEWEY BRIDGE M4 DEPOSIT

	Hbl porph	rhy/porph	feld porph	basalt	basement	vf/f Qzt	c Qzt	black vf Oqzt	T_R red f Ss-Sltst	J tan f Ss	Jm Ss	chert	Pz Ls, Ss	Km
	6	5.5	8.5	10	11.5	8.5	5.5	5	3	7	7	2	3.5	15.5
	5.5		4	5.5	6.5	5	10	6	3	5.5	6	2	1	3
	6		3	6.5	8.5	4.5	3.5	7.5	5.5	6	11.5	1.5		
	4		3	9	4	4	4.5	2.5		3.5	4.5			
	8		2	2.5	7	4.5	2.5	1.5		7.5	3.5			
			2.5	3.5	8	2.5	3.5			2	1.5			
			2	2	9.5	2.5	15.5			3.5	2			
			1.5	1.5	3.5					2.5	2			
				1	4.5					0.5				
				1.5	4									
					3									
					3									
					4									
					4									
					4.5									
					2.5									
					3.5									
					4.5									
					3.5									
					2.5									
					4									
					3									
					2.5									
					1									
					2									
					1.5									
					1.5									
					1									
					11									
n	5	1	8	10	29	7	7	5	3	9	8	3	2	2
% total	5.1	1.0	8.1	10.1	29.3	7.1	7.1	5.1	3.0	9.1	8.1	3.0	2.0	2.0
median d (cm)	6.0	5.5	2.8	3.0	4.0	4.5	4.5	5.0	3.0	3.5	4.0	2.0	2.3	9.3

TABLE B.13 CLAST TYPE AND MEDIAN DIAMETER (cm) FOR THE DEWEY BRIDGE M3 DEPOSIT

	Hbl porph	rhy/porph	feld porph	basalt	basement	vf/f Qzt	c Qzt	black vf Oqzt	T_R red f Ss-Sltst	J tan f Ss	Jm Ss	carb	chert	Pz Ls, Ss
	4.5	1.5	1.5	3.5	7	4	16.5	6	7.5	2.5	4	1	6.5	1.5
		1	6	1.5	3.5	3	3	8.5	4	3.5	6.5			2
		1.5	2.5	3.5	2.5	4.5	6.5	3.5		3.5	1.5			
		2	3	2.5	4	4	2	5.5		2	3.5			
		5.5	2	3	7	5.5	9.5	6.5			2			
		2	4.5	3	7	8.5	3.5				4			
			5	2	9	2	6.5							
			4	2.5	3	2	4							
			7	5.5	2.5	2.5	4							
			4	3.5	4	3.5	4.5							
			3.5		4.5	9.5	5.5							
			7		4.5	3.5								
			3		3.5	3								
					2	2.5								
					2	4.5								
					2.5	5								
					4	5.5								
					1.5	4.5								
					5									
					1.5									
n	1	6	13	10	20	18	11	5	2	4	6	1	1	2
% total	1.0	5.9	12.9	9.9	19.8	17.8	10.9	5.0	2.0	4.0	5.9	1.0	1.0	2.0
median d (cm)	4.5	1.8	4.0	3.0	3.8	4.0	4.5	6.0	5.8	3.0	3.8	1.0	6.5	1.8

TABLE B.14 CLAST TYPE AND MEDIAN DIAMETER (cm) FOR THE DEWEY BRIDGE M2 DEPOSIT

	Hbl porph	rhy/porph	feld porph	basalt	basement	vf/f Qzt	T_R red f Ss-Sltst	Jm Ss	chert	Pz Ls, Ss
	1	1	1	1	1	1	1	1	1	1
	1	1	1	1	1	1		1	1	
	1	1	1	1	1	1		1		
	1	1	1	1	1	1		1		
	1	1	1	1	1	1		1		
	1	1	1	1	1	1		1		
	1	1	1	1	1	1		1		
	1	1		1	1	1		1		
	1	1		1	1	1		1		
	1	1		1	1	1		1		
	1	1		1	1	1				
	1	1		1	1					
	1			1	1					
	1			1	1					
	1			1	1					
	1			1	1					
				1	1					
				1	1					
				1	1					
				1	1					
				1						
				1						
				1						
n	16	12	7	23	20	11	1	10	2	1
% total	15.5	11.7	6.8	22.3	19.4	10.7	1.0	9.7	1.9	1.0
median d (cm)[a]	NA	NA	NA	NA	NA	NA	NA	NA	NA	NA

[a] Clast diameters not measured.

TABLE B.15 CLAST TYPE AND MEDIAN DIAMETER (cm) FOR THE PROFESSOR VALLEY M7 DEPOSIT

	Hbl porph	rhy/porph	feld porph	basalt	basement	vf/f Qzt	c Qzt	J tan f Ss	Jm Ss	Pz Ls, Ss
	3.6	2.6	8	4.3	7.3	7.1	4.1	5.9	4.2	2.9
	4.4	3.1	6.6	14	2.9	4.4	5.3	6.4		7.6
	3.3	3.1	4.8	5.2	4.2	8	8.1	3.7		6
	8	1.8	6.6	4.7	4.6	3.6		6		5
	4	4.9	3.8	8	4.6	4.3		2.5		6.5
	8.1	2.5	5.9	3.5	5.5	5.6		5		2.1
	5	3.4	4	5.4	3.5	5		2.3		2.3
	6	2.1	3.7	4	3	6		3.7		2.6
	5.6		2.6	4.1	6.5	5.2				
	2.9			6.5	7.9	5				
	2.5			7.3	2.3	5				
				5.7	1.8	2.5				
				3	2.2	5.3				
				6	2.9	4.7				
				2.5	3	4.4				
				1.8	3.4	5.5				
				2.5	2.4	2.9				
				5.4		2.8				
n	11	8	9	18	17	18	3	8	1	8
% total	10.9	7.9	8.9	17.8	16.8	17.8	3.0	7.9	1.0	7.9
median d (cm)	4.9	2.9	5.1	5.2	4.0	4.9	5.8	4.4	4.2	4.4

TABLE B.16 CLAST TYPE AND MEDIAN DIAMETER (cm) FOR THE PROFESSOR VALLEY M5 DEPOSIT

	Hbl porph	rhy/porph	feld porph	basalt	basement	vf/f Qzt	Pc	T_R red f Ss-Sltst	J tan f Ss	Pz Ls, Ss
	2.5	3.9	1.4	4.3	3.2	2.4	3.1	3.1	3.2	1.5
	3	3.4	3.6	1.6	4.8	3.1			9	3.2
	2.5	3.5	3.4	2	2.5	9			6.1	1.8
	2.5	3	3.2	3.5	3	4.5			2.5	5.1
	3	2.8	2.5	3.8	5.7	3.7			7.6	2
	2.5	2	2.5	2.6	3.5	2.8			3	1.8
	2	6.4	4.5	4.5	8.1	4			4	2
	2.5	3.1	3.5	5.4	4	4.2				6
	3	4.1	4	2.6	3.5	11.5				4.7
	2.3	4		3	1.9	2.5				6
	2.2	3.9		2	2	1				4
	2.8	6		13	1	2.5				
		2.7		2.5	3	3.3				
		5.9			2					
		2.9								
		6.5								
		3								
		3.4								
		2.9								
n	12	19	9	13	14	13	1	1	7	11
% total	12.0	19.0	9.0	13.0	14.0	13.0	1.0	1.0	7.0	11.0
median d (cm)	2.5	3.4	3.4	3.0	3.1	3.3	3.1	3.1	4.0	3.2

TABLE B.17 CLAST TYPE AND MEDIAN DIAMETER (cm) FOR THE UPPER GRAVEL OF THE PROFESSOR VALLEY M3 DEPOSIT

	Hbl porph	rhy/porph	feld porph	basalt	basement	vf/f Qzt	c Qzt	black vf Oqzt	T_R red f Ss-Sltst	J tan f Ss	Jm Ss	Pz Ls, Ss
	4.1	2.5	4.2	4.9	3	5.5	2.9	3.1	3.5	2.6	4.2	2.9
	3	2.5	5	3.2	6.6	2	6.7		3	6.1	2.4	2.3
	3		8	8.6	2.7	10	5.5		3	6.2	4.7	1.6
	2		3	2.4	11	2	4.5		3	9	8	5.8
	2.5		2.5	1.5	3.5					3.5	2	1
	2		3.5	10.5	3					4.6	4.5	7
	2.5		3.6	5.3	8.6					9	4.5	3.5
	4.5		5.2	3.3	2					3.3	2.5	
	4				1.5					2	3	
	2				5					8	2.5	
	8				2.5					4	3	
	2				3.9					6	4	
					1.5					7		
					2					3.2		
					1.5							
					2							
					8.5							
					4.5							
					3.5							
					6							
					3.5							
					4.5							
					5.6							
					4							
					3							
					1							
n	12	2	8	8	26	4	4	1	4	14	12	7
% total	11.8	2.0	7.8	7.8	25.5	3.9	3.9	1.0	3.9	13.7	11.8	6.9
median d (cm)	2.8	2.5	3.9	4.1	3.5	3.8	5.0	3.1	3.0	5.3	3.5	2.9

TABLE B.18 CLAST TYPE AND MEDIAN DIAMETER (cm) FOR THE LOWER GRAVEL OF THE PROFESSOR VALLEY M3 DEPOSIT

	Hbl porph	rhy/porph	feld porph	basalt	basement	vf/f Qzt	Pc	T_R red f Ss-Sltst	J tan f Ss	Jm Ss	Pz Ls, Ss
	3.3	7.3	9.4	10	2.1	2.8	2.4	2.8	6	1.8	4.2
	3.9	1.8	3	1.3	2.7	3	3.1	3.5	18	3.7	4.4
	2.5	1	3.6	5.8	4.7	5.7	4		2.7	2.5	2.5
	3.4	3.8	4.8	6.8	2.3	4			2.8		3.8
	4.8	2.5	4.1	6	2.9	3.1			6		5.5
	5	2.2	6	5.5	2.1	5.8			2.7		3.1
	3.8	3.3	2.7	5.5	7	4			3.5		3
	2		3.1	5.6	5.5	2			3.5		4
	2		3.3	2.4	5.3	3.5					3.7
	14		3.4	2.4	2.4						
	7.4		3.4	2.1	2.8						
	3.9		5.3	2.6	2.5						
	9		2	3.3	5.7						
			2.2	2.5	3.2						
			2	4.2							
				2.3							
				2.9							
n	13	7	15	17	14	9	3	2	8	3	9
% total	13.0	7.0	15.0	17.0	14.0	9.0	3.0	2.0	8.0	3.0	9.0
median d (cm)	3.9	2.5	3.4	3.3	2.9	3.5	3.1	3.2	3.5	2.5	3.8

TABLE B.19 CLAST TYPE AND MEDIAN DIAMETER (cm) FOR THE CACHE VALLEY GRABEN M6 DEPOSIT

	Hbl porph	rhy/porph	feld porph	basalt	basement	vf/f Qzt	c Qzt	black vf Oqzt	Pc	T_R red f Ss-Sltst	J tan f Ss	Jm Ss	carb	chert
	3	2	4.5	3.5	7.5	6	5.5	5	1.5	18	11	6	8	1
	4	2.5	4	2.5	3.5	3.5	6.5		3	2	6.5	6		1.5
	3.5	2	4.5	7.5	5				2	10	9	5		
	8	6	9	5	3				10	8	7	9		
	6	2	8	5	1				5.5	40	8	2.5		
	6.5		6	5	6.5				5	4	6			
	5		6	5	1					20	10			
	7		9	5	1.5					10	35			
	8		4.5	2	3					5	7.5			
	1			5	13						2.5			
	6			1.5							3			
	3			1.5							25			
	5			4										
	3													
	4													
	6.5													
	4													
	5													
	4.5													
	1.5													
	9													
n	21	5	9	13	10	2	2	1	6	9	12	5	1	2
% total	21.4	5.1	9.2	13.3	10.2	2.0	2.0	1.0	6.1	9.2	12.2	5.1	1.0	2.0
median d (cm)	5.0	2.0	6.0	5.0	3.3	4.8	6.0	5.0	4.0	10.0	7.8	6.0	8.0	1.3

TABLE B.20 CLAST TYPE AND MEDIAN DIAMETER (cm) FOR THE IDA GULCH M6 DEPOSIT

	Hbl porph	rhy/porph	feld porph	basalt	basement	vf/f Qzt	c Qzt	black vf Oqzt	Pc	T_R red f Ss-Sltst	J tan f Ss	Jm Ss	carb	chert	Pz Ls, Ss
	2	2.5	2	2.5	0.5	10.5	7.5	2.5	2.5	8	2	4	5	3.5	3.5
	5		6.5	7.5	2	6.5	2	4.5	4.5	2	8.5	8.5	1.5		1.5
	4		2.5	2.5	1	6	2	2.5	4.5	9	13	1.5			1.5
	2		1	2	2	4	6.5	3	1.5		9	2.5			
			9.5		1.5	2		8	8.5		3	3.5			
			8.5		5.5			2	2		12.5	1			
			0.5		10						1				
			6		4						11.5				
			2.5		4.5						12				
			8.5		4						5.5				
			10		5						1.5				
			3.5		1						9				
			1.5		9						5				
			7		9						2.5				
			7		2										
			6		2.5										
			2.5		2										
			2.5		1										
			7.5		4										
					4										
					2										
					11.5										
					1.5										
n	4	1	19	4	23	5	4	6	6	3	14	6	2	1	3
% total	4.0	1.0	18.8	4.0	22.8	5.0	4.0	5.9	5.9	3.0	13.9	5.9	2.0	1.0	3.0
median d (cm)	3.0	2.5	6.0	2.5	2.5	6.0	4.3	2.8	3.5	8.0	7.0	3.0	3.3	3.5	1.5

TABLE B.21 CLAST TYPE AND MEDIAN DIAMETER (cm) FOR THE IDA GULCH M4 DEPOSIT

	Hbl porph	rhy/porph	feld porph	basalt	basement	vf/f Qzt	c Qzt	black vf Oqzt	Pc	T_R red f Ss-Sltst	J tan f Ss	Jm Ss	carb	chert	Pz Ls, Ss
	10.5	3.5	9	11	2.5	7.5	6.5	7	3.5	7.5	8	4.5	6.5	2.5	2
	4	3	4	3	8.5	9.5	2.5	2.5		6	9	6		2.5	
	4.5	2.5	4	2.5	3.5	6	3.5	4.5		1.5	11	2		3.5	
	12		5	6	4.5	5	6.5	6.5			2	1.5			
	1.5		2.5	5.5	8	3	4	4			12				
	2.5		4.5	5	5	3.5	1.5	1.5			3.5				
	2.5		1.5	4	2.5	3.5	2	2							
	9		1.5	9	4	2.5									
			2	3	3.5	3									
				2	5.5	3.5									
				2.5	4.5	2.5									
				2.5	3	3									
					2	3.5									
					2.5	2									
					2.5	2									
					3	1									
						2.5									
						4									
						3									
						3									
n	8	3	9	12	16	20	7	7	1	3	6	4	1	3	1
% total	7.9	3.0	8.9	11.9	15.8	19.8	6.9	6.9	1.0	3.0	5.9	4.0	1.0	3.0	1.0
median d (cm)	4.3	3.0	4.0	3.5	3.5	3.0	3.5	4.0	3.5	6.0	8.5	3.3	6.5	2.5	2.0

TABLE B.22 CLAST TYPE AND MEDIAN DIAMETER (cm) FOR THE IDA GULCH M3 DEPOSIT

	Hbl porph	feld porph	basalt	basement	black vf Oqzt	Pc	T_R red f Ss-Sltst	J tan f Ss	Jm Ss	chert
	1	1	1	1	1	1	1	1	1	1
	1	1	1	1	1	1	1	1	1	
	1	1	1	1	1	1	1	1	1	
	1	1		1	1	1	1	1	1	
	1			1	1	1	1	1	1	
	1			1	1	1	1	1		
	1			1	1	1				
	1			1	1	1				
	1			1	1	1				
	1			1		1				
	1			1		1				
	1			1		1				
	1			1		1				
	1			1		1				
	1			1		1				
	1			1		1				
	1			1		1				
	1			1		1				
	1									
	1									
	1									
	1									
	1									
	1									
	1									
	1									
	1									
	1									
	1									
	1									
n	31	4	3	18	9	18	6	6	5	1
% total	30.7	4.0	3.0	17.8	8.9	17.8	5.9	5.9	5.0	1.0
median d (cm)[a]	NA	NA	NA	NA	NA	NA	NA	NA	NA	NA

[a] Clast diameters not measured.

Appendix C. Real-time kinematic (RTK) GPS survey data

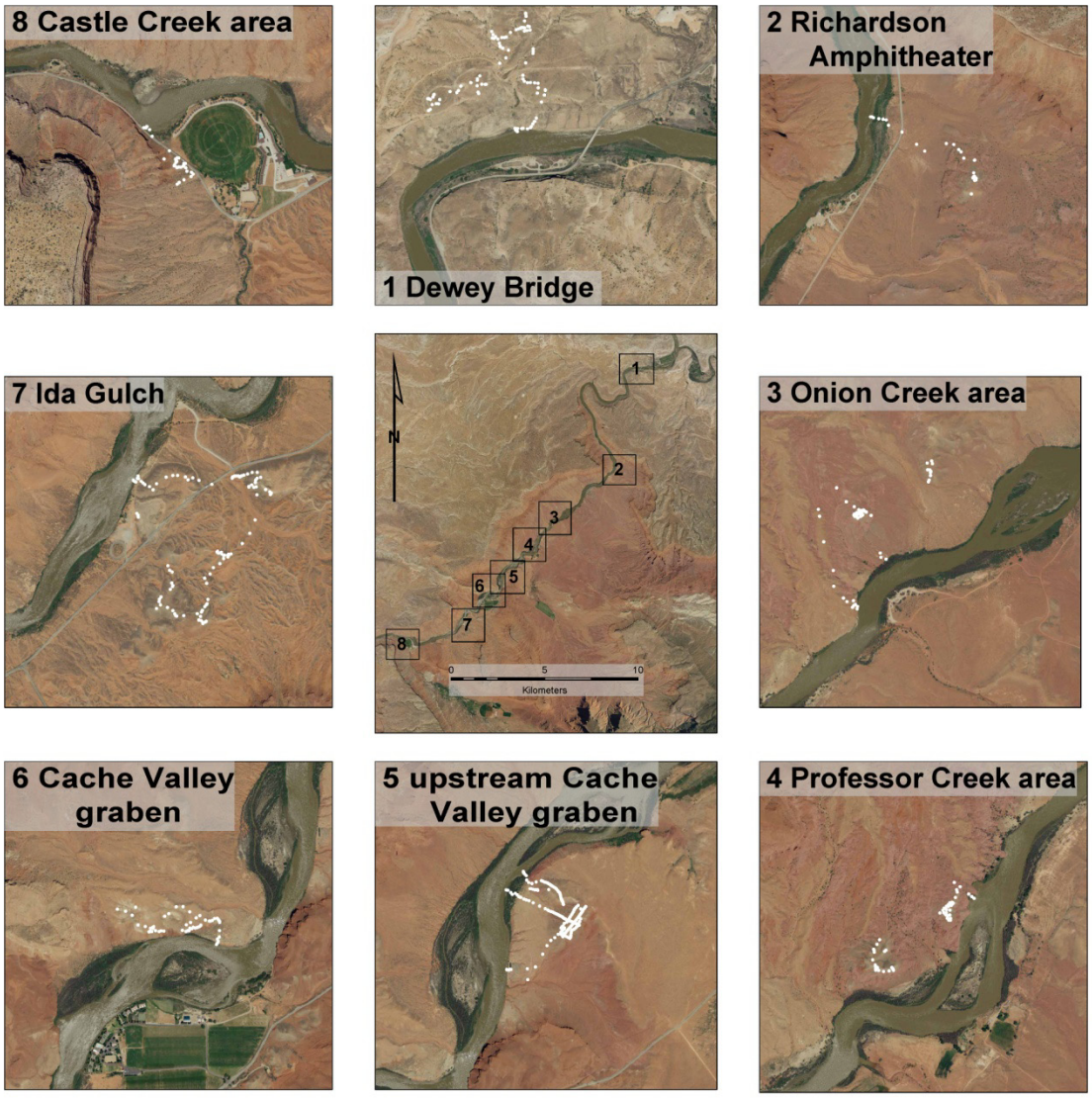

Figure C.1. Locations of study area surveys. Survey points shown in white. Eight surveys were performed.

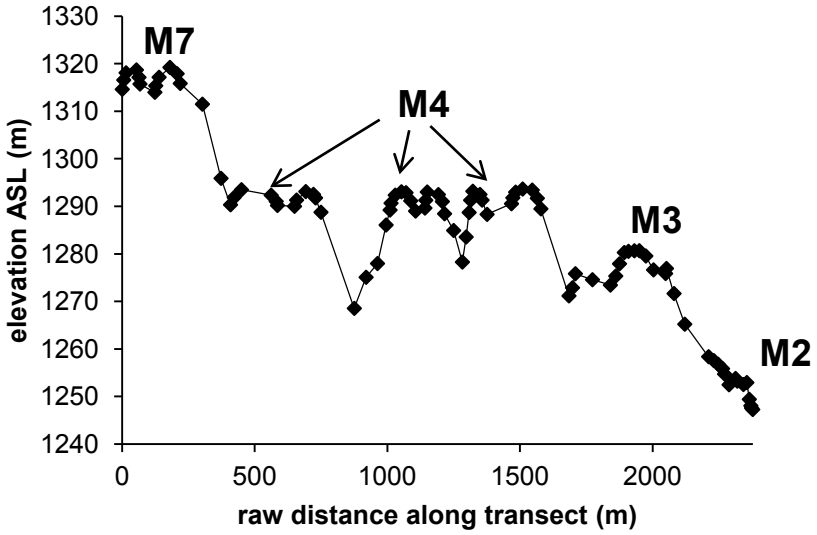

Figure C.2. Raw survey transect of Dewey Bridge terrace deposits.

TABLE C.1 SURVEY DATA FOR DEWEY BRIDGE TERRACE SUITE

Survey Transect 1: Dewey Bridge terrace suite	
Instrument height (m)	1.15
Instrument location	N 4297578.89 E 646580.09
Instrument elevation ASL (m)	1294.15

point ID	northing	easting	elevation ASL (m)	elevation above river (m)	raw distance along transect (m)	notes
101	4297493.23	646348.92	1314.60	67.34	0.00	strath
102	4297493.34	646354.53	1316.56	69.30	5.61	riser
103	4297489.18	646362.29	1318.07	70.81	14.42	tread
104	4297466.49	646394.15	1318.68	71.42	53.54	tread
105	4297466.65	646403.78	1317.13	69.86	63.17	riser
106	4297465.32	646407.25	1315.72	68.45	66.88	strath
107	4297516.04	646383.01	1313.98	66.72	123.10	strath
108	4297513.81	646380.71	1315.35	68.09	126.30	riser
109	4297501.82	646376.79	1317.14	69.88	138.92	tread
110	4297461.21	646372.73	1319.21	71.95	179.73	tread
111	4297435.89	646362.67	1317.88	70.62	206.97	riser
112	4297429.67	646352.84	1315.84	68.58	218.61	strath
113	4297488.92	646412.02	1311.48	64.22	302.36	bedrock
114	4297530.84	646468.30	1295.88	48.61	372.53	bedrock

115	4297525.57	646503.68	1290.32	43.06	408.29	strath
116	4297536.51	646512.24	1291.87	44.61	422.18	riser
117	4297560.35	646525.72	1293.49	46.23	449.57	tread
118	4297570.65	646637.18	1292.34	45.07	561.50	tread
119	4297569.77	646656.18	1291.03	43.77	580.52	riser
120	4297570.46	646660.90	1290.18	42.92	585.29	strath
121	4297520.64	646620.31	1290.00	42.73	649.54	strath
122	4297528.02	646617.47	1291.31	44.05	657.44	riser
123	4297562.26	646612.19	1293.10	45.83	692.09	tread
124	4297591.20	646613.23	1292.51	45.25	721.04	tread
125	4297599.01	646613.81	1291.76	44.50	728.88	riser
126	4297614.74	646626.94	1288.75	41.49	749.37	strath
127	4297682.18	646733.06	1268.53	21.27	875.11	channel
128	4297711.40	646766.55	1275.07	27.81	919.56	piedmont
129	4297752.21	646779.92	1277.97	30.70	962.49	piedmont
130	4297762.92	646749.34	1286.06	38.80	994.89	bedrock
131	4297771.36	646737.00	1289.21	41.95	1009.84	strath
132	4297775.08	646736.57	1290.66	43.40	1013.58	riser
133	4297789.98	646731.46	1292.35	45.09	1029.34	tread
134	4297811.99	646723.70	1293.05	45.79	1052.68	tread
135	4297824.43	646711.54	1292.86	45.60	1070.07	tread
136	4297835.77	646697.87	1291.15	43.89	1087.83	riser
137	4297852.43	646690.62	1289.00	41.73	1106.00	strath
138	4297817.27	646694.15	1289.63	42.37	1141.33	strath
139	4297816.62	646697.30	1291.28	44.01	1144.54	riser
140	4297815.96	646702.79	1293.01	45.75	1150.08	tread
141	4297820.77	646744.50	1292.47	45.21	1192.06	tread
142	4297820.60	646759.39	1291.00	43.74	1206.96	riser
143	4297823.01	646767.39	1288.43	41.17	1215.31	strath
144	4297847.57	646791.38	1284.91	37.65	1249.64	piedmont
145	4297861.78	646821.12	1278.27	31.01	1282.60	channel
146	4297866.96	646834.38	1283.55	36.28	1296.84	bedrock
147	4297870.57	646844.95	1288.70	41.44	1308.01	strath
148	4297873.49	646849.67	1291.28	44.02	1313.56	riser
149	4297873.43	646858.10	1293.17	45.91	1321.99	tread
150	4297881.03	646883.98	1292.49	45.23	1348.96	tread
151	4297879.09	646891.62	1291.30	44.04	1356.84	riser
152	4297860.70	646895.99	1288.30	41.04	1375.74	strath
153	4297949.45	646872.12	1290.54	43.28	1467.64	strath
154	4297944.47	646873.17	1291.78	44.52	1472.74	riser
155	4297933.99	646874.36	1292.98	45.72	1483.28	tread
156	4297908.65	646866.47	1293.63	46.37	1509.81	tread
157	4297872.48	646867.12	1293.41	46.15	1545.99	tread
158	4297857.49	646879.09	1291.69	44.43	1565.17	riser

159	4297854.49	646865.99	1289.47	42.20	1578.61	strath
160	4297759.49	646912.61	1271.16	23.90	1684.43	channel
161	4297746.12	646912.43	1272.86	25.60	1697.80	bedrock
162	4297735.26	646911.82	1275.82	28.56	1708.68	strath
163	4297684.41	646872.39	1274.56	27.30	1773.02	strath
164	4297618.28	646857.93	1273.43	26.17	1840.72	strath
165	4297598.15	646858.37	1275.33	28.07	1860.85	strath
166	4297585.95	646865.56	1277.91	30.64	1875.01	riser
167	4297578.95	646882.16	1280.28	33.02	1893.03	tread
168	4297579.34	646898.03	1280.53	33.26	1908.91	tread
169	4297577.50	646920.23	1280.64	33.38	1931.18	tread
170	4297575.84	646938.71	1280.66	33.40	1949.73	tread
171	4297551.23	646939.56	1279.55	32.29	1974.36	tread
172	4297522.68	646934.71	1276.62	29.36	2003.32	riser
173	4297537.26	646977.79	1275.86	28.59	2048.80	strath
174	4297540.50	646977.18	1276.92	29.66	2052.10	riser
175	4297512.42	646971.83	1271.65	24.39	2080.69	bedrock
176	4297475.03	646956.66	1265.20	17.94	2121.04	bedrock
177	4297389.33	646929.40	1258.37	11.11	2210.98	tread
178	4297371.87	646919.77	1257.54	10.28	2230.92	tread
179	4297358.83	646910.43	1256.77	9.51	2246.95	tread
180	4297344.61	646901.80	1255.86	8.60	2263.59	riser
181	4297337.96	646898.56	1254.72	7.46	2270.98	riser
182	4297331.99	646882.57	1252.47	5.20	2288.05	strath
183	4297334.49	646858.13	1253.80	6.54	2312.61	strath
184	4297333.09	646851.65	1253.23	5.96	2319.24	strath
185	4297333.16	646828.70	1252.51	5.25	2342.20	strath
186	4297335.03	646815.83	1252.93	5.67	2355.20	strath
187	4297326.11	646818.19	1249.40	2.14	2364.43	bedrock
188	4297322.64	646822.88	1248.06	0.80	2370.27	riser
189	4297320.49	646824.15	1247.58	0.32	2372.76	riser
190	4297317.43	646827.65	1247.26	0.00	2377.40	Colorado River (2760 cfs)

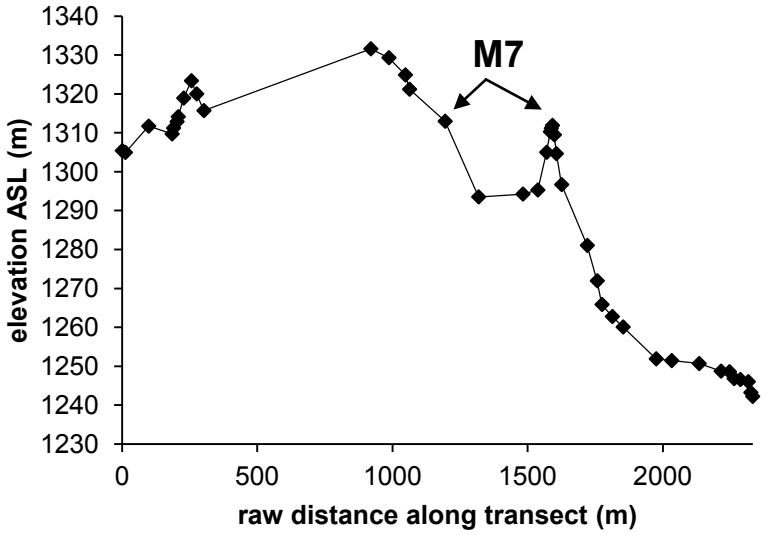

Figure C.3. Raw survey transect of Richardson Amphitheater terrace deposits.

TABLE C.2 SURVEY DATA FOR RICHARDSON AMPHITHEATER TERRACE SUITE

Survey Transect 2: Richardson Amphitheater M7 terrace

Instrument height (m)	1.11
Instrument location	N 4291777.23 E 646335.15
Instrument elevation ASL (m)	1284.44

point ID	northing	easting	elevation ASL (m)	elevation above river (m)	raw distance along transect (m)	notes
101	4291691.21	646334.36	1305.42	63.18	0.00	strath
102	4291682.86	646326.30	1304.97	62.73	11.60	strath
103	4291597.20	646317.96	1311.72	69.48	97.66	strath
104	4291679.88	646343.94	1309.72	67.48	184.33	strath
105	4291682.45	646339.44	1311.23	68.98	189.50	tread
106	4291669.71	646336.02	1312.89	70.64	202.69	tread
107	4291665.61	646334.49	1314.14	71.89	207.07	piedmont
108	4291645.44	646333.17	1318.93	76.69	227.28	piedmont
109	4291617.75	646339.90	1323.39	81.15	255.77	piedmont
110	4291619.16	646320.31	1320.01	77.77	275.41	piedmont
111	4291614.70	646294.04	1315.72	73.47	302.06	piedmont
112	4291264.34	646802.49	1331.60	89.36	919.53	piedmont
113	4291282.05	646738.05	1329.31	87.07	986.36	piedmont
114	4291309.89	646683.75	1324.89	82.65	1047.38	piedmont

115	4291322.90	646675.59	1321.21	78.96	1062.74	piedmont
116	4291384.46	646559.18	1312.98	70.73	1194.42	piedmont
117	4291498.73	646511.11	1293.53	51.29	1318.40	piedmont
118	4291633.93	646418.55	1294.26	52.01	1482.24	bedrock
119	4291678.72	646386.46	1295.30	53.06	1537.34	bedrock
120	4291680.12	646353.80	1305.00	62.76	1570.03	bedrock
121	4291671.77	646343.05	1310.29	68.05	1583.65	strath
122	4291674.09	646340.56	1311.17	68.93	1587.04	riser
123	4291677.19	646337.65	1311.92	69.67	1591.30	tread
124	4291684.26	646336.49	1309.49	67.25	1598.47	riser
125	4291689.66	646331.49	1304.65	62.40	1605.83	strath
126	4291709.37	646330.97	1296.69	54.45	1625.54	bedrock
127	4291788.23	646278.28	1281.07	38.82	1720.39	bedrock
128	4291821.92	646263.51	1271.96	29.72	1757.18	bedrock
129	4291833.89	646250.56	1265.87	23.63	1774.81	bedrock
130	4291860.86	646223.72	1262.78	20.53	1812.86	bedrock
131	4291866.74	646184.08	1260.09	17.85	1852.93	piedmont
132	4291825.53	646068.94	1251.90	9.66	1975.22	piedmont
133	4291862.73	646025.20	1251.45	9.20	2032.63	piedmont
134	4291928.20	645947.44	1250.69	8.45	2134.29	highway
135	4291963.95	645874.90	1248.74	6.50	2215.16	piedmont
136	4291992.64	645863.09	1248.59	6.35	2246.19	tread
137	4291996.52	645846.29	1246.82	4.57	2263.43	tread
138	4291999.83	645823.37	1246.59	4.35	2286.59	tread
139	4292004.23	645794.41	1246.03	3.79	2315.87	tread
140	4292008.79	645786.19	1243.25	1.00	2325.28	tread
141	4292008.90	645779.38	1242.24	0.00	2332.10	Colorado River (2760 cfs)

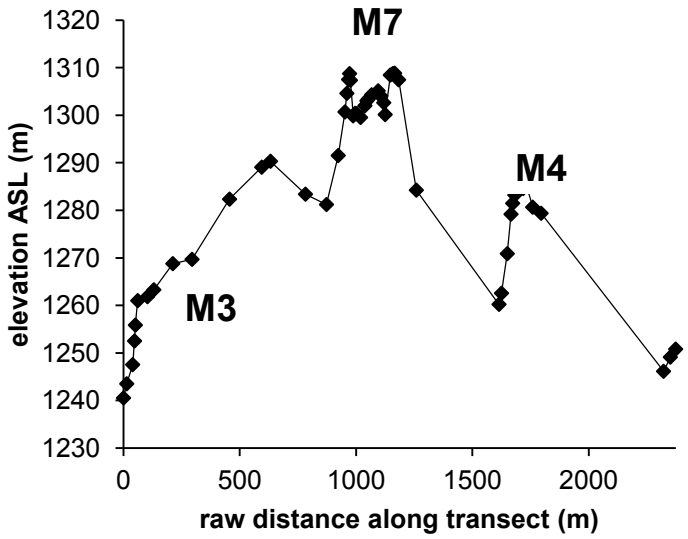

Figure C.4. Raw survey transect of Onion Creek area terrace deposits.

TABLE C.3 SURVEY DATA FOR ONION CREEK TERRACE SUITE

Survey Transect 3: Terrace suite upstream of Onion Creek confluence	
Instrument height (m)	1.16
Instrument location	N 4288905.86 E 642256.77
Instrument elevation ASL (m)	1258.42

point ID	northing	easting	elevation ASL (m)	elevation above river (m)	raw distance along transect (m)	notes
101	4288874.63	642278.48	1240.53	0.00	0.00	Colorado River (2620 cfs)
102	4288861.16	642275.51	1243.51	2.98	13.79	strath
103	4288884.94	642266.48	1247.53	7.00	39.23	riser
104	4288880.76	642259.57	1252.52	11.99	47.31	riser
105	4288878.24	642256.88	1255.85	15.33	50.99	riser
106	4288870.26	642250.59	1261.00	20.48	61.15	tread
107	4288900.09	642221.40	1261.84	21.31	102.88	tread
108	4288919.80	642202.31	1263.28	22.75	130.32	tread
109	4288983.01	642150.74	1268.78	28.25	211.90	tread
110	4289065.65	642148.10	1269.68	29.16	294.57	tread
111	4289218.42	642096.66	1282.34	41.82	455.78	tread
112	4289354.97	642074.41	1289.07	48.54	594.12	tread
113	4289392.28	642068.66	1290.32	49.79	631.88	tread

114	4289506.91	642165.95	1283.39	42.86	782.23	bedrock
115	4289432.64	642217.25	1281.22	40.69	872.50	bedrock
116	4289406.45	642260.45	1291.52	50.99	923.01	bedrock
117	4289389.77	642284.16	1300.69	60.17	952.00	bedrock
118	4289383.14	642288.84	1304.60	64.07	960.11	strath
119	4289377.73	642293.72	1307.51	66.99	967.40	riser
120	4289373.66	642295.65	1308.75	68.22	971.90	tread
121	4289370.82	642298.00	1307.35	66.82	975.59	riser
122	4289362.36	642305.75	1299.86	59.34	987.06	strath
123	4289357.52	642298.99	1300.39	59.87	995.38	strath
124	4289353.86	642292.76	1300.32	59.80	1002.61	strath
125	4289344.88	642278.92	1299.52	59.00	1019.10	strath
126	4289354.85	642263.12	1302.00	61.47	1037.78	strath
127	4289361.98	642258.30	1303.04	62.51	1046.40	strath
128	4289367.15	642261.22	1303.42	62.89	1052.33	strath
129	4289374.37	642273.49	1304.29	63.77	1066.57	strath
130	4289386.22	642299.13	1305.13	64.61	1094.82	strath
131	4289388.57	642310.09	1304.03	63.51	1106.02	strath
132	4289380.55	642319.95	1302.63	62.10	1118.73	strath
133	4289378.06	642325.54	1300.14	59.61	1124.85	strath
134	4289380.57	642303.63	1308.44	67.92	1146.91	tread
135	4289373.78	642295.34	1308.74	68.22	1157.62	tread
136	4289369.46	642288.61	1308.84	68.31	1165.62	tread
137	4289360.60	642274.12	1307.45	66.93	1182.60	tread
138	4289359.90	642350.43	1284.24	43.71	1258.91	bedrock
139	4289539.15	642657.35	1260.22	19.69	1614.34	channel
140	4289549.20	642660.91	1262.56	22.04	1625.01	piedmont
141	4289573.06	642668.08	1270.88	30.35	1649.92	bedrock
142	4289589.00	642668.13	1279.18	38.66	1665.85	strath
143	4289595.93	642669.78	1281.47	40.94	1672.98	riser
144	4289603.12	642664.29	1283.22	42.69	1682.03	tread
145	4289636.75	642677.82	1284.59	44.06	1718.28	tread
146	4289650.63	642674.72	1285.27	44.74	1732.50	tread
147	4289639.84	642650.60	1280.66	40.13	1758.93	strath
148	4289603.50	642652.93	1279.38	38.85	1795.34	strath
149	4289126.23	642431.24	1246.14	5.61	2321.59	strath
150	4289135.91	642403.71	1249.12	8.59	2350.77	tread
151	4289158.35	642399.42	1250.80	10.28	2373.62	tread

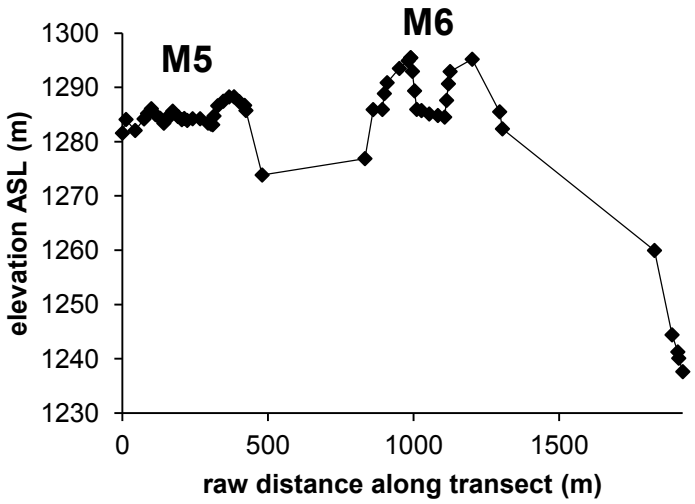

Figure C.5. Raw survey transect of Professor Creek area terrace deposits.

TABLE C.4 SURVEY DATA FOR PROFESSOR CREEK TERRACE SUITE

Survey Transect 4: M6 and M5 terraces upstream of Professor Creek confluence	
Instrument height (m)	1.10
Instrument location	N 4288030.41 E 641415.60
Instrument elevation ASL (m)	1274.42

point ID	northing	easting	elevation ASL (m)	elevation above river (m)	raw distance along transect (m)	notes
101	4287991.44	641428.75	1281.58	43.96	0.00	bedrock
102	4287979.33	641431.58	1284.09	46.47	12.43	strath
103	4287949.50	641421.93	1282.06	44.44	43.79	strath
104	4287924.75	641404.19	1284.19	46.57	74.24	strath
105	4287921.60	641392.72	1285.19	47.57	86.14	strath
106	4287911.36	641384.47	1286.07	48.45	99.29	strath
107	4287902.24	641373.10	1284.97	47.35	113.87	strath
108	4287892.32	641360.98	1284.31	46.69	129.53	strath
109	4287881.11	641355.08	1283.40	45.78	142.19	strath
110	4287868.81	641359.79	1284.25	46.63	155.36	strath
111	4287861.53	641366.74	1285.10	47.48	165.42	strath
112	4287856.22	641371.68	1285.62	48.00	172.67	strath
113	4287839.43	641378.20	1284.63	47.01	190.69	strath
114	4287829.06	641386.50	1284.05	46.43	203.97	strath
115	4287827.97	641394.78	1284.27	46.65	212.32	strath

116	4287838.09	641396.13	1283.91	46.29	222.53	strath
117	4287856.03	641391.72	1284.22	46.60	241.00	strath
118	4287881.83	641392.67	1284.22	46.60	266.83	strath
119	4287908.00	641399.40	1283.42	45.80	293.85	strath
120	4287915.51	641406.01	1283.24	45.62	303.85	strath
121	4287919.74	641410.45	1283.12	45.50	309.99	strath
122	4287922.55	641407.05	1284.73	47.11	314.40	riser
123	4287917.36	641395.37	1286.62	49.00	327.17	tread
124	4287901.39	641385.00	1287.45	49.83	346.21	tread
125	4287884.71	641373.65	1288.25	50.63	366.39	tread
126	4287867.85	641373.29	1288.27	50.65	383.25	tread
127	4287851.95	641380.28	1287.39	49.77	400.62	tread
128	4287835.13	641389.20	1286.69	49.07	419.66	tread
129	4287834.89	641384.83	1285.74	48.12	424.03	riser
130	4287866.99	641339.29	1273.85	36.23	479.75	bedrock
131	4287724.07	641016.68	1276.87	39.25	832.60	bedrock
132	4287699.72	641002.55	1285.91	48.29	860.75	strath
133	4287673.49	640984.71	1285.93	48.31	892.48	strath
134	4287667.04	640986.71	1288.86	51.24	899.23	riser
135	4287657.50	640988.04	1290.86	53.24	908.86	tread
136	4287616.55	640979.21	1293.49	55.87	950.76	tread
137	4287589.47	640993.03	1294.91	57.29	981.16	tread
138	4287581.27	640994.99	1295.47	57.85	989.58	tread
139	4287581.19	640994.70	1295.45	57.83	989.89	tread
140	4287575.49	640996.10	1292.95	55.33	995.76	riser
141	4287568.22	640995.78	1289.36	51.74	1003.03	riser
142	4287560.87	640995.54	1285.95	48.33	1010.39	strath
143	4287558.86	641011.79	1285.73	48.11	1026.76	strath
144	4287553.88	641037.93	1285.10	47.48	1053.37	strath
145	4287556.90	641067.43	1284.82	47.20	1083.03	strath
146	4287559.90	641090.59	1284.52	46.90	1106.37	strath
147	4287566.21	641088.64	1287.61	49.99	1112.97	riser
148	4287571.57	641085.53	1290.66	53.04	1119.17	riser
149	4287575.95	641081.59	1292.92	55.30	1125.06	tread
150	4287575.48	641005.77	1295.19	57.57	1200.89	tread
151	4287662.01	641043.17	1285.50	47.88	1295.16	riser
152	4287667.90	641050.59	1282.36	44.74	1304.63	strath
153	4288006.94	641447.54	1259.95	22.33	1826.67	bedrock
154	4287967.81	641493.43	1244.40	6.78	1886.98	bedrock
155	4287955.21	641508.69	1241.26	3.64	1906.77	tread
156	4287953.70	641511.44	1240.10	2.48	1909.91	riser
157	4287944.85	641522.26	1237.62	0.00	1923.88	Colorado River (2620 cfs)

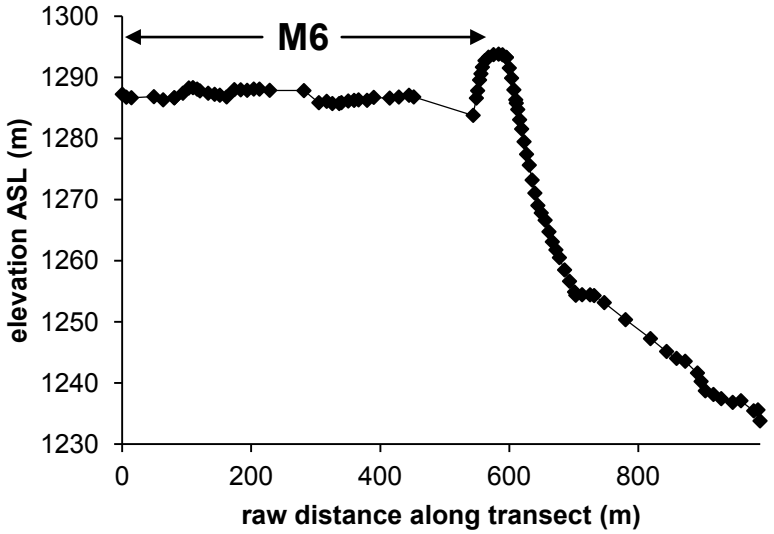

Figure C.6. Raw survey transect of upstream Cache Valley graben M6 terrace deposit.

TABLE C.5 SURVEY DATA FOR UPSTREAM CACHE VALLEY GRABEN M6 TERRACE

Survey Transect 5A: Terrace suite upstream of Cache Valley graben

Instrument height (m)	1.75 m
Instrument location	N 4286070.05 E 640175.54
Instrument elevation ASL (m)	1294.46

point ID	northing	easting	elevation ASL (m)	elevation above river (m)	raw distance along transect (m)	notes
100	4286079.65	640167.37	1287.22	53.43	0.00	strath
101	4286075.86	640162.42	1286.74	52.95	6.24	strath
102	4286069.59	640157.69	1286.65	52.86	14.09	strath
103	4286034.71	640158.86	1286.82	53.04	49.00	strath
104	4286023.09	640167.30	1286.31	52.52	63.35	strath
105	4286025.27	640184.42	1286.64	52.86	80.61	strath
106	4286025.28	640184.42	1286.64	52.86	80.63	strath
107	4286019.08	640196.21	1287.39	53.60	93.95	strath
108	4286014.66	640204.27	1288.25	54.46	103.14	strath
109	4286020.04	640207.67	1288.30	54.51	109.51	strath
110	4286026.31	640209.45	1288.06	54.27	116.02	strath
111	4286030.62	640209.53	1287.77	53.98	120.33	strath
112	4286043.25	640211.47	1287.39	53.60	133.11	strath
113	4286053.13	640213.01	1287.21	53.42	143.11	strath

114	4286059.51	640217.92	1287.07	53.28	151.16	strath
115	4286063.69	640227.60	1286.78	53.00	161.70	strath
116	4286071.19	640236.90	1287.97	54.19	173.65	strath
117	4286078.66	640243.39	1287.94	54.16	183.55	strath
118	4286087.50	640248.05	1287.86	54.08	193.54	strath
119	4286096.79	640252.30	1288.07	54.28	203.76	strath
120	4286104.46	640256.76	1288.06	54.27	212.63	strath
121	4286119.05	640262.85	1287.86	54.07	228.43	strath
122	4286172.15	640262.93	1287.82	54.03	281.54	strath
123	4286190.46	640248.79	1285.84	52.05	304.68	strath
124	4286182.24	640239.89	1286.06	52.28	316.79	strath
125	4286175.55	640234.18	1285.70	51.91	325.59	strath
126	4286167.27	640227.49	1285.70	51.91	336.24	strath
127	4286164.05	640226.43	1285.85	52.06	339.62	strath
128	4286154.34	640222.19	1286.12	52.33	350.22	strath
129	4286146.57	640217.48	1286.22	52.43	359.30	strath
130	4286140.64	640213.99	1286.30	52.51	366.19	strath
131	4286130.05	640206.11	1286.23	52.44	379.38	strath
132	4286120.57	640201.93	1286.71	52.92	389.75	strath
133	4286100.39	640187.66	1286.59	52.80	414.46	strath
134	4286094.76	640174.66	1286.77	52.98	428.63	strath
135	4286080.40	640168.19	1287.05	53.27	444.38	strath
136	4286075.84	640162.41	1286.78	52.99	451.75	strath
137	4286084.44	640254.09	1283.77	49.98	543.83	bedrock
138	4286086.16	640249.40	1286.59	52.80	548.82	bedrock
139	4286087.79	640248.37	1287.81	54.02	550.75	strath
140	4286089.04	640245.61	1289.55	55.76	553.78	riser
141	4286089.58	640243.57	1290.57	56.79	555.89	riser
142	4286090.49	640241.51	1291.66	57.87	558.14	riser
143	4286092.60	640238.12	1292.72	58.93	562.14	tread
144	4286095.15	640233.26	1293.29	59.50	567.62	tread
145	4286098.43	640226.19	1293.70	59.91	575.42	tread
146	4286101.95	640219.16	1293.79	60.00	583.28	tread
147	4286104.10	640213.49	1293.68	59.89	589.35	tread
148	4286105.99	640207.87	1293.25	59.46	595.27	tread
149	4286106.00	640207.89	1293.25	59.46	595.30	tread
150	4286106.91	640203.42	1291.51	57.72	599.85	riser
151	4286107.50	640199.95	1289.86	56.07	603.37	riser
152	4286108.78	640196.64	1287.94	54.16	606.93	riser
153	4286109.84	640193.93	1286.31	52.52	609.83	riser
154	4286110.41	640193.31	1285.77	51.98	610.67	strath
155	4286111.24	640191.21	1284.73	50.94	612.93	bedrock
156	4286113.07	640188.97	1283.05	49.26	615.82	bedrock
157	4286114.59	640186.20	1281.54	47.75	618.98	bedrock

158	4286116.85	640183.23	1279.46	45.67	622.72	bedrock
159	4286118.78	640179.86	1277.40	43.62	626.60	bedrock
160	4286120.29	640175.92	1275.62	41.84	630.82	bedrock
161	4286122.65	640172.17	1273.18	39.39	635.25	bedrock
162	4286125.21	640168.81	1271.05	37.26	639.48	bedrock
163	4286128.55	640165.58	1269.02	35.23	644.12	bedrock
164	4286131.15	640161.03	1267.80	34.01	649.36	bedrock
165	4286133.95	640155.74	1266.62	32.83	655.35	bedrock
166	4286136.22	640150.23	1264.73	30.94	661.31	bedrock
167	4286139.06	640145.85	1263.08	29.29	666.52	bedrock
168	4286141.26	640140.74	1261.76	27.98	672.09	bedrock
169	4286143.82	640135.96	1260.49	26.70	677.51	bedrock
170	4286146.75	640128.52	1258.48	24.69	685.51	bedrock
171	4286150.40	640121.76	1256.63	22.84	693.19	bedrock
172	4286153.99	640114.88	1254.88	21.09	700.95	bedrock
173	4286154.85	640113.17	1254.34	20.55	702.87	bedrock
174	4286157.72	640103.80	1254.43	20.64	712.67	piedmont
175	4286162.44	640092.32	1254.41	20.62	725.08	piedmont
176	4286165.71	640086.99	1254.29	20.50	731.33	piedmont
177	4286173.46	640073.29	1253.14	19.35	747.07	piedmont
178	4286186.97	640043.25	1250.35	16.56	780.01	piedmont
179	4286204.23	640008.70	1247.25	13.46	818.63	piedmont
180	4286215.70	639986.47	1245.14	11.35	843.64	piedmont
181	4286219.84	639971.59	1244.01	10.22	859.09	piedmont
182	4286224.13	639958.89	1243.54	9.75	872.49	piedmont
183	4286233.57	639942.42	1241.62	7.84	891.48	piedmont
184	4286235.44	639937.08	1240.24	6.45	897.14	piedmont
185	4286237.84	639931.02	1238.71	4.92	903.65	piedmont
186	4286246.96	639922.31	1238.11	4.32	916.27	riser
187	4286255.46	639913.71	1237.43	3.64	928.36	riser
188	4286249.26	639897.08	1236.81	3.03	946.10	riser
189	4286259.15	639888.94	1237.08	3.29	958.90	riser
190	4286271.33	639873.40	1235.43	1.64	978.65	riser
191	4286272.42	639866.88	1235.58	1.80	985.26	riser
192	4286273.29	639863.78	1233.79	0.00	988.48	Colorado River (5420 cfs)

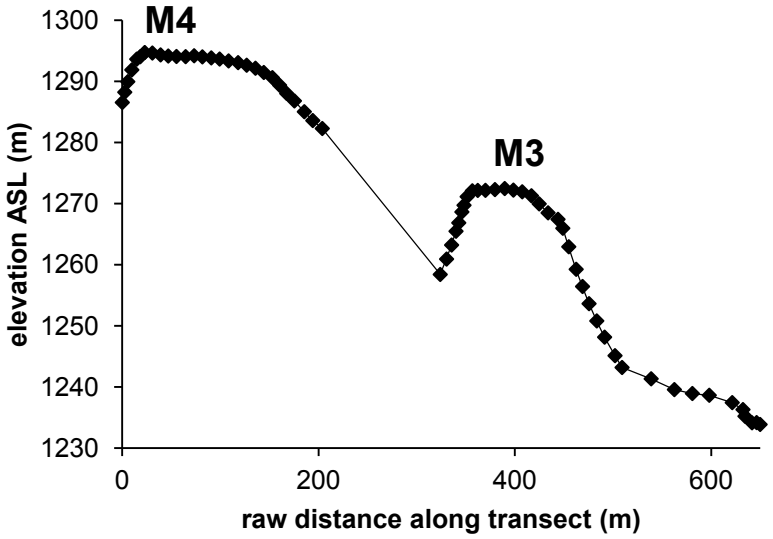

Figure C.7. Raw survey transect of upstream Cache Valley graben M4 and M3 terrace deposits.

TABLE C.6 SURVEY DATA FOR UPSTREAM CACHE VALLEY GRABEN M4 AND M3 TERRACES

Survey Transect 5B: Terrace suite upstream of Cache Valley graben

Instrument height (m)	1.75 m
Instrument location	N 4286070.05 E 640175.54
Instrument elevation ASL (m)	1294.46

point ID	northing	easting	elevation ASL (m)	elevation above river (m)	raw distance along transect (m)	notes
193	4286023.12	640167.35	1286.53	52.67	0.00	strath
194	4286025.47	640168.25	1288.21	54.35	2.51	riser
195	4286028.10	640169.88	1289.93	56.08	5.60	riser
196	4286031.85	640171.52	1291.86	58.00	9.70	riser
197	4286036.53	640173.22	1293.62	59.76	14.68	riser
198	4286039.51	640175.33	1294.01	60.16	18.33	riser
199	4286042.19	640178.98	1294.71	60.85	22.86	tread
200	4286048.04	640184.10	1294.62	60.76	30.64	tread
201	4286054.57	640189.32	1294.31	60.45	39.00	tread
202	4286060.57	640194.34	1294.13	60.27	46.81	tread
203	4286066.61	640200.13	1294.05	60.20	55.18	tread
204	4286073.56	640206.35	1294.02	60.17	64.51	tread
205	4286080.42	640211.64	1294.17	60.31	73.17	tread

206	4286086.74	640217.19	1293.99	60.13	81.58	tread
207	4286093.64	640223.05	1293.82	59.96	90.64	tread
208	4286100.20	640228.48	1293.63	59.78	99.15	tread
209	4286107.48	640233.98	1293.33	59.47	108.28	tread
210	4286115.09	640239.97	1293.04	59.19	117.96	tread
211	4286121.75	640245.63	1292.62	58.77	126.71	tread
212	4286128.81	640251.13	1292.13	58.27	135.66	tread
213	4286135.64	640256.18	1291.43	57.58	144.15	tread
214	4286142.98	640260.95	1290.59	56.74	152.90	tread
215	4286148.90	640265.33	1289.35	55.49	160.26	tread
216	4286154.77	640269.51	1288.00	54.14	167.47	riser
217	4286161.47	640273.63	1286.78	52.93	175.34	riser
218	4286170.01	640279.00	1285.02	51.16	185.42	riser
219	4286177.03	640284.01	1283.57	49.72	194.05	riser
220	4286184.74	640289.87	1282.27	48.41	203.73	strath
221	4286195.69	640170.22	1258.39	24.54	323.88	bedrock
222	4286201.92	640168.50	1260.91	27.05	330.34	bedrock
223	4286207.02	640167.92	1263.21	29.35	335.47	bedrock
224	4286211.02	640165.89	1265.46	31.61	339.96	bedrock
225	4286212.82	640163.75	1266.84	32.98	342.76	strath
226	4286215.78	640162.58	1268.62	34.76	345.94	riser
227	4286217.67	640161.53	1269.71	35.86	348.10	riser
228	4286220.67	640160.48	1271.12	37.26	351.28	riser
229	4286225.55	640158.36	1272.08	38.22	356.60	tread
230	4286230.90	640157.05	1272.14	38.28	362.11	tread
231	4286238.61	640155.78	1272.16	38.30	369.93	tread
232	4286248.09	640153.70	1272.28	38.42	379.63	tread
233	4286257.54	640150.61	1272.45	38.59	389.57	tread
234	4286263.81	640144.36	1272.19	38.34	398.42	tread
235	4286270.91	640138.84	1271.92	38.06	407.42	tread
236	4286277.86	640132.56	1271.27	37.41	416.79	tread
237	4286283.35	640126.87	1269.94	36.08	424.69	tread
238	4286288.07	640119.16	1268.47	34.62	433.74	tread
239	4286293.76	640110.76	1267.41	33.56	443.88	tread
240	4286295.82	640106.35	1265.95	32.10	448.75	bedrock
241	4286299.77	640101.73	1262.92	29.07	454.82	bedrock
242	4286304.09	640095.54	1259.24	25.38	462.37	bedrock
243	4286307.39	640089.96	1256.43	22.57	468.86	bedrock
244	4286310.91	640084.35	1253.61	19.76	475.48	bedrock
245	4286313.41	640076.88	1250.79	16.94	483.35	bedrock
246	4286315.17	640069.10	1248.14	14.28	491.33	bedrock
247	4286320.12	640059.72	1245.11	11.25	501.94	bedrock
248	4286322.82	640053.07	1243.18	9.32	509.12	channel
249	4286315.70	640024.30	1241.32	7.47	538.75	channel

250	4286307.43	640002.15	1239.56	5.70	562.39	channel
251	4286313.20	639984.74	1238.92	5.06	580.73	channel
252	4286326.50	639973.82	1238.63	4.78	597.95	riser
253	4286349.82	639971.90	1237.43	3.57	621.34	riser
254	4286357.43	639964.04	1236.29	2.43	632.29	riser
255	4286358.92	639962.71	1235.20	1.35	634.29	riser
256	4286364.92	639958.71	1234.13	0.27	641.49	riser
257	4286368.58	639955.78	1234.16	0.31	646.18	riser
258	4286372.15	639955.81	1233.86	0.00	649.75	Colorado River (5420 cfs)

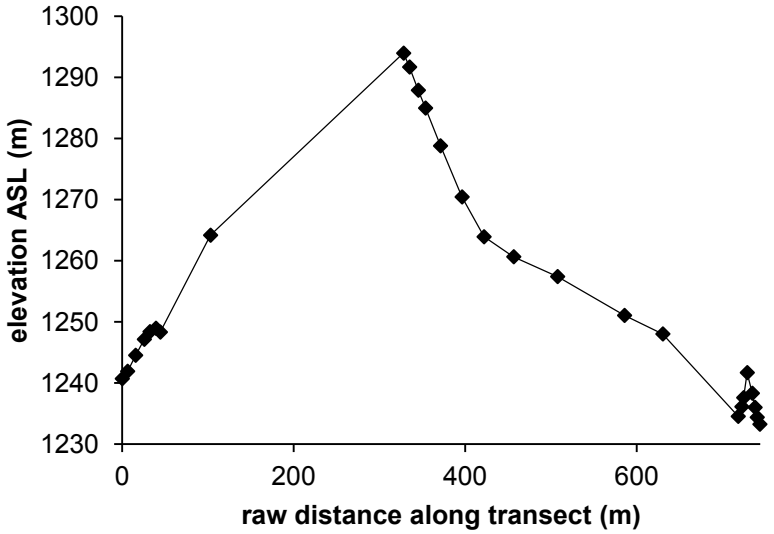

Figure C.8. Raw survey transect of upstream Cache Valley graben M2 terrace deposit.

TABLE C.7 SURVEY DATA FOR UPSTREAM CACHE VALLEY GRABEN M2 TERRACE

Survey Transect 5C: Terrace suite upstream of Cache Valley graben

Instrument height (m)	1.75 m
Instrument location	N 4286070.05 E 640175.54
Instrument elevation ASL (m)	1294.46

point ID	northing	easting	elevation ASL (m)	elevation above river (m)	raw distance along transect (m)	notes
259	4286279.75	639992.23	1240.69	7.45	0.00	channel
260	4286279.04	639998.43	1241.90	8.66	6.25	riser
261	4286276.71	640007.48	1244.52	11.28	15.59	riser
262	4286273.79	640017.20	1247.13	13.89	25.74	riser
263	4286273.77	640023.76	1248.38	15.14	32.30	tread
264	4286274.88	640030.66	1248.94	15.70	39.29	tread
265	4286270.84	640033.82	1248.31	15.07	44.42	bedrock
266	4286275.18	640092.22	1264.16	30.92	102.98	strath
267	4286065.09	640173.13	1293.94	60.70	328.11	tread
268	4286060.01	640168.37	1291.67	58.43	335.07	strath
269	4286051.77	640162.39	1287.88	54.64	345.25	strath
270	4286046.65	640155.72	1284.96	51.72	353.66	strath
271	4286036.18	640141.81	1278.78	45.54	371.07	strath
272	4286018.48	640123.90	1270.42	37.18	396.25	strath

273	4286003.67	640103.02	1263.90	30.66	421.85	piedmont
274	4285976.01	640082.17	1260.64	27.40	456.48	piedmont
275	4285930.19	640059.45	1257.39	24.16	507.63	piedmont
276	4285862.20	640021.14	1251.04	17.80	585.68	piedmont
277	4285852.07	639977.63	1248.01	14.77	630.35	section line
278	4285847.83	639889.86	1234.53	1.29	718.22	bedrock
279	4285848.54	639885.67	1236.11	2.87	722.47	strath
280	4285848.62	639883.57	1237.58	4.34	724.58	OSL sample
281	4285845.82	639880.44	1241.68	8.44	728.77	tread
282	4285845.73	639874.51	1238.31	5.07	734.70	strath
283	4285846.25	639871.38	1235.99	2.75	737.87	riser
284	4285845.65	639868.97	1234.37	1.13	740.35	riser
285	4285847.87	639866.78	1233.24	0.00	743.47	Colorado River (5420 cfs)

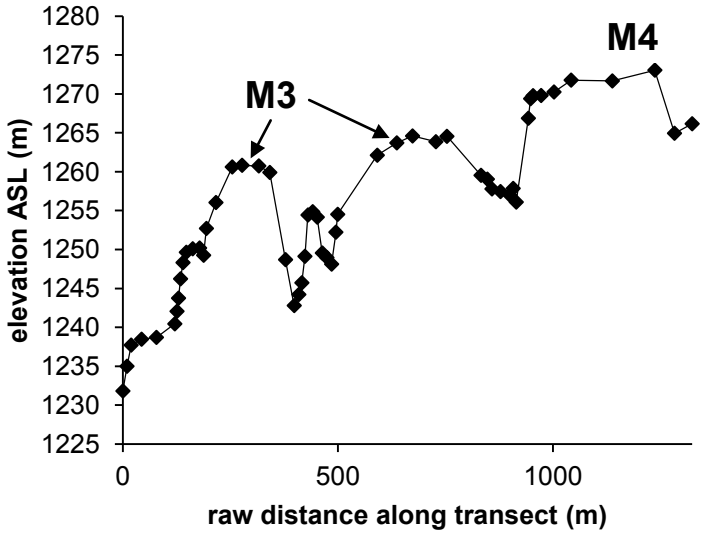

Figure C.9. Raw survey transect of Cache Valley graben terrace deposits.

TABLE C.8 SURVEY DATA FOR CACHE VALLEY GRABEN TERRACE SUITE

Survey Transect 6: Cache Valley graben terrace suite

Instrument height (m)	1.19
Instrument location	N 4285290.52 E 639343.30
Instrument elevation ASL (m)	1239.07

point ID	northing	easting	elevation ASL (m)	elevation above river (m)	raw distance along transect (m)	notes
100	4285261.41	639338.18	1231.82	0.00	0.00	Colorado River (2620 cfs)
101	4285269.31	639343.52	1235.00	3.18	9.53	riser
102	4285278.25	639347.28	1237.72	5.90	19.24	tread
103	4285301.49	639353.89	1238.47	6.66	43.39	tread
104	4285336.03	639354.08	1238.71	6.89	77.94	tread
105	4285378.77	639355.27	1240.45	8.63	120.69	tread
106	4285383.86	639354.87	1242.06	10.25	125.80	riser
107	4285386.73	639352.79	1243.75	11.94	129.35	riser
108	4285390.61	639350.12	1246.23	14.42	134.06	riser
109	4285395.11	639346.67	1248.32	16.51	139.73	riser
110	4285401.43	639342.28	1249.65	17.83	147.42	tread
111	4285399.68	639327.45	1250.10	18.28	162.35	tread
112	4285389.61	639315.06	1250.20	18.38	178.32	tread

113	4285385.81	639306.47	1249.26	17.45	187.71	strath
114	4285386.92	639300.10	1252.71	20.90	194.17	riser
115	4285391.85	639278.49	1256.04	24.23	216.34	riser
116	4285415.56	639248.96	1260.61	28.80	254.22	tread
117	4285403.72	639229.37	1260.83	29.01	277.10	tread
118	4285378.71	639199.57	1260.75	28.93	316.01	tread
119	4285366.59	639177.04	1259.91	28.09	341.59	tread
120	4285336.87	639155.69	1248.70	16.88	378.19	strath
121	4285331.11	639175.02	1242.80	10.98	398.36	strath
122	4285335.39	639184.89	1244.22	12.41	409.11	strath
123	4285335.30	639191.92	1245.73	13.91	416.15	strath
124	4285341.70	639194.90	1249.13	17.31	423.21	strath
125	4285348.67	639196.32	1254.44	22.62	430.32	strath
126	4285345.02	639206.72	1254.86	23.05	441.35	strath
127	4285353.30	639213.37	1254.16	22.34	451.97	strath
128	4285349.38	639224.40	1249.56	17.74	463.67	strath
129	4285352.10	639234.81	1248.96	17.14	474.43	strath
130	4285355.62	639245.10	1248.12	16.31	485.31	strath
131	4285360.97	639253.41	1252.23	20.42	495.19	strath
132	4285365.03	639254.71	1254.52	22.71	499.46	strath
133	4285435.39	639195.35	1262.12	30.30	591.51	tread
134	4285463.29	639159.58	1263.71	31.89	636.87	tread
135	4285462.22	639123.02	1264.60	32.78	673.45	tread
136	4285425.20	639083.32	1263.86	32.04	727.73	tread
137	4285412.16	639061.26	1264.55	32.73	753.36	tread
138	4285333.01	639056.37	1259.54	27.72	832.66	strath
139	4285334.39	639041.65	1259.05	27.23	847.44	strath
140	4285330.52	639031.73	1257.79	25.97	858.09	strath
141	4285335.25	639012.43	1257.45	25.64	877.96	strath
142	4285329.90	638991.56	1257.00	25.19	899.50	strath
143	4285331.56	638983.79	1257.86	26.04	907.45	strath
144	4285329.01	638977.11	1256.10	24.28	914.60	strath
145	4285347.83	638998.06	1266.87	35.06	942.76	riser
146	4285353.06	638997.94	1269.39	37.57	947.98	riser
147	4285356.45	639002.55	1269.78	37.96	953.71	tread
148	4285347.91	638985.88	1269.80	37.98	972.44	tread
149	4285357.22	638957.46	1270.25	38.43	1002.35	tread
150	4285365.27	638918.47	1271.78	39.96	1042.16	tread
151	4285460.33	638906.04	1271.67	39.86	1138.02	tread
152	4285449.61	638807.73	1273.06	41.24	1236.91	tread
153	4285438.71	638852.01	1264.94	33.13	1282.51	tread
154	4285416.98	638886.87	1266.16	34.35	1323.58	tread

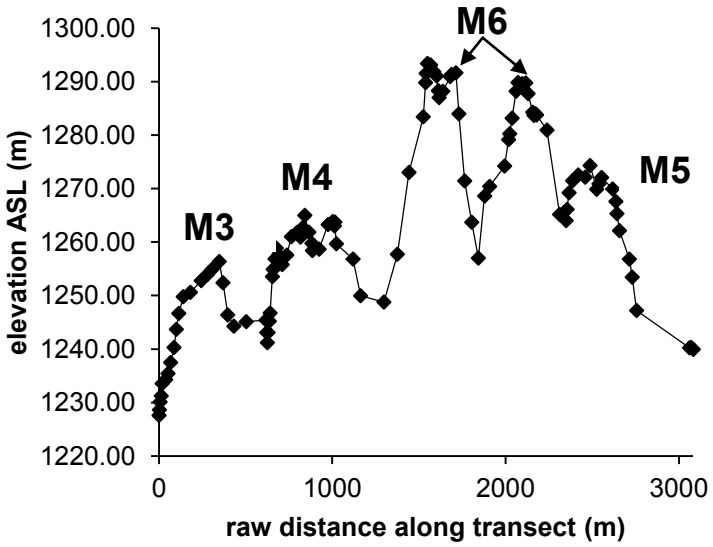

Figure C.10. Raw survey transect of Ida Gulch terrace deposits.

TABLE C.9 SURVEY DATA FOR IDA GULCH TERRACE SUITE

Survey Transect 7: Ida Gulch terrace suite	
Instrument height (m)	1.15
Instrument location	N 4283787.49 E 637892.87
Instrument elevation ASL (m)	1250.40

point ID	northing	easting	elevation ASL (m)	elevation above river (m)	raw distance along transect (m)	notes
101	4283839.25	637786.42	1227.59	0.00	0.00	Colorado River (2730 cfs)
102	4283837.55	637788.10	1228.64	1.04	2.39	riser
103	4283834.29	637790.20	1230.11	2.52	6.27	riser
104	4283830.30	637795.23	1231.24	3.65	12.69	tread
105	4283828.91	637800.33	1233.55	5.95	17.98	strath
106	4283847.92	637806.99	1234.28	6.69	38.13	strath
107	4283860.85	637811.49	1235.42	7.83	51.82	strath
108	4283846.36	637814.64	1237.49	9.89	66.65	riser
109	4283832.43	637828.67	1240.30	12.70	86.42	riser
110	4283823.11	637838.42	1243.69	16.09	99.91	riser
111	4283814.19	637849.21	1246.66	19.07	113.91	riser
112	4283803.95	637872.92	1249.79	22.19	139.74	tread
113	4283819.32	637911.23	1250.60	23.01	181.01	tread

114	4283854.68	637962.43	1252.80	25.20	243.23	tread
115	4283863.80	637998.10	1253.97	26.37	280.05	tread
116	4283864.26	638023.17	1254.87	27.28	305.13	piedmont
117	4283855.62	638064.99	1256.37	28.77	347.83	piedmont
118	4283840.10	638079.27	1252.39	24.80	368.93	piedmont
119	4283850.57	638104.64	1246.38	18.78	396.36	piedmont
120	4283838.01	638137.80	1244.27	16.68	431.82	piedmont
121	4283816.10	638205.95	1245.12	17.53	503.41	highway
122	4283848.69	638315.15	1245.41	17.81	617.37	piedmont
123	4283852.78	638316.02	1243.08	15.48	621.55	piedmont
124	4283855.88	638318.02	1241.19	13.59	625.24	channel
125	4283857.32	638322.02	1243.10	15.51	629.49	piedmont
126	4283860.08	638328.65	1245.20	17.61	636.67	piedmont
127	4283860.88	638332.97	1246.73	19.14	641.07	bedrock
128	4283860.72	638346.11	1253.54	25.95	654.21	bedrock
129	4283860.09	638350.41	1254.90	27.31	658.55	strath
130	4283855.64	638355.60	1255.10	27.51	665.39	strath
131	4283857.86	638358.70	1256.84	29.25	669.21	riser
132	4283861.93	638365.48	1258.86	31.27	677.11	tread
133	4283866.06	638377.66	1257.61	30.02	689.97	riser
134	4283872.13	638397.68	1255.79	28.19	710.89	strath
135	4283880.30	638422.74	1257.57	29.98	737.24	riser
136	4283880.24	638449.29	1261.01	33.41	763.80	tread
137	4283853.43	638468.04	1261.81	34.22	796.52	tread
138	4283848.54	638449.18	1260.92	33.33	816.00	tread
139	4283838.82	638441.25	1262.69	35.09	828.54	riser
140	4283826.32	638439.48	1265.00	37.40	841.17	tread
141	4283813.02	638419.98	1261.86	34.26	864.78	tread
142	4283804.73	638404.71	1259.77	32.18	882.15	riser
143	4283802.02	638405.12	1258.41	30.82	884.89	strath
144	4283802.58	638444.06	1258.67	31.07	923.84	strath
145	4283788.27	638494.13	1263.28	35.68	975.91	strath
146	4283776.10	638517.19	1263.83	36.24	1001.99	strath
147	4283767.68	638523.57	1263.02	35.43	1012.56	strath
148	4283769.85	638523.76	1263.74	36.15	1014.74	riser
149	4283761.79	638520.13	1259.68	32.09	1023.58	bedrock
150	4283800.23	638431.98	1256.83	29.23	1119.75	strath
151	4283760.11	638447.96	1249.97	22.38	1162.93	piedmont
152	4283625.70	638438.57	1248.79	21.19	1297.67	channel
153	4283553.83	638409.87	1257.73	30.13	1375.07	piedmont
154	4283499.65	638369.57	1273.03	45.43	1442.59	piedmont
155	4283444.21	638309.07	1283.42	55.83	1524.65	piedmont
156	4283441.57	638295.62	1289.81	62.21	1538.36	strath
157	4283439.92	638293.02	1291.54	63.95	1541.44	riser

158	4283432.44	638292.06	1293.39	65.79	1548.98	tread
159	4283438.11	638274.71	1293.12	65.52	1567.23	tread
160	4283444.73	638258.70	1291.90	64.30	1584.56	tread
161	4283448.45	638241.80	1291.07	63.48	1601.86	tread
162	4283454.95	638234.33	1288.30	60.71	1611.76	riser
163	4283458.40	638236.93	1287.01	59.41	1616.08	strath
164	4283452.67	638257.72	1288.19	60.60	1637.65	strath
165	4283435.05	638296.15	1290.94	63.35	1679.93	strath
166	4283427.52	638292.74	1291.35	63.75	1688.20	strath
167	4283436.42	638269.23	1291.65	64.05	1713.34	riser
168	4283419.28	638269.19	1283.97	56.38	1730.48	bedrock
169	4283392.36	638249.30	1271.43	43.84	1763.95	bedrock
170	4283371.08	638214.78	1263.71	36.11	1804.50	bedrock
171	4283337.07	638197.13	1257.00	29.41	1842.83	channel
172	4283315.37	638168.26	1268.61	41.01	1878.94	piedmont
173	4283288.56	638178.79	1270.40	42.80	1907.73	piedmont
174	4283202.22	638185.17	1274.21	46.62	1994.32	piedmont
175	4283179.68	638181.18	1279.16	51.57	2017.21	piedmont
176	4283174.54	638177.43	1280.25	52.66	2023.57	strath
177	4283163.58	638168.80	1283.16	55.57	2037.52	riser
178	4283144.56	638155.84	1288.21	60.61	2060.53	riser
179	4283135.11	638151.08	1289.83	62.24	2071.12	tread
180	4283111.31	638145.48	1289.62	62.03	2095.56	tread
181	4283092.44	638137.00	1289.75	62.16	2116.25	tread
182	4283088.60	638149.82	1287.76	60.16	2129.64	riser
183	4283085.44	638176.34	1284.27	56.67	2156.35	strath
184	4283081.05	638170.71	1283.69	56.09	2163.49	strath
185	4283078.46	638161.92	1283.98	56.38	2172.66	strath
186	4283073.78	638158.32	1283.76	56.17	2178.56	strath
187	4283125.90	638127.82	1280.94	53.35	2238.95	strath
188	4283115.46	638056.14	1265.17	37.58	2311.39	piedmont
189	4283113.18	638018.26	1264.02	36.42	2349.34	piedmont
190	4283115.66	638013.22	1266.12	38.53	2354.95	strath
191	4283125.82	638008.46	1269.21	41.62	2366.17	riser
192	4283142.98	637997.73	1271.47	43.88	2386.42	tread
193	4283159.40	637969.40	1272.55	44.95	2419.16	tread
194	4283173.11	637931.72	1272.13	44.54	2459.25	tread
195	4283154.26	637911.15	1274.31	46.71	2487.15	tread
196	4283190.48	637924.02	1269.86	42.27	2525.58	strath
197	4283203.38	637926.99	1270.89	43.29	2538.82	riser
198	4283216.29	637934.96	1272.07	44.48	2553.99	tread
199	4283256.40	637984.28	1269.93	42.34	2617.56	tread
200	4283271.28	637995.75	1267.59	39.99	2636.35	riser
201	4283277.00	637997.86	1265.32	37.72	2642.44	strath

202	4283290.70	637992.51	1262.14	34.54	2657.15	piedmont
203	4283347.69	637994.30	1256.81	29.22	2714.18	piedmont
204	4283356.84	637980.83	1253.44	25.85	2730.45	piedmont
205	4283380.89	637972.02	1247.20	19.61	2756.07	channel
206	4283641.04	637812.34	1240.23	12.63	3061.31	strath
207	4283651.16	637811.28	1240.29	12.69	3071.48	strath
208	4283660.64	637804.78	1239.93	12.34	3082.98	strath

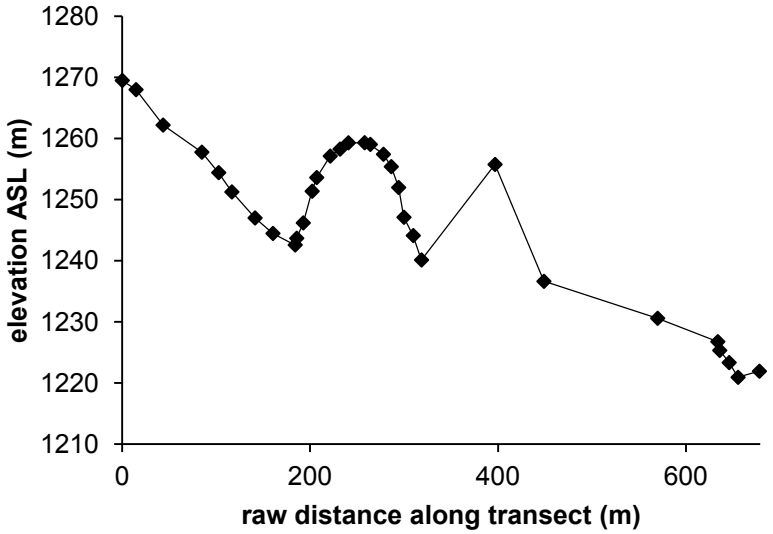

Figure C.11. Raw survey transect of Castle Creek area M3 terrace deposit.

TABLE C.10 SURVEY DATA FOR CASTLE CREEK AREA TERRACE SUITE

Survey Transect 8: M3 terrace near Castle Creek confluence	
Instrument height (m)	1.14
Instrument location	N 4282421.59 E 634595.02
Instrument elevation ASL (m)	1259.20

point ID	northing	easting	elevation ASL (m)	elevation above river (m)	raw distance along transect (m)	notes
101	4282330.84	634507.77	1269.48	48.56	0.00	bedrock
102	4282340.90	634518.41	1267.97	47.06	14.64	piedmont
103	4282354.70	634543.66	1262.17	41.26	43.41	piedmont
104	4282371.74	634581.22	1257.74	36.83	84.66	piedmont
105	4282385.23	634593.07	1254.39	33.48	102.61	piedmont
106	4282395.35	634583.39	1251.24	30.33	116.62	piedmont
107	4282400.15	634559.20	1246.98	26.07	141.28	piedmont
108	4282418.40	634553.69	1244.45	23.54	160.35	channel
109	4282441.89	634550.88	1242.56	21.65	184.01	riser
110	4282440.43	634550.16	1243.66	22.75	185.64	riser
111	4282441.52	634543.28	1246.17	25.26	192.60	riser
112	4282432.20	634541.70	1251.35	30.44	202.06	riser
113	4282427.72	634539.80	1253.59	32.68	206.92	tread
114	4282422.76	634526.31	1257.10	36.19	221.30	tread

115	4282422.88	634515.86	1258.25	37.33	231.75	tread
116	4282421.32	634507.13	1259.28	38.36	240.62	piedmont
117	4282428.72	634491.50	1259.29	38.38	257.91	piedmont
118	4282434.35	634493.74	1259.02	38.11	263.97	tread
119	4282446.73	634500.16	1257.40	36.49	277.91	tread
120	4282453.28	634505.34	1255.38	34.46	286.27	tread
121	4282459.96	634501.26	1251.96	31.05	294.09	riser
122	4282465.11	634498.90	1247.09	26.18	299.76	riser
123	4282471.63	634506.35	1244.10	23.19	309.67	riser
124	4282471.64	634515.12	1240.11	19.20	318.43	riser
125	4282465.98	634437.08	1255.74	34.82	396.68	bedrock
126	4282509.42	634465.68	1236.61	15.70	448.69	highway
127	4282587.74	634373.45	1230.57	9.66	569.69	highway
128	4282633.34	634328.49	1226.74	5.83	633.73	piedmont
129	4282633.60	634330.52	1225.31	4.40	635.78	riser
130	4282631.35	634340.29	1223.32	2.41	645.80	riser
131	4282639.37	634345.38	1220.91	0.00	655.30	Colorado River (2730 cfs)
132	4282622.19	634360.22	1221.91	1.00	678.00	riser

Appendix D. Supplemental GIS data and figures

This appendix contains figures and data for basic topographic analyses completed using 10 m digital elevation models (DEMs) in ArcGIS (ESRI, 2011). These analyses include tributary catchment gradient distributions and hypsometry (Table D.1, Figures D.1 and D.2). Also included is a map of the three study area catchments (Onion, Professor, and Castle creeks) displaying the distribution of steepness index (k_{sn}) values and knickzones throughout these streams (Fig. D.3). Finally, the mathematical derivation of k_{sn} is provided.

TABLE D.1 TOPOGRAPHIC METRICS OF STUDY AREA TRIBUTARY DRAINAGES

	elevation (m)						slope (°)				steepness index (k_{sn})	
catchment	min	max	mean	relief	HI	R_{VA} (m)	median	mean	σ	skew	mean[a]	θ[b]
Onion Creek	1234	2466	1688	1232	0.37	190	20.7	26.4	25.5	-0.01	9	0.41
Professor Creek	1233	2702	1825	1469	0.40	193	10.2	17.9	20.9	-0.05	18	0.15
Castle Creek	1221	3756	2129	2535	0.36	226	9.0	19.8	18.5	-0.02	21	0.33

[a] Calculated using reference concavity (θ_{ref}) of 0.35.
[b] Regressed concavity over entire tributary length.

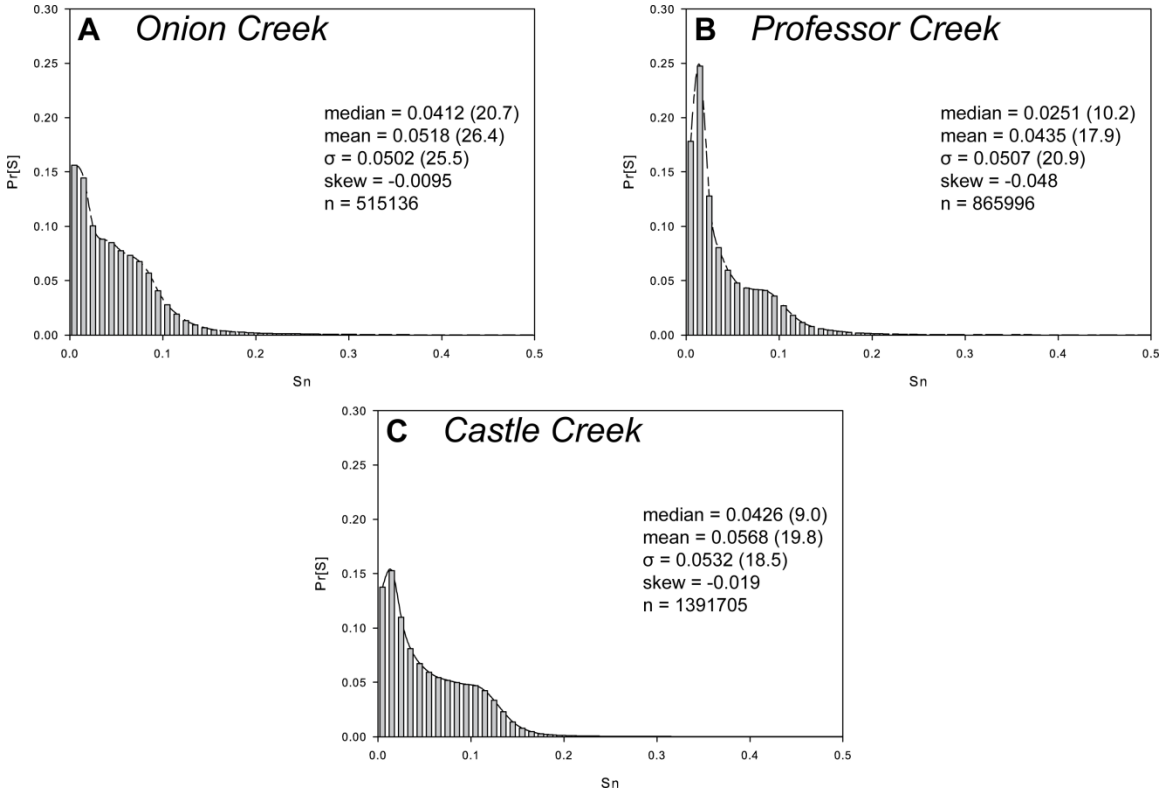

Figure D.1. Slope probability Pr[S] distributions for study area tributary catchments. S_n is mean gradient normalized to maximum gradient (Wolinsky and Pratson, 2005). Values in parentheses are in degrees. All three tributary slope distributions are skewed toward lower slopes. (A) Onion Creek, with the highest mean gradient. (B) Professor Creek. (C) Castle Creek.

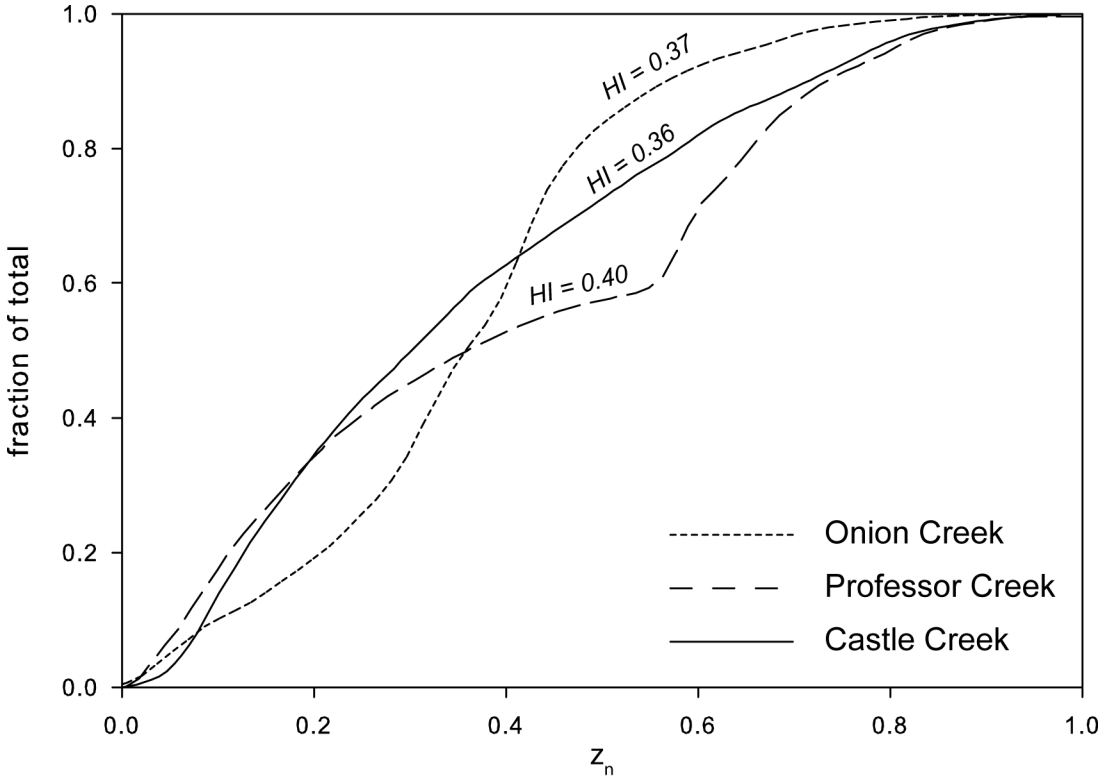

Figure D.2. Hypsometric integrals for study area tributary catchments. z_n is normalized elevation. Values for all three catchments are moderate, with little apparent relation to active salt tectonism.

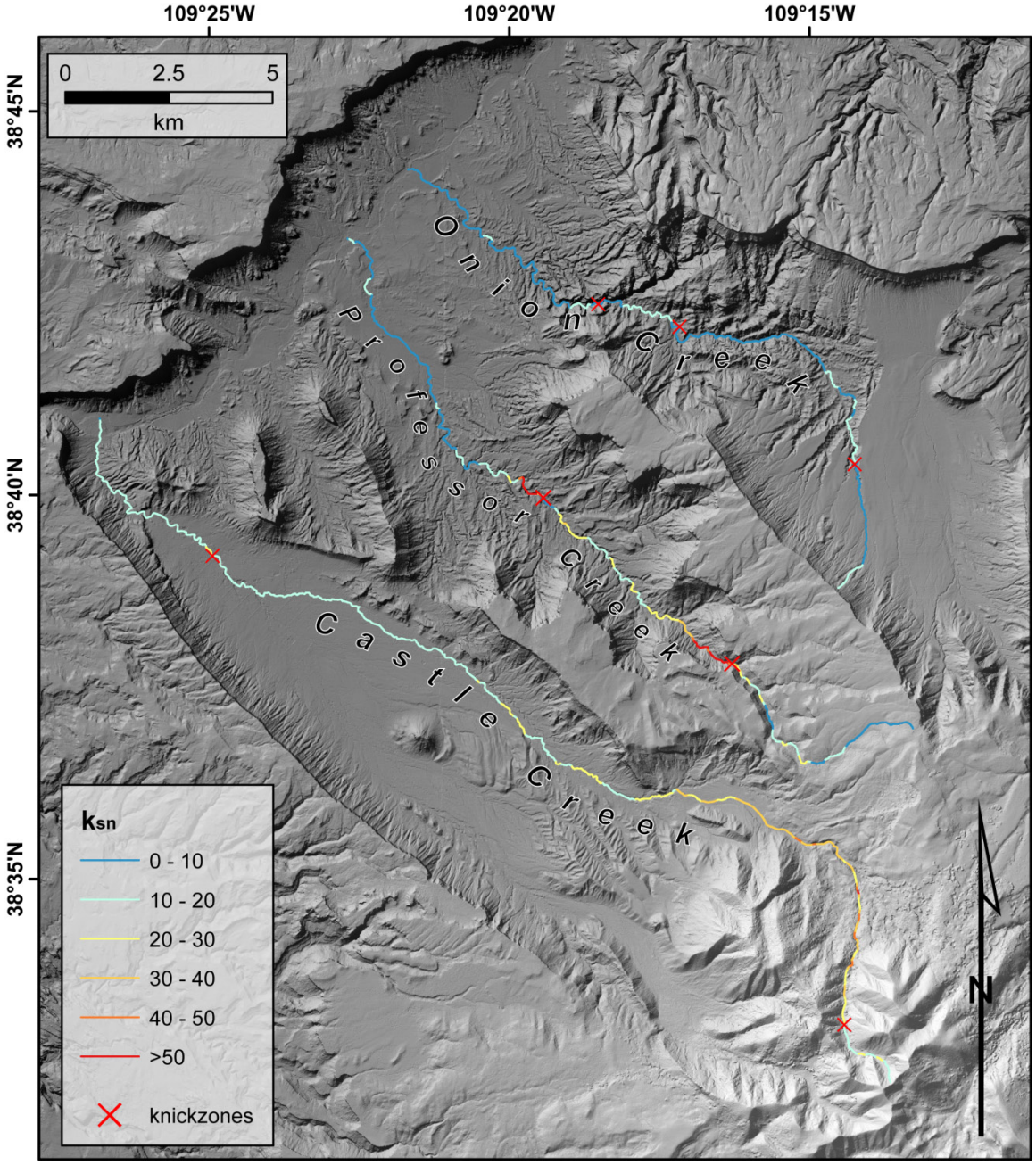

Figure D.3. Map of steepness index (k_{sn}) distributions for study area tributary catchments. Castle Creek drainage features the highest overall k_{sn} values, Onion Creek features the lowest. Knickzones are associated with mass movement debris in Castle Creek, transient and structural factors in Professor Creek, and active diapirism in Onion Creek.

Derivation of k_{sn}

The normalized steepness index (k_{sn}) is a generalized form of the stream-gradient index of Hack (1973) that allows broad comparison between drainages based on a reference profile concavity, θ_{ref}. The calculation of profile concavity and k_{sn} assumes that the river profile is in steady state with respect to uplift and climate, and that uplift rate and erosivity are uniform throughout each reach (Snyder et al., 2000). Derivation of k_{sn} begins with the stream power erosion model:

$$\frac{\delta z}{\delta t} = U - E = U - KA^m S^n, \quad (1)$$

where $\frac{\delta z}{\delta t}$ is the time rate of change of river-bed elevation, U is uplift rate, E is erosion rate, K is a dimensional coefficient of erosion, A is upstream drainage area, S is slope, and m and n are variables related to basin hydrology, hydraulic geometry, and erosion processes (Whipple and Tucker, 1999; Snyder et al., 2000; Wobus et al., 2006). In a steady-state landscape $\frac{\delta z}{\delta t} = 0$, $E = U$, and the stream power erosion model takes the form:

$$U = KA^m S^n. \quad (2)$$

Solving for S gives the equilibrium slope, S_e:

$$S_e = \left(\frac{U}{K}\right)^{1/n} A^{-m/n}, \quad (3)$$

where m/n is a measure of concavity, θ (Snyder et al., 2000; Kirby and Whipple, 2001). Assuming reach uniformity of U and K, this power function can then be written as:

$$S = k_s A^{-\theta}, \text{ where} \quad (4)$$

$$k_s = \left(\frac{U}{K}\right)^{1/n}. \quad (5)$$

Equation 4 is known as "Flint's Law" and utilizes conservation of mass in order to express the rate of change in river-bed slope (Flint, 1974; Howard et al., 1994). Finally, k_s is normalized according to a reference concavity, θ_{ref}, to give the normalized steepness index, k_{sn}:

$$S = k_{sn}A^{-\theta_{ref}}. \quad (6)$$

The value of θ_{ref} is chosen based on the characteristic concavity of stream profiles, and typically $0.4 \leq \theta_{ref} \leq 0.6$ in steady-state landscapes (Wobus et al., 2006; Kirby and Whipple, 2012).